

ESA Climate Change Initiative (CCI)

Sea Level Budget Closure (SLBC_cci)

Product Description Document D2.4.2
ESA_SLBC_cci_D2.4.2_v1.2

Description of data set and uncertainty assessment,
version 2

Prime & Science Lead: Martin Horwath
Technische Universität Dresden (TUDr)
Martin.Horwath@tu-dresden.de

Technical Officer: Jérôme Benveniste
ESA ESRIN, Frascati, Italy
Jerome.Benveniste@esa.int

Consortium: Laboratoire d'Etudes en Géophysique et Océanographie Spatiales (LEGOS)
Universität Bremen (UB)
Universität Zürich (UZH)
University of Leeds (UoL)
Goethe-Universität Frankfurt (GUF)
Danmarks Tekniske Universitet, DTU Space, Geodynamics (DTU-GDK)
Danmarks Tekniske Universitet, DTU Space, Geodesy (DTU-GEK)
Nansen Environmental and Remote Sensing Center (NERSC)
University of Reading (UoR)
Mercator Ocean, Toulouse (MerO)



CCI Sea Level Budget Closure

ESA/ESRIN contract 4000119910/17/I-NB

Reference: ESA_SLBC_cci_D2.4.2

Version: v1.2

Date: 18.06.2019



Page: 2 of 116

To be cited as:

Horwath, M.; Novotny, K.; Cazenave, A.; Palanisamy, H.; Marzeion, B.; Paul, F.; Döll, P.; Cáceres, D.; Hogg, A.; Shepherd, A.; Otosaka, I.; Forsberg, R.; Barletta, V.R.; Simonsen, S.; Andersen, O.B.; Rose, S.K.; Rannal, H.; Johannessen, J.A.; Raj, R.P.; Gutknecht, B.D.; Merchant, Ch.J.; von Schuckmann, K.: *ESA Climate Change Initiative (CCI) Sea Level Budget Closure (SLBC_cci). Product Description Document D2.4.2: Version 2 data sets and uncertainty assessments. Version 1.2, 18 June 2019.*

		<p>CCI Sea Level Budget Closure</p> <p>ESA/ESRIN contract 4000119910/17/I-NB</p> <p>Reference: ESA_SLBC_cci_D2.4.2</p> <p>Version: v1.2</p> <p>Date: 18.06.2019</p> <p>Page: 3 of 116</p>
---	---	---

Signatures page

<p>Prepared by</p>	<p>Kristin Novotny Project Manager, TUDr Martin Horwath Science Leader, TUDr</p> <p>Anny Cazenave, Hindumathi Palanisamy, LEGOS; Ben Marzeion, UB; Frank Paul, Raymond Le Bris, UZH; Petra Döll, Denise Cáceres, GUF; Anna Hogg, Andrew Shepherd, Inés Ootosaka, UOL; Rene Forsberg, Valentina Barletta, DTU-GDK; Ole B. Andersen, Stine K. Rose, Heidi Rannal, DTU-GEK; Johnny Johannessen, Roshin P. Raj, NERSC; Benjamin D. Gutknecht, TUDr; Christopher John Merchant, UoR; Karina von Schuckmann, MerO</p>	<p>Date: 2019-06-18</p> 
<p>Checked by</p>	<p>Martin Horwath Science Leader, TUDr</p>	<p>Date: 2019-06-18</p> 
<p>Approved by</p>	<p>Jérôme Benveniste Technical Officer, ESA</p>	<p>Date:</p>

		CCI Sea Level Budget Closure
		ESA/ESRIN contract 4000119910/17/I-NB Reference: ESA_SLBC_cci_D2.4.2 Version: v1.2 Date: 18.06.2019 Page: 4 of 116

Change Log

Issue	Author, Org.	Affected Section	Reason/Description	Status
1.0	M. Horwath / TUDr	All	Document Creation	Released to ESA 2019-02-14
1.1	M. Horwath / TUDr	All	Document Revision after Review by ESA	Released to ESA 2019-06-12
1.2	M. Horwath / TUDr	8.1	Small Revision after Review by ESA	Released to ESA 2019-06-18

Distribution List

Organization	Consortium Member
TUDr	Martin Horwath
LEGOS	Anny Cazenave
UB	Ben Marzeion
UZH	Frank Paul
UoL	Andrew Shepherd, Anna Hogg
DTU- GDK	Rene Forsberg
GUF	Petra Döll
NERSC	Johnny Johannessen
DTU-GEK	Ole B. Andersen
UoR	Christopher Merchant
MerO	Karina von Schuckmann
ESA	Jérôme Benveniste Marco Restano Américo Ambrózio

		CCI Sea Level Budget Closure ESA/ESRIN contract 4000119910/17/I-NB Reference: ESA_SLBC_cci_D2.4.2 Version: v1.2 Date: 18.06.2019 Page: 5 of 116
---	---	--

Table of Contents

Change Log	4
Table of Contents	5
Acronyms and Abbreviations	8
1 Introduction	12
1.1 Purpose and Scope	12
1.2 Document Structure	12
1.3 Data Structure	12
2 Total Sea Level Change	17
2.1 Data access and requirements	17
2.2 Algorithms	17
2.2.1 Review of scientific background	17
2.2.2 Algorithms	17
2.3 Product Specification.....	19
2.3.1 Product geophysical data content	19
2.3.2 Coverage and resolution in time and space	19
2.3.3 Product data format	19
2.4 Uncertainty Assessment.....	19
2.4.1 Sources of error	19
2.4.2 Methodology for uncertainty assessment	20
2.4.3 Results of uncertainty assessment	20
2.4.4 Uncertainty documentation in the data products	21
2.5 References.....	21
3 Steric Sea Level Change	22
3.1 Data Access and Requirements	22
3.2 Algorithm theoretical basis	22
3.2.1 Scientific background	22
3.2.2 Algorithm theoretical basis	23
3.3 Product Specification.....	35
3.3.1 Product geophysical data content	35
3.3.2 Coverage and resolution in time and space	36
3.3.3 Product data format	36
3.3.4 Product grid and projection	36
3.4 Uncertainty Assessment.....	36
3.4.1 Sources of error	36
3.4.2 Methodology for uncertainty assessment	36
3.4.3 Results of uncertainty assessment	36
3.4.4 Uncertainty documentation in the data products	36
3.5 References.....	37

		<p>CCI Sea Level Budget Closure</p> <p>ESA/ESRIN contract 4000119910/17/I-NB</p> <p>Reference: ESA_SLBC_cci_D2.4.2</p> <p>Version: v1.2</p> <p>Date: 18.06.2019</p> <p>Page: 6 of 116</p>
---	---	---

4	Ocean Mass Change	38
4.1	Data Access and Requirements	38
4.2	Algorithms	39
4.2.1	Review of scientific background	39
4.2.2	Algorithms	41
4.2.3	Algorithms for Continental Mass Change	45
4.3	Product specification	48
4.3.1	Product geophysical data content	48
4.3.2	Coverage and resolution in time and space	51
4.3.3	Product data format	52
4.3.4	Product grid and projection	52
4.4	Uncertainty assessment	53
4.4.1	Sources of error	53
4.4.2	Methodology and Results of Uncertainty Assessment	54
4.4.3	Uncertainty documentation in the data products	58
4.5	References	58
5	Glacier Contribution to Sea Level Change	61
5.1	Data Access and Requirements	61
5.2	Algorithms	62
5.2.1	Review of scientific background	62
5.2.2	Algorithms	62
5.3	Product Specification	65
5.3.1	Product geophysical data content	65
5.3.2	Coverage and resolution in time and space	66
5.3.3	Product data format	67
5.3.4	Product grid and projection	67
5.4	Uncertainty assessment	67
5.4.1	Sources of error	67
5.4.2	Methodology for uncertainty assessment	68
5.4.3	Results of uncertainty assessment	69
5.4.4	Uncertainty documentation in the data products	70
5.5	References	70
6	Ice Sheets Contribution to Sea Level Change	71
6.1	Data access and requirements	71
6.2	Algorithms	72
6.2.1	Review of scientific background	72
6.2.2	Algorithms	73
6.3	Product Specification	76
6.3.1	Product geophysical data content	76
6.3.2	Coverage and resolution in time and space	83
6.3.3	Product data format	83
6.3.4	Product grid and projection	84

		<p>CCI Sea Level Budget Closure</p> <p>ESA/ESRIN contract 4000119910/17/I-NB</p> <p>Reference: ESA_SLBC_cci_D2.4.2</p> <p>Version: v1.2</p> <p>Date: 18.06.2019</p> <p>Page: 7 of 116</p>
---	---	---

6.4	Uncertainty Assessment.....	84
6.4.1	Sources of error	84
6.4.2	Methodology for uncertainty assessment	85
6.4.3	Results of uncertainty assessment	88
6.4.4	Uncertainty documentation in the data products	88
6.5	References.....	88
7	Total Land Water Storage Change	91
7.1	Data Access and Requirements.....	91
7.2	Algorithms	91
7.2.1	Review of scientific background	91
7.2.2	Algorithms	92
7.3	Product Specification.....	97
7.3.1	Product geophysical data content	97
7.3.2	Coverage and resolution in time and space	99
7.3.3	Product data format	99
7.3.4	Product grid and projection	100
7.4	Uncertainty Assessment.....	100
7.4.1	Sources of error	100
7.4.2	Methodology for uncertainty assessment	100
7.4.3	Results of uncertainty assessment	100
7.4.4	Uncertainty documentation in the data products	101
7.5	References.....	102
8	Arctic Sea Level Change	103
8.1	Data Access and Requirements.....	103
8.2	Algorithms	103
8.2.1	Review of scientific background	103
8.2.2	Algorithms	104
8.3	Product Specification.....	106
8.3.1	Product geophysical data content	106
8.3.2	Coverage and resolution in time and space	109
8.3.3	Product data format	109
8.3.4	Product grid and projection	109
8.4	Uncertainty assessment	109
8.4.1	Sources of error	109
8.4.2	Methodology for uncertainty assessment	110
8.4.3	Results of uncertainty assessment	110
8.4.4	Uncertainty documentation in the data products	110
8.5	References.....	111
	Appendix.....	113

		<p>CCI Sea Level Budget Closure</p> <p>ESA/ESRIN contract 4000119910/17/I-NB</p> <p>Reference: ESA_SLBC_cci_D2.4.2</p> <p>Version: v1.2</p> <p>Date: 18.06.2019</p> <p>Page: 8 of 116</p>
---	---	---

Acronyms and Abbreviations


Acronym	Explanation
20CRv2	Twentieth Century Reanalysis (V2) (NOAA)
AIS	Antarctic Ice Sheet
ALES, ALES+	Adaptive Leading Edge Subwaveform retracker
AOD	atmospheric and oceanic de-aliasing
AP	Antarctic Peninsula
ASCII	American Standard Code for Information Interchange
ATBD	Algorithm Theoretical Baseline Document
AVISO	Archiving, Validation and Interpretation of Satellite Oceanographic data
BISICLES	Berkeley Ice Sheet Initiative for Climate Extremes
CCI, cci	Climate Change Initiative (initiated by ESA)
CECR	Comprehensive Error Characterisation Report
CF	Climate and Forecast
CFSR	NCEP Climate Forecast System Reanalysis
CMC	Continental Mass Change
CMEMS	Copernicus Marine Environment Monitoring Service
CPOM	Centre for Polar Observation and Modelling
CRU	Climatic Research Unit (University of East Anglia, Norwich, UK)
CRU CL, CRU TS	CRU Timeseries (grids of observed climate)
CSIRO	Australia's Commonwealth Scientific and Industrial Research Organisation
CSR	Center for Space Research (University of Texas at Austin)
CSV, csv	Comma-separated values
DAC	Dynamic Atmospheric Correction
DTU	Danmarks Tekniske Universitet
DTU18MSS	MSS model by DTU Space
EAIS	East Antarctic Ice Sheet
ECMWF	European Centre for Medium-Range Weather Forecasts
ECV	Essential Climate Variables
ELA	Equilibrium Line Altitude
EN4	version 4 of the Met Office Hadley Centre "EN" series of data sets of global quality controlled ocean temperature and salinity profiles
Envisat	"Environmental Satellite", Earth-observing satellite operated by ESA
EOF	End Of Header
EOS-80	1980 International Equation of State for Seawater
EPSG	European Petroleum Survey Group
EPSG3031	EPSG Projection 3031 - WGS 84 / Antarctic Polar Stereographic
EPSG3413	EPSG Projection 3413 - WGS 84 / NSIDC Sea Ice Polar Stereographic North
ERA	Earth system ReAnalysis
ERS-1/2	European Remote Sensing Satellite -1/2

		<p>CCI Sea Level Budget Closure</p> <p>ESA/ESRIN contract 4000119910/17/I-NB</p> <p>Reference: ESA_SLBC_cci_D2.4.2</p> <p>Version: v1.2</p> <p>Date: 18.06.2019</p> <p>Page: 9 of 116</p>
---	---	---

ESA	European Space Agency
ESM	ESA Earth System Model
ETOPO5	global 5-minute gridded elevations/bathymetry NOAA product
EWH	equivalent water height
FES2014	Finite Element Solution) tide model
GAA, GAB, GAC, GAD	Names of data products related to GRACE atmospheric and oceanic background models (refer to section 3.2.2)
GFO	GRACE Follow-On mission
GFZ	GeoForschungsZentrum Potsdam
GGM	Global Glacier Model
GIA	Glacial Isostatic Adjustment
GIS	Greenland Ice Sheet
GMB	Gravimetric Mass Balance / GRACE Mass Balance
GMSL	Global Mean Sea Level
GMSSLA	Global Mean Steric Sea Level Anomaly (SSLA)
GPCC	Global Precipitation Climatology Centre
GPS / GNSS	Global Positioning System / Global Navigation Satellite System
GRACE	Gravity Recovery and Climate Experiment
GRACE-FO	GRACE-Follow On
GrIS	Greenland Ice Sheet
GSFC	Goddard Space Flight Center
GSSL	Global mean Steric Sea Level
GSSLA	Global Steric Sea Level Anomaly
GT, Gt	Gigatons
HYCOM	Hybrid Coordinate Ocean Model
IB	Inverse Barometer
ICE-4, ICE-5G, ICE-6G_C	models of postglacial relative sea-level history
ICESat	Ice, Cloud, and land Elevation Satellite, part of NASA's Earth Observing System
ITSG	Institute of Geodesy, Theoretical Geodesy and Satellite Geodesy (TU Graz)
JPL	Jet Propulsion Laboratory
JRA-25	Japanese 25-year ReAnalysis
JRA-55	Japanese 55-year ReAnalysis
LARS	Lars Advanced Retracking System
LRM	Low Rate Mode (CryoSat-2)
MERRA-2	Modern-Era Retrospective analysis for Research and Applications, Version 2
MOG2D	Modèle d'Onde de Gravité à 2 Dimensions
MSS	Mean Sea Surface
NASA	National Aeronautics and Space Administration
NERSC	Nansen Environmental and Remote Sensing Center

		<p>CCI Sea Level Budget Closure</p> <p>ESA/ESRIN contract 4000119910/17/I-NB</p> <p>Reference: ESA_SLBC_cci_D2.4.2</p> <p>Version: v1.2</p> <p>Date: 18.06.2019</p> <p>Page: 10 of 116</p>
---	---	--

netCDF	Network Common Data Form (to support the creation, access, and sharing of array-oriented scientific data)
NSE	Nash-Sutcliffe efficiency
OBP	Ocean Bottom Pressure
OMC	Ocean Mass Change
OMCT	Ocean Model for Circulation and Tides
PGR	post-glacial rebound
PP	Pulse Peakiness
PSD	Product Specification Document
PUG	Product User Guide
RADS	Radar Altimetry Database System
RGI	Randolph Glacier Inventory
RL05, RL06	(GRACE) solution Release 05/06
RMS	Root Mean Square
RMSE	Root Mean Square Error
SAR	Synthetic Aperture Radar
SARAL	Satellite with ARGos and ALtiKa, cooperative altimetry technology mission of Indian Space Research Organisation (ISRO) and CNES (Space Agency of France)
SARIn	SAR Interferometric mode (CryoSat-2)
SEC	Surface Elevation Change
SH	spherical harmonic
SLA	sea level anomaly
SLE	Sea Level Equivalent
SLR	Satellite Laser Ranging
SR	Standard Deviation Ratio
SSH, ssh	Sea Surface Height
SSL	Steric Sea Level
SSL4SLBC	Steric Sea Level for Sea Level Budget Closure
SST	Sea Surface Temperature
TOPAZ	(Towards) an Operational Prediction system for the North Atlantic European coastal Zones
TOPEX	TOPOgraphy EXperiment, part of the TOPEX/Poseidon satellite(joint radar altimetry project, NASA and CNES)
TS	Time Series
TUDr	TU Dresden
TWS	Total Water Storage
TWSA	Total Water Storage Anomaly
UK	United Kingdom
UNF	WaterGAP-defined binary data format
UoL	University of Leeds
v0, v1	version 0/1 data set within SLBC_cci project
v2	version 2 data set (final data set) within SLBC_cci project

		<p>CCI Sea Level Budget Closure</p> <p>ESA/ESRIN contract 4000119910/17/I-NB</p> <p>Reference: ESA_SLBC_cci_D2.4.2</p> <p>Version: v1.2</p> <p>Date: 18.06.2019</p> <p>Page: 11 of 116</p>
---	---	--

VM	model of the radial viscoelastic structure of the Earth (used fo ICE-5G)
w.e.	water equivalent
WAIS	West Antarctic Ice Sheet
WATCH	The WATER and global CHange project
WFDEI	Watch Forcing Data based on ERA-Interim reanalysis
wg22d_gl	non-standard version of WaterGAP2.2d global hydrology model, including glaciers
wg22d_std	WaterGAP2.2d standard global hydrology model
WGMS	World Glacier Monitoring Service

		CCI Sea Level Budget Closure ESA/ESRIN contract 4000119910/17/I-NB Reference: ESA_SLBC_cci_D2.4.2 Version: v1.2 Date: 18.06.2019 Page: 12 of 116
---	---	---

1 Introduction

1.1 Purpose and Scope

This document describes the Version 2 (v2) datasets on individual sea level budget components. Starting with the version 0 (v0) data sets at the beginning of the project, these time series have been continuously revised. As a preliminary result, version 1 (v1) “preliminary improved” data series were released in August 2018. Further improvement finally led to the “final improved” v2 data set (Deliverable D2.4.1) described in this document (Deliverable D2.4.2). They will be the basis for the final budget assessment within SLBC_cci.

1.2 Document Structure

Sections 2 to 8 contain the descriptions for the sea level and steric component, the ocean mass component, the glacier contribution, the ice sheet contribution, the land water contribution, and the dedicated datasets for the Arctic area, respectively. Each section has the same subdivision into subsections describing sources of the datasets, algorithms, product specification, uncertainty assessments, and finally the reference list.

University of Reading (UoR) contributes to this project within SSL4SBC_cci. Data provided by UoR are described in the present document in Section 3.

1.3 Data Structure

All data described in this documentation are stored at a project’s data drive at TU Dresden. Access is managed by Kristin Novotny (Kristin.Novotny@tu-dresden.de).

Data files are organized in the following structure:

```

/D2.4_Data_v2_final_2019-02-14_frozen
  /WP213_gmsl_steric_v2
    /Data_LEGOS
      ts_CCI_GMSL_with_errors_1993_2015_no_seasonal_signal_GIA_applied_TopexA_driftcorrected_v2.nc
      0ReadMe.txt
    /Data_UoR
      steric_r604z.nc
  /WP223_ocean_mass_v2
    0Readme.txt
    /CMC_GraceTimeSeries
      CMCts_SLBC_cci_v2.00_CSR_RL06sh_2006.00-2016.00_F100_noc5_GAD-0_GIA-a2013_i5v2.csv
      CMCts_SLBC_cci_v2.00_CSR_RL06sh_2006.00-2016.00_F100_noc5_GAD-0_GIA-caron2018.csv
      CMCts_SLBC_cci_v2.00_CSR_RL06sh_2006.00-2016.00_F100_noc5_GAD-0_GIA-ice6g_vm5a.csv

```



CCI Sea Level Budget Closure

ESA/ESRIN contract 4000119910/17/I-NB

Reference: ESA_SLBC_cci_D2.4.2

Version: v1.2

Date: 18.06.2019

Page: 13 of 116

CMCts_SLBC_cci_v2.00_CSR_RL06sh_2006.00-2016.00_F100_noc5_GAD-0_GIA-no.csv
CMCts_SLBC_cci_v2.00_GFZ_RL06sh_2006.00-2016.00_F100_noc5_GAD-0_GIA-a2013_i5v2.csv
CMCts_SLBC_cci_v2.00_GFZ_RL06sh_2006.00-2016.00_F100_noc5_GAD-0_GIA-caron2018.csv
CMCts_SLBC_cci_v2.00_GFZ_RL06sh_2006.00-2016.00_F100_noc5_GAD-0_GIA-ice6g_vm5a.csv
CMCts_SLBC_cci_v2.00_GFZ_RL06sh_2006.00-2016.00_F100_noc5_GAD-0_GIA-no.csv
CMCts_SLBC_cci_v2.00_ITSG2018_2006.00-2016.00_F100_noc5_GAD-0_GIA-a2013_i5v2.csv
CMCts_SLBC_cci_v2.00_ITSG2018_2006.00-2016.00_F100_noc5_GAD-0_GIA-caron2018.csv
CMCts_SLBC_cci_v2.00_ITSG2018_2006.00-2016.00_F100_noc5_GAD-0_GIA-ice6g_vm5a.csv
CMCts_SLBC_cci_v2.00_ITSG2018_2006.00-2016.00_F100_noc5_GAD-0_GIA-no.csv
CMCts_SLBC_cci_v2.00_JPL_RL06sh_2006.00-2016.00_F100_noc5_GAD-0_GIA-a2013_i5v2.csv
CMCts_SLBC_cci_v2.00_JPL_RL06sh_2006.00-2016.00_F100_noc5_GAD-0_GIA-caron2018.csv
CMCts_SLBC_cci_v2.00_JPL_RL06sh_2006.00-2016.00_F100_noc5_GAD-0_GIA-ice6g_vm5a.csv
CMCts_SLBC_cci_v2.00_JPL_RL06sh_2006.00-2016.00_F100_noc5_GAD-0_GIA-no.csv
v200_doc.png

/ OMC_GraceTimeSeries

OReadme.txt

/ArcticOc

AOMCts_SLBCv2.01_ITSG2018_2003.000-2016.650_ShFil-0_c21-0_GAD1-111_GIA-A2013-Ice5Gv2_R2.csv
AOMCts_SLBCv2.01_ITSG2018_2003.000-2016.650_ShFil-0_c21-0_GAD1-111_GIA-CaronIvins2018_R2.csv
AOMCts_SLBCv2.01_ITSG2018_2003.000-2016.650_ShFil-0_c21-0_GAD1-111_GIA-Ice-6Gv5a_R2

/GlobalOc

OMCts_SLBCv2.01_ITSG2018_2003.000-2016.650_ShFil-0_c21-0_GAD1-111_GIA-A2013-Ice5Gv2_R2.csv
OMCts_SLBCv2.01_ITSG2018_2003.000-2016.650_ShFil-0_c21-0_GAD1-111_GIA-CaronIvins2018_R2.csv
OMCts_SLBCv2.01_ITSG2018_2003.000-2016.650_ShFil-0_c21-0_GAD1-111_GIA-Ice-6Gv5a_R2.csv

/RestGlobalOc

OMC65ts_SLBCv2.01_ITSG2018_2003.000-2016.650_ShFil-0_c21-0_GAD1-111_GIA-A2013-Ice5Gv2_R2.csv
OMC65ts_SLBCv2.01_ITSG2018_2003.000-2016.650_ShFil-0_c21-0_GAD1-111_GIA-CaronIvins2018_R2.csv
OMC65ts_SLBCv2.01_ITSG2018_2003.000-2016.650_ShFil-0_c21-0_GAD1-111_GIA-Ice-6Gv5a_R2.csv

/SupplementaryOmcTimeSeries

/arctic

AOMCts_SLBCv2.01_CSR_RL06sh_2003.000-2016.650_ShFil-0_c21-0_GAD1-111_GIA-A2013-Ice5Gv2_R2.csv
AOMCts_SLBCv2.01_CSR_RL06sh_2003.000-2016.650_ShFil-0_c21-0_GAD1-111_GIA-CaronIvins2018_R2.csv
AOMCts_SLBCv2.01_CSR_RL06sh_2003.000-2016.650_ShFil-0_c21-0_GAD1-111_GIA-Ice-6Gv5a_R2.csv
AOMCts_SLBCv2.01_CSR_RL06sh_2003.000-2016.650_ShFil-0_c21-0_GAD1-111_GIA-no_R2.csv
AOMCts_SLBCv2.01_GFZ_RL06sh_2003.000-2016.650_ShFil-0_c21-0_GAD1-111_GIA-A2013-Ice5Gv2_R2.csv
AOMCts_SLBCv2.01_GFZ_RL06sh_2003.000-2016.650_ShFil-0_c21-0_GAD1-111_GIA-CaronIvins2018_R2.csv
AOMCts_SLBCv2.01_GFZ_RL06sh_2003.000-2016.650_ShFil-0_c21-0_GAD1-111_GIA-Ice-6Gv5a_R2.csv
AOMCts_SLBCv2.01_GFZ_RL06sh_2003.000-2016.650_ShFil-0_c21-0_GAD1-111_GIA-no_R2.csv
AOMCts_SLBCv2.01_GSFCm_2003.000-2016.650.csv
AOMCts_SLBCv2.01_ITSG2018_2003.000-2016.650_ShFil-0_c21-0_GAD1-111_GIA-no_R2.csv
AOMCts_SLBCv2.01_JPL_RL06sh_2003.000-2016.650_ShFil-0_c21-0_GAD1-111_GIA-A2013-Ice5Gv2_R2.csv
AOMCts_SLBCv2.01_JPL_RL06sh_2003.000-2016.650_ShFil-0_c21-0_GAD1-111_GIA-CaronIvins2018_R2.csv
AOMCts_SLBCv2.01_JPL_RL06sh_2003.000-2016.650_ShFil-0_c21-0_GAD1-111_GIA-Ice-6Gv5a_R2.csv



CCI Sea Level Budget Closure

ESA/ESRIN contract 4000119910/17/I-NB

Reference: ESA_SLBC_cci_D2.4.2

Version: v1.2

Date: 18.06.2019

Page: 14 of 116

AOMCts_SLBCv2.01_JPL_RL06sh_2003.000-2016.650_ShFil-0_c21-0_GAD1-111_GIA-no_R2.csv

/global

CHAMBERS_ocean_mass_orig.txt

OMCts_SLBCv2.01_CSR_RL06sh_2003.000-2016.650_ShFil-0_c21-0_GAD1-111_GIA-A2013-Ice5Gv2_R2.csv

OMCts_SLBCv2.01_CSR_RL06sh_2003.000-2016.650_ShFil-0_c21-0_GAD1-111_GIA-CaronIvins2018_R2.csv

OMCts_SLBCv2.01_CSR_RL06sh_2003.000-2016.650_ShFil-0_c21-0_GAD1-111_GIA-Ice-6Gv5a_R2.csv

OMCts_SLBCv2.01_CSR_RL06sh_2003.000-2016.650_ShFil-0_c21-0_GAD1-111_GIA-no_R2.csv

OMCts_SLBCv2.01_GFZ_RL06sh_2003.000-2016.650_ShFil-0_c21-0_GAD1-111_GIA-A2013-Ice5Gv2_R2.csv

OMCts_SLBCv2.01_GFZ_RL06sh_2003.000-2016.650_ShFil-0_c21-0_GAD1-111_GIA-CaronIvins2018_R2.csv

OMCts_SLBCv2.01_GFZ_RL06sh_2003.000-2016.650_ShFil-0_c21-0_GAD1-111_GIA-Ice-6Gv5a_R2.csv

OMCts_SLBCv2.01_GFZ_RL06sh_2003.000-2016.650_ShFil-0_c21-0_GAD1-111_GIA-no_R2.csv

OMCts_SLBCv2.01_GSFCm_2003.000-2016.650.csv

OMCts_SLBCv2.01_ITSG2018_2003.000-2016.650_ShFil-0_c21-0_GAD1-111_GIA-no_R2.csv

OMCts_SLBCv2.01_JPL_RL06sh_2003.000-2016.650_ShFil-0_c21-0_GAD1-111_GIA-A2013-Ice5Gv2_R2.csv

OMCts_SLBCv2.01_JPL_RL06sh_2003.000-2016.650_ShFil-0_c21-0_GAD1-111_GIA-CaronIvins2018_R2.csv

OMCts_SLBCv2.01_JPL_RL06sh_2003.000-2016.650_ShFil-0_c21-0_GAD1-111_GIA-Ice-6Gv5a_R2.csv

OMCts_SLBCv2.01_JPL_RL06sh_2003.000-2016.650_ShFil-0_c21-0_GAD1-111_GIA-no_R2.csv

/restglobal

OMC65ts_SLBCv2.01_CSR_RL06sh_2003.000-2016.650_ShFil-0_c21-0_GAD1-111_GIA-A2013-Ice5Gv2_R2.csv

OMC65ts_SLBCv2.01_CSR_RL06sh_2003.000-2016.650_ShFil-0_c21-0_GAD1-111_GIA-CaronIvins2018_R2.csv

OMC65ts_SLBCv2.01_CSR_RL06sh_2003.000-2016.650_ShFil-0_c21-0_GAD1-111_GIA-Ice-6Gv5a_R2.csv

OMC65ts_SLBCv2.01_CSR_RL06sh_2003.000-2016.650_ShFil-0_c21-0_GAD1-111_GIA-no_R2.csv

OMC65ts_SLBCv2.01_GFZ_RL06sh_2003.000-2016.650_ShFil-0_c21-0_GAD1-111_GIA-A2013-Ice5Gv2_R2.csv

OMC65ts_SLBCv2.01_GFZ_RL06sh_2003.000-2016.650_ShFil-0_c21-0_GAD1-111_GIA-CaronIvins2018_R2.csv

OMC65ts_SLBCv2.01_GFZ_RL06sh_2003.000-2016.650_ShFil-0_c21-0_GAD1-111_GIA-Ice-6Gv5a_R2.csv

OMC65ts_SLBCv2.01_GFZ_RL06sh_2003.000-2016.650_ShFil-0_c21-0_GAD1-111_GIA-no_R2.csv

OMC65ts_SLBCv2.01_GSFCm_2003.000-2016.650.csv

OMC65ts_SLBCv2.01_ITSG2018_2003.000-2016.650_ShFil-0_c21-0_GAD1-111_GIA-no_R2.csv

OMC65ts_SLBCv2.01_JPL_RL06sh_2003.000-2016.650_ShFil-0_c21-0_GAD1-111_GIA-A2013-Ice5Gv2_R2.csv

OMC65ts_SLBCv2.01_JPL_RL06sh_2003.000-2016.650_ShFil-0_c21-0_GAD1-111_GIA-CaronIvins2018_R2.csv

OMC65ts_SLBCv2.01_JPL_RL06sh_2003.000-2016.650_ShFil-0_c21-0_GAD1-111_GIA-Ice-6Gv5a_R2.csv

OMC65ts_SLBCv2.01_JPL_RL06sh_2003.000-2016.650_ShFil-0_c21-0_GAD1-111_GIA-no_R2.csv

/ OMC_GriddedOMC

EWH_OMC-Grid_GSFCm_SLBC-v2.01_1x1.nc

EWH_OMC-Grid_ITSG2018_SLBC-v2.01_1x1_buf300_A2013Ice5Gv2.nc

EWH_OMC-Grid_ITSG2018_SLBC-v2.01_1x1_buf300_Caron2018.nc

EWH_OMC-Grid_ITSG2018_SLBC-v2.01_1x1_buf300_Ice6Gv5a.nc

		<p>CCI Sea Level Budget Closure</p> <p>ESA/ESRIN contract 4000119910/17/I-NB</p> <p>Reference: ESA_SLBC_cci_D2.4.2</p> <p>Version: v1.2</p> <p>Date: 18.06.2019</p> <p>Page: 15 of 116</p>
---	---	--

EWH_OMC-Grid_ITSG2018_SLBC-v2.01_1x1_filt_buf300_A2013Ice5Gv2.nc
 EWH_OMC-Grid_ITSG2018_SLBC-v2.01_1x1_filt_buf300_Caron2018.nc
 EWH_OMC-Grid_ITSG2018_SLBC-v2.01_1x1_filt_buf300_Ice6Gv5a.nc
 info.txt

/WP233_glaciers_v2

glaciers_rgi_v6_annually.nc
 glaciers_rgi_v6_annually_greenland_periphery.nc
 glaciers_rgi_v6_monthly.nc
 glaciers_rgi_v6_monthly_greenland_periphery.nc

/WP243_icesheets_v2

/AIS_Altim

annual_mean_v1_EAIS.csv
 annual_mean_v1_WAIS.csv
 AIS_timeseries_and_uncertainty_varying_err_dens.csv
 APIS_timeseries_and_uncertainty_varying_err_dens.csv
 EAIS_timeseries_and_uncertainty_varying_err_dens.csv
 WAIS_timeseries_and_uncertainty_varying_err_dens.csv
 slbc_apis_1yr_epoch.csv
 slbc_eais_1yr_epoch.csv
 slbc_wais_1yr_epoch.csv
 slbc_error_apis_140dr_epoch_noncumul.csv
 slbc_error_eais_140dyr_epoch_noncumul.csv
 slbc_error_wais_140dyr_epoch_noncumul.csv
 slbc_error_apis_1yr_epoch_noncumul.csv
 slbc_error_eais_1yr_epoch_noncumul.csv
 slbc_error_wais_1yr_epoch_noncumul.csv

/AIS_GMB

AIS_GMB_basin.dat
 AIS_GMB_trend.dat
 AIS_GMB_grid.nc

/GIS_Altim

SLBC_GrIS_RA_MB_vers2.1.nc

/GIS_GMB

CCI_GMB_RL06_time_series_NO_GIA.zip
 (contains GISNN_grace.dat, NN = 00 ... 08)
 GIS00_grace.png
 README.txt

/WP253_landwater_v2

/globally_averaged_twsa

twsa_WaterGAP22d_std_wfdeigpcc_mm_irr70_version2_month1992_2016.txt
 twsa_WaterGAP22d_std_wfdeigpcc_mm_irr70_version2_year1992_2016.txt
 twsa_WaterGAP22d_std_wfdeigpcc_mm_irr70_version2_yearinmonth1992_2016.txt
 twsa_WaterGAP22d_std_wfdeigpcc_mm_irr100_version2_month1992_2016.txt
 twsa_WaterGAP22d_std_wfdeigpcc_mm_irr100_version2_year1992_2016.txt
 twsa_WaterGAP22d_std_wfdeigpcc_mm_irr100_version2_yearinmonth1992_2016.txt
 twsa_WaterGAP22d_gl_wfdeigpcc_mm_irr70_version2_month1992_2016.txt
 twsa_WaterGAP22d_gl_wfdeigpcc_mm_irr70_version2_year1992_2016.txt



CCI Sea Level Budget Closure

ESA/ESRIN contract 4000119910/17/I-NB

Reference: ESA_SLBC_cci_D2.4.2

Version: v1.2

Date: 18.06.2019

Page: 16 of 116

twsa_WaterGAP22d_gl_wfdeigpcc_mm_irr70_version2_yearinmonth1992_2016.txt
twsa_WaterGAP22d_gl_wfdeigpcc_mm_irr100_version2_month1992_2016.txt
twsa_WaterGAP22d_gl_wfdeigpcc_mm_irr100_version2_year1992_2016.txt
twsa_WaterGAP22d_gl_wfdeigpcc_mm_irr100_version2_yearinmonth1992_2016.txt
twsa_WaterGAP22d_std_wfdeicru_mm_irr70_version2_month1992_2016.txt
twsa_WaterGAP22d_std_wfdeicru_mm_irr70_version2_year1992_2016.txt
twsa_WaterGAP22d_std_wfdeicru_mm_irr70_version2_yearinmonth1992_2016.txt
twsa_WaterGAP22d_std_wfdeicru_mm_irr100_version2_month1992_2016.txt
twsa_WaterGAP22d_std_wfdeicru_mm_irr100_version2_year1992_2016.txt
twsa_WaterGAP22d_std_wfdeicru_mm_irr100_version2_yearinmonth1992_2016.txt
twsa_WaterGAP22d_gl_wfdeicru_mm_irr70_version2_month1992_2016.txt
twsa_WaterGAP22d_gl_wfdeicru_mm_irr70_version2_year1992_2016.txt
twsa_WaterGAP22d_gl_wfdeicru_mm_irr70_version2_yearinmonth1992_2016.txt
twsa_WaterGAP22d_gl_wfdeicru_mm_irr100_version2_month1992_2016.txt
twsa_WaterGAP22d_gl_wfdeicru_mm_irr100_version2_year1992_2016.txt
twsa_WaterGAP22d_gl_wfdeicru_mm_irr100_version2_yearinmonth1992_2016.txt

/gridded

/additional_data

contarea_wghm_wlm.nc

/twsa

twsa_WaterGAP22d_std_WFDEI_GPCC_mm_irr70_version2.nc
twsa_WaterGAP22d_std_WFDEI_GPCC_mm_irr100_version2.nc
twsa_WaterGAP22d_gl_WFDEI_GPCC_mm_irr70_version2.nc
twsa_WaterGAP22d_gl_WFDEI_GPCC_mm_irr100_version2.nc
twsa_WaterGAP22d_std_WFDEI_CRU_mm_irr70_version2.nc
twsa_WaterGAP22d_std_WFDEI_CRU_mm_irr100_version2.nc
twsa_WaterGAP22d_gl_WFDEI_CRU_mm_irr70_version2.nc
twsa_WaterGAP22d_gl_WFDEI_CRU_mm_irr100_version2.nc

README.txt

/WP263_ArcticOcean_v2

/data_DTU

arctic_sla_dac_v2.nc
arctic_sla_nodac_v2.nc

/data_NERSC

TopazSSH20032017.nc
TopazStericht20032017.nc

ESA_SLBC_cci_D2.4.2_v1.0.pdf

		<p>CCI Sea Level Budget Closure</p> <p>ESA/ESRIN contract 4000119910/17/I-NB</p> <p>Reference: ESA_SLBC_cci_D2.4.2</p> <p>Version: v1.2</p> <p>Date: 18.06.2019</p> <p>Page: 17 of 116</p>
---	---	--

2 Total Sea Level Change

The time series of Global Mean Sea Level (GMSL) change are derived from satellite altimetry observations. The following section describes this product.

2.1 Data access and requirements

The final v2 altimetry based GMSL data file consists of GMSL time series from the ESA CCI project that has been corrected for TOPEX A instrumental drift over 1993 – February 1999 based on Ablain et al. (2017a). The novelty of the v2 data when compared to the previous versions is the availability of a dedicated monthly time step uncertainty estimation.

The time series is available as a netcdf file with the name:

```
ts_CCI_GMSL_with_errors_1993_2015_no_seasonal_signal_GIA_applied_TopexA_driftcorrected_v2.nc
```

The CCI GMSL time series is available at webpage <http://www.esa-sealevel-cci.org/>, access to the data directory (password) can be obtained by e-mail as stated on the web page. The original GMSL error covariance matrix that has been used to extract the monthly time step error estimate for CCI GMSL is available online at <https://doi.org/10.17882/58344>.

2.2 Algorithms

2.2.1 Review of scientific background

The CCI GMSL time series uses version 2.0 of the European Space Agency/ESA Climate Change Initiative/CCI ‘Sea Level’ project and combines data from the TOPEX/Poseidon, Jason-1/2, GFO, ERS-1/2, Envisat, CryoSat-2 and SARAL/Altika missions and is based on a new processing system with dedicated algorithms and adapted data processing strategies (Ablain et al., 2015, 2017b; Quartly et al., 2017; Legeais et al., 2018). It is available as a global gridded 1°x1° resolution data over 82°N and 82°S latitudinal range. The CCI sea level product has been validated using different approaches including a comparison with tide gauge records as well as to ocean re-analyses and climate model outputs.

2.2.2 Algorithms

The CCI gridded sea level data has been averaged over 65°N and 65°S latitudinal range to obtain the SLBC_cci version 2 GMSL time series. Furthermore, TOPEX A instrumental drift due to aging of the TOPEX A altimeter placed in the TOPEX/Poseidon mission from January 1993 to early 1999 has also been corrected from the CCI GMSL time series based on Ablain et al. (2017a). The TOPEX A drift value based on this methodology corresponds to

		CCI Sea Level Budget Closure ESA/ESRIN contract 4000119910/17/I-NB
		Reference: ESA_SLBC_cci_D2.4.2 Version: v1.2 Date: 18.06.2019 Page: 18 of 116

(1.0 +/- 1.0) mm/yr over January 1993 to July 1995 and (3 +/- 1.0) mm/yr over August 1995 to February 1999. The Glacial Isostatic Adjustment (GIA) correction of -0.3 mm/yr (Peltier, 2004) has been applied to the CCI GMSL time series. Annual and semi-annual signals were removed from the time series through a least square fit of 12 month and 6 month period sinusoids. A 60 day smoothing has also been applied on the GMSL time series.

Figure 2.1 displays the evolution of CCI based GMSL averaged over 65°N and 65°S latitudes after TOPEX A drift correction over Jan. 1993–Feb. 1999. The uncertainty envelope based on Ablain et al. (in review) is in red whereas the blue envelope denotes the root mean square dispersion of all available GMSL time series from the ensemble mean (see Section 2.4 for explanation).

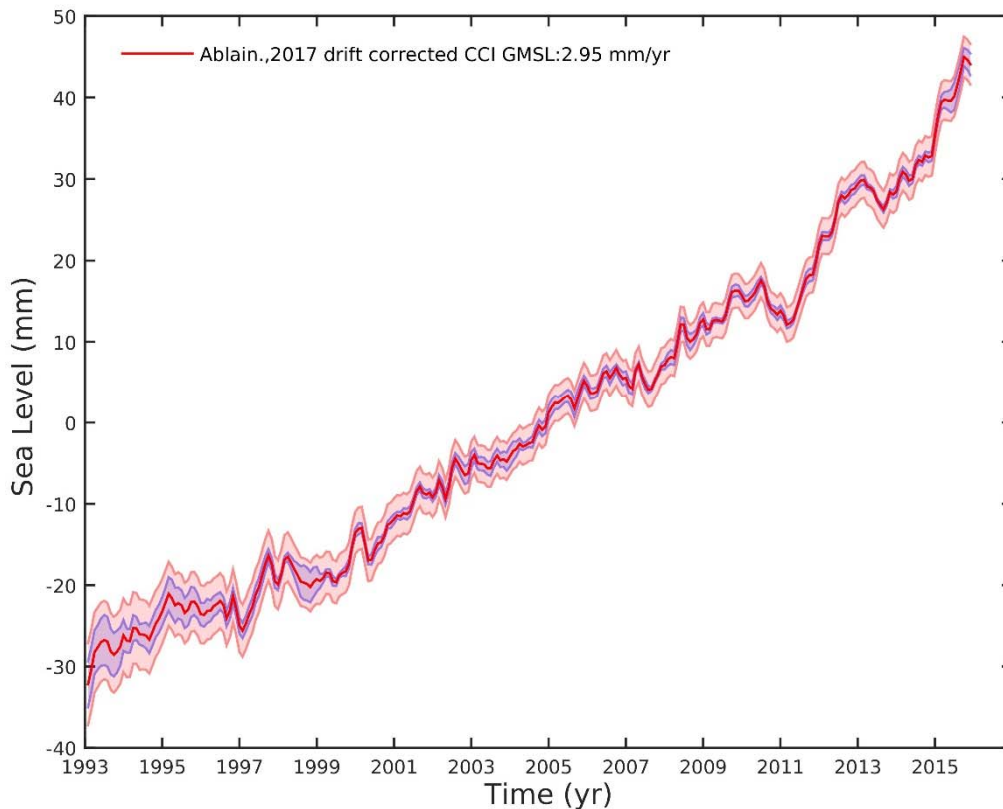


Figure 2.1: CCI based GMSL averaged over 65°N and 65°S latitudes, TOPEX A drift correction over Jan. 1993–Feb. 1999 applied

		CCI Sea Level Budget Closure
		ESA/ESRIN contract 4000119910/17/I-NB Reference: ESA_SLBC_cci_D2.4.2 Version: v1.2 Date: 18.06.2019 Page: 19 of 116

2.3 Product Specification

2.3.1 Product geophysical data content

Global mean sea level data in file

ts_CCI_GMSL_with_errors_1993_2015_no_seasonal_signal_GIA_applied_TopexA_driftcorrected_v2.nc

Geophysical Variable	Name in product	Unit
Time	Time	Decimal year
Global mean sea level anomaly	ts_GMSL	mm
Uncertainty	Uncertainty	mm

2.3.2 Coverage and resolution in time and space

The CCI GMSL time series has been averaged over 65°N and 65°S latitudes and is at monthly time resolution covering January 1993 to December 2015.

2.3.3 Product data format

The GMSL time series has been stored as a single netCDF4 file. The variables are one-dimensional array with dimension corresponding to time steps.

2.4 Uncertainty Assessment

2.4.1 Sources of error

Over the recent years, several articles (Ablain et al., 2015, 2017b; Dieng et al, 2017; Quartly et al., 2017; Legeais et al., 2018) have discussed sources of errors in GMSL trend estimation. Ablain et al. (in review) extends this work by considering new altimeter missions (Jason-2, Jason-3) and recent findings on altimetry error estimates. Three major types of errors are considered in the uncertainty estimation of altimetric GMSL: (a) biases in GMSL between successive altimetry missions characterized by bias uncertainties at any given time; (b) drifts in GMSL due to onboard instrumental drifts or long-terms drifts such as GIA, orbit etc. characterized by trend uncertainty, and (c) other measurement errors such as due to geophysical corrections (wet tropospheric, orbital, etc.) which exhibit time-correlation and are characterized by their standard deviation. These different terms of the GMSL error are combined to build the error variance-covariance matrix.

		<p>CCI Sea Level Budget Closure</p> <p>ESA/ESRIN contract 4000119910/17/I-NB</p> <p>Reference: ESA_SLBC_cci_D2.4.2</p> <p>Version: v1.2</p> <p>Date: 18.06.2019</p> <p>Page: 20 of 116</p>
---	---	--

2.4.2 Methodology for uncertainty assessment

The uncertainty data for GMSL time series provided here for SLBC version 2 are obtained from Ablain et al. (in review). This manuscript provides a very detailed explanation for the methodology adapted for the GMSL uncertainty assessment. Below we give a brief explanation on the uncertainty assessment.

The three main categories of GMSL error mentioned in Section 2.4.1 are combined to build the total error variance-covariance matrix (Σ). All the error sources are assumed to be independent from each other. The individual variance-covariance matrix of each of the error sources discussed in Section 2.4.1 is calculated from a large number of random draws (>1000) of simulated error using fed with a standard normal distribution. Thus, the total error variance-covariance matrix (Σ) is the sum of the individual variance-covariance matrix of each error source in the error budget. The dominating error terms are in the diagonal of the total matrix. The GMSL uncertainty envelope is estimated from the square root of the diagonal terms of the total matrix. The different terms of the altimeter GMSL error are based on the current knowledge of altimetry measurement errors. As the altimetry record increases in length with new altimeter missions, the knowledge of the altimetry measurement also increases, and the description of the errors improves. This implies that the error variance-covariance matrix is expected to improve and change in the future (Ablain et al., in review).

With the v1 data set we provided an uncertainty estimate at each time step for the ensemble mean of the three GMSL time series based on the root mean square (RMS) of the dispersion of each of the three GMSL time series from the ensemble mean. This calculation based on Dieng et al. (2017) provides (at least partially) the random error when no other uncertainty estimate is available over each time step.

2.4.3 Results of uncertainty assessment

In Figure 2.1, the uncertainty envelope based on Ablain et al. (in review) is represented as a red shaded envelope. We can observe that the GMSL time series shows a larger uncertainty during the TOPEX/Poseidon period (5 mm to 8 mm) than during the Jason period (close to 4 mm) mainly due to the TOPEX A instrumental drift issue. The blue shaded uncertainty envelope is the uncertainty estimate based on the root mean square of the dispersion of each of the available GMSL time series from different processing groups such as NASA, AVISO, University of Colorado, CSIRO from the ensemble mean. This uncertainty envelope based on the dispersion from their ensemble mean is due to the use of different processing technique, different versions of auxiliary data and different interpolation methods applied by the different groups (Henry et al., 2014; Masters et al., 2012). We can observe that this blue envelop is smaller than the real uncertainty envelope (in red) in GMSL because all groups use similar

		<p>CCI Sea Level Budget Closure</p> <p>ESA/ESRIN contract 4000119910/17/I-NB</p> <p>Reference: ESA_SLBC_cci_D2.4.2</p> <p>Version: v1.2</p> <p>Date: 18.06.2019</p> <p>Page: 21 of 116</p>
---	---	--

methods and corrections to process the raw data and thus several sources of systematic uncertainty is not accounted for in the spread.

In terms of trend uncertainty, Ablain et al. (in review) estimates the GMSL trend uncertainty to be ± 0.4 mm/yr (90% confidence level, after correcting the TOPEX A drift) which means that at 1 sigma the uncertainty is ± 0.24 mm/yr.

2.4.4 Uncertainty documentation in the data products

Refer to data format and file content in Section 2.3.1. Monthly time step GMSL uncertainty estimate based on Ablain et al. (in review) is provided in the netcdf file.

2.5 References

- Ablain, M., et al. (2015): Improved sea level record over the satellite altimetry era (1993–2010) from the climate change Initiative project, *Ocean Sci.*, 11, 67–82, doi:10.5194/os-11-67-2015.
- Ablain M., R. Jugier, L. Zawadzki, and N. Taburet (2017a): The TOPEX-A Drift and Impacts on GMSL Time Series. *AVISO Website*. October 2017. https://meetings.aviso.altimetry.fr/fileadmin/user_upload/tx_ausyclsseminar/files/Poster_OSTST17_GMSL_Drift_TOPEX-A.pdf.
- Ablain, M., J. F. Legeais, P. Prandi, M. Marcos, L. Fenoglio-Marc, H. B. Dieng, J. Benveniste, and A. Cazenave (2017b): Altimetry-based sea level at global and regional scales, *Surv. Geophys.*, 38, 7–31, doi:10.1007/s10712-016-9389-8.
- Ablain M, Meyssignac B, Zawadzki L, Jugier R, Ribes A, Cazenave A, Picot N (*in review*): Uncertainty in Satellite estimate of Global Mean Sea Level changes, trend and acceleration, *Earth Syst. Sci. Data Discuss.*, <https://doi.org/10.5194/essd-2019-10>
- Dieng, H.B, A. Cazenave, B. Meyssignac, and M. Ablain (2017): New estimate of the current rate of sea level rise from a sea level budget approach, *Geophysical Research Letters*, 44, doi:10.1002/2017GL073308.
- Henry O, Ablain M, Meyssignac B, Cazenave A, Masters D, Nerem S, Leuliette E, and Garric G (2014): Investigating and reducing differences between the satellite altimetry-based global mean sea level time series provided by different processing groups. *J Geod* 88:351–361. doi: 10.1007/s00190-013-0687-3.
- Legeais J.F., Ablain M., Zawadzki L., Zuo H., Johannessen J.A., Scharffenberg M.G., Fenoglio-Marc L., Fernandes J., Andersen O.B., Rudenko S., Cipollini P., Quartly G.D., Passaro M., Cazenave A., and Benveniste J. (2018): An improved and homogeneous altimeter sea level record from the ESA Climate Change Initiative, *Earth Syst. Sci. Data*, 10, 281–301, doi: 10.5194/essd-10-281-2018.
- Masters D, Nerem RS, Choe C, Leuliette E, Beckley B, White N, and Ablain M (2012): Comparison of global mean sea level time series from TOPEX/Poseidon, Jason-1, and Jason-2. *Mar Geod* 35:20–41, doi: 10.1080/01490419.2012.717862.
- Peltier W.R. (2004): Global glacial isostasy and the surface of the ice-age Earth: the ICE-5G (VM2) model and GRACE, *Annual Review of Earth and Planetary Sciences* 32:111, doi: 10.1146/annurev.earth.32.082503.144359.
- Quartly G.D., Legeais J.F., Ablain M., Zawadzki L., Fernandes J., Rudenko S., Carrère L., García P.N., Cipollini P., Andersen O.B., Poisson J.C., Sabrina Mbajon Njiche S.M., Cazenave A., and Benveniste J. (2017): A new phase in the production of quality-controlled sea level data, *Earth Syst. Sci. Data*, 9, 557–572, doi: 10.5194/essd-9-557-2017.

		<p>CCI Sea Level Budget Closure</p> <p>ESA/ESRIN contract 4000119910/17/I-NB</p> <p>Reference: ESA_SLBC_cci_D2.4.2</p> <p>Version: v1.2</p> <p>Date: 18.06.2019</p> <p>Page: 22 of 116</p>
---	---	--

3 Steric Sea Level Change

The following content is a copy of the SSL4SLBC_cci Product Description Document 1 that was submitted to ESA by Ch. Merchant, University of Reading on 17 Dec. 2018 and is slightly updated here.

3.1 Data Access and Requirements

Product: The v2.0 product for steric sea level is available from the ESA SST CCI public pages, at http://gws-access.ceda.ac.uk/public/esacci-sst/slbc_cci/ as well as via the SLBC_cci project.

Input datasets and external code libraries:



- Argo profiles collected and quality controlled by the UK Met Office and released as dataset EN.4.2.1, available from <https://www.metoffice.gov.uk/hadobs/en4/download-en4-2-1.html>
- The UK Met Office EN.4.2.1 climatology, available from the same location
- Bathymetry from ETOPO 5, <https://www.ngdc.noaa.gov/mgg/global/etopo5.HTML>
- Equation of state for seawater, EOS-80, implemented in the libraries seawater 3.3.4, <https://libraries.io/pypi/seawater>
- Standard depths for profile calculations as defined by von Schuckmann and Le Traon (2011)
- ESA SST CCI data: L4 Analysis SSTs, <http://gws-access.ceda.ac.uk/public/esacci-sst/>, averaged to 1 degree and 1 month resolution.

3.2 Algorithm theoretical basis

3.2.1 Scientific background

Global total sea level derived from satellite altimetry can be partitioned into its steric and mass-related components (e.g. Cazenave et al., 2009; Leuliette and Miller, 2009). Steric sea level can be further separated into volume changes through ocean salinity (halosteric) and ocean temperature (thermosteric) effects, from which the latter is known to play a dominant role in observed contemporary rise of GSSL.

Several GSSL variations from Argo and other in situ observations have been derived over the past couple of years (e.g. Willis et al., 2008; Cazenave et al., 2009; Leuliette and Miller, 2009; von Schuckmann et al., 2009).

		<p>CCI Sea Level Budget Closure</p> <p>ESA/ESRIN contract 4000119910/17/I-NB</p> <p>Reference: ESA_SLBC_cci_D2.4.2</p> <p>Version: v1.2</p> <p>Date: 18.06.2019</p> <p>Page: 23 of 116</p>
---	---	--

There are substantial differences in these global statistical analyses, which have been related to instrumental biases, quality control and processing issues, role of salinity and influence of the reference depth for SSL calculation.

A given heat uptake can produce different steric height changes depending on the initial conditions. Density of sea water is a function of temperature and salinity at any given pressure, and is described through the Thermodynamic Equation of Seawater.

3.2.2 Algorithm theoretical basis

3.2.2.1 Overview of method

The basic approach is to estimate steric sea level anomaly (SSLA) fields and a grid, and average across the ocean to determine the global mean steric sea level anomaly (GMSSLA) that contributes to global mean sea level rise.

For this approach we use grid cells at $5^\circ \times 5^\circ$, monthly resolution, a grid defined collectively within the SLBC_cci project, and compatible with the resolution of gravity-base mass change estimates. Our calculation method is updated from that of von Schuckmann and Le Traon (2011), and adopts the common vertical grid used therein for profile calculations, but here the horizontal resolution is refined. This vertical grid extends to 2000 m depth, and the SSLAs are therefore effectively assuming no steric contribution from depths below 2000 m.

Cells that are partially comprised by ocean are included in proportion to their ocean area at the sea surface. Where bathymetry within the cell is <2000 m, the steric thickness anomaly is estimated for a given profile to a depth no deeper than the sea floor using the mean bathymetry at a spatial resolution of $1^\circ \times 1^\circ$. In this way, shelf seas are included, although Argo profiles are generally absent for such areas.

3.2.2.2 Core calculation: steric thickness

The “steric height” is the (small) deviation in the height of a unit-area-based column of a given mass of sea-water in comparison to the height the same mass would have if at a reference temperature and salinity.

Consider a layer, l , containing a certain mass per unit area, M . By definition of density, ρ :

$$\rho_l = \frac{M}{\Delta z_l} \quad \text{Eq. 1}$$

where Δz_l is the thickness of the layer. Designating $h_l = \Delta z_l - \Delta z_{l0}$ as the “steric thickness” of the layer *relative to a layer of reference density*, ρ_0 , we have

$$h_l = M \left(\frac{1}{\rho_l} - \frac{1}{\rho_0} \right) = \left(\frac{1}{\rho_l} - \frac{1}{\rho_0} \right) \rho_0 \Delta z_{l0} \quad \text{Eq. 2}$$

		<p>CCI Sea Level Budget Closure</p> <p>ESA/ESRIN contract 4000119910/17/I-NB</p> <p>Reference: ESA_SLBC_cci_D2.4.2</p> <p>Version: v1.2</p> <p>Date: 18.06.2019</p> <p>Page: 24 of 116</p>
---	---	--

The reference density has to be chosen. Here, we use a reference density of 1000 kg m^{-3} .

The steric thickness anomaly for the layer is $h'_l = h_l - h_{l,c}$, where c stands for “climatological”, which means in turn that

$$h'_l = \left(\frac{1}{\rho_l} - \frac{1}{\rho_{l,c}} \right) \rho_0 \Delta z_{l0} \quad \text{Eq. 3}$$

This equation is the essence of the calculation. SSLA is found by adding the evaluation of this equation for all the layers of the ocean down to a reference depth below which steric effects are not evaluated. Here, that reference depth is 2 km, determined by the depth sampling of Argo profilers.

Evaluating Eq. 3 essentially involves manipulating observational data to provide at the target monthly $5^\circ \times 5^\circ$ the following information:

- the climatological values of temperature, salinity and pressure, enabling evaluation of $\rho_{l,c}$
- the monthly mean values of temperature, T_l , and salinity, S_l , (pressure is always calculated climatologically), enabling evaluation of ρ_l

and combining this with the reference density and standard layer thickness. The SSLA is simply:

$$h' = \sum_l h'_l \quad \text{Eq. 4}$$



The practical implementation of Eq. 4 must address the following complications:

- sparsity of data and the linked issue of sensitivity to gross errors when data are sparse: these issues require some degree of infilling with and stabilisation of estimates by climatological information
- the key requirement that uncertainty in SSLA also be well estimated, which requires estimation of error covariances of inputs and propagation to the result

3.2.2.3 Estimating steric thickness, accounting for uncertainty, in one layer

The standard layer mid-points (“levels”) used here (carried across from von Schuckmann et al., 2009) are $\{1.5, 4.0, 7.5, 12.5, \dots, 97.5, 105, 115, 125, \dots, 795, 810, 830, 850, \dots, 1970, 1990\}$ metres. The levels are therefore $\{0., 2.75, 5.75, 10, 15, \dots, 1980, 2000\}$ m. There are 151 layers or levels, bounded by 152 bounds.

The Argo profile observations are typically not on the standard levels, and so are first transformed to standard layers by interpolation of temperature and salinity anomaly (anomaly

		<p>CCI Sea Level Budget Closure</p> <p>ESA/ESRIN contract 4000119910/17/I-NB</p> <p>Reference: ESA_SLBC_cci_D2.4.2</p> <p>Version: v1.2</p> <p>Date: 18.06.2019</p> <p>Page: 25 of 116</p>
---	---	--

means the deviation from the norm for the location and month of year.) For each of temperature and salinity this involves:

- interpolate the EN 4.2.1 climatology profile to the observed depths in the Argo profile
- subtract the interpolated climatological profiles to create the observed anomaly on the observed depths
- interpolate the observed anomaly to standard layer mid-point, creating the temperature or salinity anomaly for the layer

The anomaly values are then turned into steric thickness anomaly by applying Eq. 3. Let the set of n_l steric thickness anomaly estimates from different profiles for the cell-month, plus the climatological estimate, be $\mathbf{x}_l = [h'_{l,1}, h'_{l,2}, \dots, h'_{l,n_l}, h'_{l,c}]^T$.

The monthly mean steric thickness anomaly is found as the optimum combination of the steric thickness calculations from all the valid profiles in the grid cell for the month given by the follow collection of equations:

$$\begin{aligned}
 \mathbf{h}'_l &= \mathbf{w}_l^T \mathbf{x}_l & \text{Eq. 5} \\
 \mathbf{w}_l &= \frac{1}{\Sigma_l} \mathbf{S}_{x_l}^{-1} \mathbf{i} \\
 \Sigma_l &= \mathbf{i}^T \mathbf{S}_{x_l}^{-1} \mathbf{i}
 \end{aligned}$$

where \mathbf{i} is a column vector of ones, and \mathbf{S}_{x_l} is the error covariance matrix of the steric thickness anomaly estimates.

The error covariance matrix, \mathbf{S}_{x_l} , is needed for the optimal calculation of the monthly average in Eq. 5, as well as for the uncertainty estimates discussed below. To estimate this matrix, we need to be clear about what “error” means here: it is the difference between the steric thickness anomaly for the layer from a single profile (Argo, or climatological) and the (unknown) true cell-month mean. This difference has two components: the measurement error in the profile, and the difference arising from variability within the cell-month (“intra-cell variability”).

The uncertainty in the steric thickness anomaly from measurement errors is estimated using the uncertainty information in Table 3.1. Only the final column is relevant to the Argo-only results discussed here.


		CCI Sea Level Budget Closure ESA/ESRIN contract 4000119910/17/I-NB Reference: ESA_SLBC_cci_D2.4.2 Version: v1.2 Date: 18.06.2019 Page: 26 of 116

Table 3.1: Measurement uncertainties assumed for different profile sources.

Variable	XBT	XCTD	ARGO
T	± 0.2 °C	± 0.03 °C	± 0.002 °C
S	Climatological variability	± 0.03	± 0.01

To transform these measurement uncertainties into steric thickness anomaly uncertainty, the equation used is:

$$u(h'_l) = \left(\frac{1}{\rho(S_l, T_l, p_l)} - \frac{1}{\rho(S_l + u(S_l), T_l - u(T_l), p_l)} \right) \rho_0 \Delta z_{l0} \quad \text{Eq. 6}$$

which is a conservative (worst-case) combination of the effect of error in temperature and salinity.

Measurement uncertainties are taken to be independent between profiles, so that the measurement error covariance matrix, S_{x_m} , is diagonal. A better assumption may be that measurement errors are independent between platforms, and perfectly correlated for profiles from the same platform within the month, and the impact of changing to this assumption should be addressed in future improvements to the product.

The uncertainty in the steric thickness anomaly from intra-cell variability (known as representativity uncertainty) has to be estimated. Here, we model the intra-cell variability as equal to the inter-annual variability of the cell, which is equal to the uncertainty in using the climatology as an estimate for a particular month. In other words, a single profile within a cell-month is assumed to be as useful as knowledge of the climatological profile for estimating the true profile of the cell-month. The proportionality of intra-cell variability and inter-annual variability is reasonable (both will be greater in more active parts of the ocean), but the scale factor of 1 that is assumed is presently speculative: in future work, this assumption for representativity uncertainty should be improved, for example by considering the relationship between these quantities in high resolution ocean models.

Representativity errors cannot be considered to be independent between profiles. The model for their error covariance is

$$S_{x_r} = u^2(h'_{l,c}) R_{x_l} \quad \text{Eq. 7}$$

under the assumption about the uncertainty just discussed. R_{x_l} is the matrix of error correlation coefficients between profiles, a given element of which is modelled as

		<p>CCI Sea Level Budget Closure</p> <p>ESA/ESRIN contract 4000119910/17/I-NB</p> <p>Reference: ESA_SLBC_cci_D2.4.2</p> <p>Version: v1.2</p> <p>Date: 18.06.2019</p> <p>Page: 27 of 116</p>
---	---	--

$$\exp\left(-\frac{|d_p - d_{p'}|}{\Delta_d} - \frac{|t_p - t_{p'}|}{\Delta_t}\right) r_{l,l'} \quad \text{Eq. 8}$$

for the pair of profiles p and p' , where $|d_p - d_{p'}|$ is the magnitude of horizontal separation, $|t_p - t_{p'}|$ the time separation, and Δ_d and Δ_t are a length and time scale respectively. (The term $r_{l,l'}$ is the between-layer error correlation coefficient, which is 1 when considering a single layer, $l' = l$.) This model expresses the fact that two profiles obtained very close in space and time will tend to differ in the same way from the true cell mean. Their representativity errors are therefore highly correlated (close to 1) and this is evident in Eq. 8 because as $|d_p - d_{p'}|$ and $|t_p - t_{p'}|$ tend to zero, the exponential term tends to $\exp(-0) = 1$. Combining more separated profiles gives a better estimate of the true cell mean. We must attribute values to the scale parameters in reference to the scales of the space-time box whose mean we are estimating: by construction these scales cannot be longer than 1 month and 5° respectively. Thus we assume $\Delta_d \sim 0.5 \times 5^\circ = 2.5^\circ$, so that at cell-corner-to-opposite-corner separation, the error correlation is small, $e^{-2\sqrt{2}} \sim 0.06$. Similarly, by construction, the error correlation should be small at a timescale of 1 month. $\Delta_t \sim \frac{1}{3}$ month = 10 days is assumed, so that the correlation between start-and-end-of-month is about 0.05 (roughly matching the length-scale assumption). (The scale parameters can in future be refined using high resolution model outputs and differences in observed profiles for the minority of intensely observed cells.)

The error covariance required in Eq. 5 is then calculated as:

$$\mathbf{S}_{x_l} = \mathbf{S}_{x_m} + \mathbf{S}_{x_r} \quad \text{Eq. 9}$$

which in turn defines the weighting of the steric thickness anomalies from different profiles in the estimated cell mean value and enables calculation of the steric thickness anomaly for the layer.

Note that the climatological profile is included in the average, partly because in some cells and/or some depths it is the only available estimate, and partly to help stabilise the estimate when the number of profiles is few against the influence of outliers. The climatological anomaly is by definition zero, but below it is explained that the ‘‘climatological profile’’ used is in fact a conditional climatological estimate – i.e., is the climatology additionally constrained by a surface SST observation. The error correlation between the measured profiles and the (conditioned) climatological estimate is zero.

3.2.2.4 Vertical integration to SSLA and its uncertainty

The steric sea-level height anomaly (SSLA) is the sum of the layer-by-layer optimal estimates of steric thickness anomaly, i.e., $h' = \sum_l h'_l = \sum_l \mathbf{w}_l^T \mathbf{x}_l$. If we define $\mathbf{w}^T = [\mathbf{w}_1^T, \dots, \mathbf{w}_l^T, \dots]$ and $\mathbf{x}^T = [\mathbf{x}_1^T, \dots, \mathbf{x}_l^T, \dots]$ then

		<p>CCI Sea Level Budget Closure</p> <p>ESA/ESRIN contract 4000119910/17/I-NB</p> <p>Reference: ESA_SLBC_cci_D2.4.2</p> <p>Version: v1.2</p> <p>Date: 18.06.2019</p> <p>Page: 28 of 116</p>
---	---	--

$$h' = \mathbf{w}^T \mathbf{x} \quad \text{Eq. 10}$$

which is a useful form, since it makes obvious the uncertainty estimate for the SSLA:

$$\mathbf{u}_{h'} = (\mathbf{w}^T \mathbf{S}_x \mathbf{w})^{0.5} \quad \text{Eq. 11}$$

The evaluation of the SSLA in Eq. 10 is simple once we have determined the \mathbf{w}_l in the layer-by-layer calculations. The remaining task is to formulate \mathbf{S}_x . The diagonal blocks corresponding to each layer in \mathbf{S}_x are the matrices \mathbf{S}_{x_l} that have already been calculated at Eq. 9. Now we must make assumptions about the error correlations between layers in order to complete the off-diagonal elements of \mathbf{S}_x . The assumptions made are:



- measurement errors are perfectly correlated vertically in a given profile; this is equivalent to saying that the sensor calibration bias dominates all other sources of measurement uncertainty in each profile, which is a reasonable conservative assumption;
- representativity errors are perfectly correlated vertically, i.e., $r_{l,l'} = 1$ in Eq. 8 for all $\{l, l'\}$; this implies that relative to the cell-mean average profile, each measured profile differs in the same direction at all layers and in proportion to the representativity uncertainty of the layers; while vertical correlations over some scale are likely, applying this to the whole profile is conservative (tends to over-estimate uncertainty).

The evaluation of Eq. 10 and Eq. 11 completes the calculation of cell-month SSLA. The only aspect yet to be described is that of the conditioning of the climatology with SST, described in the next section.

3.2.2.5 Using SST to condition the climatology

The degree of constraint provided by sea surface temperature on steric sea level is generally limited: in some circumstances it may be useful, and often it will be negligible. The potential benefits of including SST constraints arise because:

- SST anomalies at monthly $5^\circ \times 5^\circ$ scales are well observed (with minimal representativity uncertainty) throughout the Argo period from satellite measurements across the whole ocean, including areas and times that Argo profiles were sparse or non-existent; of course, Argo profiles are persistently absent for coastal regions and shelf seas
- while the mixed layer depth of the ocean is highly variable, in those times and places where it is of significant depth (typically mid-latitude winters), precise knowledge of SST gives some integrated constraint
- we can condition the climatological profile used for SSLA using SST, reducing the tendency of inclusion of the climatological information to dampen the changes in the SSLA

		<p>CCI Sea Level Budget Closure</p> <p>ESA/ESRIN contract 4000119910/17/I-NB</p> <p>Reference: ESA_SLBC_cci_D2.4.2</p> <p>Version: v1.2</p> <p>Date: 18.06.2019</p> <p>Page: 29 of 116</p>
---	---	--

Thus, the way in which SST data have been introduced is by conditioning the climatology. This idea can be expressed as replacing the climatology and its variability, $(\mathbf{x}_c; \mathbf{V}_c)$ with $(\mathbf{x}'_c = \mathbf{x}|\mathbf{x}_c, \mathbf{V}_c, x_{sst}; \mathbf{S}_{x'_c})$, the profile best estimate given the climatology, its variability and the SST observation, and the error covariance matrix of that best estimate. (Here, the tick mark refers to “conditioned” and x_{sst} is the SST value introduced which is independent of the profile information available.)

This approach is adopted here for the purpose of step-wise development from the earlier methods, where a static climatology was used. A more radical approach could be developed where SST and Argo data are used jointly in one step, which in principle could be more optimal, and could be considered in future.

The starting point is that we have a climatological profile of temperature and salinity for a given cell and, layer-by-layer, the inter-annual variability. Only the temperature climatology is conditioned.



Under the assumption of Gaussian distribution variability and errors, the general expression for updating a prior state, \mathbf{x}_a , given partially or indirectly informative observations, \mathbf{y} is (as presented in, for example, Rodgers, 2000, Eq 2.31):

$$\hat{\mathbf{x}} = \mathbf{x}_a + \mathbf{S}_a \mathbf{K}^T (\mathbf{K} \mathbf{S}_a \mathbf{K}^T + \mathbf{S}_\epsilon)^{-1} (\mathbf{y} - \mathbf{K} \mathbf{x}_a) \quad \text{Eq. 12}$$

In the present the following substitutions into Rodgers’ nomenclature apply:

- \mathbf{x}_a is replaced with \mathbf{x}_c , the (unconditional) climatological profile of temperature
- \mathbf{S}_a is replaced with the covariance matrix of inter-annual variability of the temperature profile, \mathbf{V}_c
- \mathbf{y} is the added (conditioning) observation, which here comprises only x_{sst}
- \mathbf{K} is the matrix of partial derivatives of the observation with respect to the state, which here means $\mathbf{K} = [1 \ 0 \ \dots]$, since x_{sst} is taken as identical to the first element of the state, the temperature in the top layer
- $\mathbf{y} - \mathbf{K} \mathbf{x}_a$ therefore equals $x_{sst} - \mathbf{x}_{c,1}$ which we will write as Δx_{sst}
- \mathbf{S}_ϵ is the error covariance matrix of the observations, which here just means the uncertainty in the SST, σ_{sst}^2
- considering $\mathbf{V}_c \mathbf{K}^T$ and writing the i, j term of \mathbf{V}_c as $v_i v_j r_{ij}$, we have $\mathbf{V}_c \mathbf{K}^T = [v_1^2 \ v_1 v_2 r_{12} \ v_1 v_3 r_{13} \ \dots]^T = v_1 [v_1 r_{11} \ v_2 r_{12} \ v_3 r_{13} \ \dots]^T = v_1 \mathbf{v}'$, defining \mathbf{v}' which as the vector of interannual variability at each level modified by its correlation with surface temperature variability
- $\mathbf{K} \mathbf{S}_a \mathbf{K}^T = v_1^2$

Applying these substitutions gives the equation for the conditional climatology

		<p>CCI Sea Level Budget Closure</p> <p>ESA/ESRIN contract 4000119910/17/I-NB</p> <p>Reference: ESA_SLBC_cci_D2.4.2</p> <p>Version: v1.2</p> <p>Date: 18.06.2019</p> <p>Page: 30 of 116</p>
---	---	---

$$\mathbf{x}'_c = \mathbf{x}_c + \frac{\mathbf{v}_1 \Delta \mathbf{x}_{sst}}{\mathbf{v}_1^2 + \sigma_{sst}^2} \mathbf{v}' \quad \text{Eq. 13}$$

The error covariance of the conditional climatology is, in Rodgers' notation (eq. 2.53 therein):

$$\mathbf{S} = \mathbf{S}_a - \mathbf{S}_a \mathbf{K}^T (\mathbf{K} \mathbf{S}_a \mathbf{K}^T + \mathbf{S}_\epsilon)^{-1} \mathbf{K} \mathbf{S}_a \quad \text{Eq. 14}$$

Using the substitutions for the current case:

$$\mathbf{S}_{\mathbf{x}'_c} = \mathbf{V}_c - \frac{\mathbf{v}_1^2}{\mathbf{v}_1^2 + \sigma_{sst}^2} \mathbf{v}' \mathbf{v}'^T \quad \text{Eq. 15}$$

In the current implementation, only the diagonal terms are required. The diagonal of $\mathbf{S}_{\mathbf{x}'_c}$, designated $s_{\mathbf{x}'_c}$, has as its i^{th} term:

$$s_{\mathbf{x}'_c}[i] = \mathbf{v}_i^2 - \frac{\mathbf{v}_1^2}{\mathbf{v}_1^2 + \sigma_{sst}^2} \mathbf{v}_i^2 r_{1i}^2 = \mathbf{v}_i^2 \left(\frac{\mathbf{v}_1^2 (1 - r_{1i}^2) + \sigma_{sst}^2}{\mathbf{v}_1^2 + \sigma_{sst}^2} \right) \quad \text{Eq. 16}$$

We can see in this equation that as the correlation from the surface to a given depth reduces to zero, the uncertainty tends to the variability of the original climatology, $\sqrt{\mathbf{v}_i^2}$, while the uncertainty of the uppermost layer is equal to $\sqrt{\sigma_{sst}^2}$, as expected.

To be able to calculate $(\mathbf{x}'_c; \mathbf{S}_{\mathbf{x}'_c})$ therefore requires estimation of: the climatological profile, the column vector of interannual variability (which is the same as the estimate of the uncertainty in using the climatology for a given month), the correlation coefficient between the surface and each level in the profile, and SST with its uncertainty (taken from SST CCI level 4 analysis data).

To compute the vector of correlation coefficients for a given well-populated ($n_p > 30$) cell, the procedure is:

- gather all Argo profiles per cell for the target month of the year
- turn into anomalies by subtracting the climatology
- calculate the mean of each remaining anomaly profile and subtract this (this guards against a biased profile introducing unrealistic correlations)
- calculate the correlation coefficient between the top level and each level below, including its 95% confidence interval
- where the confidence interval encompasses zero, set the correlation to zero, since this is non-significant; also set the correlation to zero for all depths below, to avoid spurious statistically significant deep correlations

		<p>CCI Sea Level Budget Closure</p> <p>ESA/ESRIN contract 4000119910/17/I-NB</p> <p>Reference: ESA_SLBC_cci_D2.4.2</p> <p>Version: v1.2</p> <p>Date: 18.06.2019</p> <p>Page: 31 of 116</p>
---	---	--

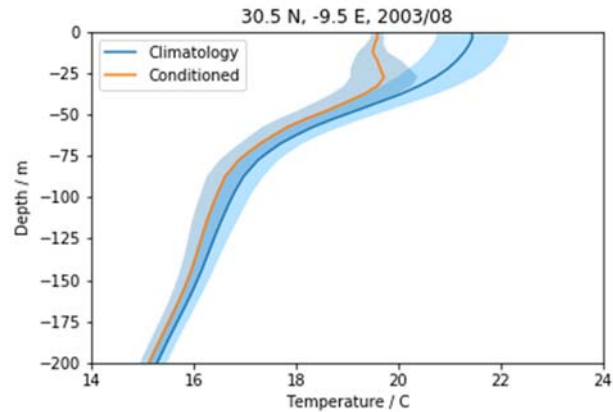


Figure 3.1: Example of conditioned climatology in comparison with unconditioned case.

The correlation coefficient vectors then need to be infilled from well populated cells to all ocean cells. This is done by filling the additional cells with the mean correlation profile from the well-populated cells.

The effect of conditioning the climatology is illustrated in Figure 3.1. For this particular month (August), year (2003) and location (30.5°N, -9.5°E), the SST is about 2°C below the climatology value. The conditioning is strong for the upper ~50 m of the ocean, which is a modest depth range, and the conditioned profile is clearly more realistic given the SST (approximately isothermal over a mixed layer). The uncertainty is reduced at the surface, where the cell-month SST is well known from the satellite data. Below about 150 m, the effect of conditioning decays towards zero (conditioned and unconditioned profiles converge).

3.2.2.6 The baseline period and climatology

SLBC_cci adopted 2006 to 2015 inclusive as the baseline period for calculation of anomalies. The EN 4.2.1 climatology used here is therefore the average for each month of the year of the EN 4.2.1 analysis for that baseline period. The interannual variability used as climatological uncertainty is the standard deviation over the 10 year period. 10 years is a short period for estimating variability, and this may be a significant underestimate for the series as a whole.

However, different weightings and input data ensure that the result of the methods applied are not exactly zero mean when averaged across this baseline, despite anomalies being calculated with respect to a climatological product adapted to the baseline period. Therefore, the final step in making the product is to re-zero the results to the baseline period. This is done for each cell for each month of the year, by subtracting the 10-year mean result.

		<p>CCI Sea Level Budget Closure</p> <p>ESA/ESRIN contract 4000119910/17/I-NB</p> <p>Reference: ESA_SLBC_cci_D2.4.2</p> <p>Version: v1.2</p> <p>Date: 18.06.2019</p> <p>Page: 32 of 116</p>
---	---	--

3.2.2.7 Calculation of GMSSLA and its uncertainty

The global mean steric sea level height anomaly (GMSSLA) is the area-weighted average of the gridded SSLA results. Because of the re-zeroing step, the GMSSLA is zero-mean over the period 2006–2015 inclusive. The “global” timeseries is by project agreement calculated over the range 65°S to 65°N. The calculation is as follows. Let the vector \mathbf{a} contain the normalised areas per cell, i , such that $\sum a_i = 1$; $a_i \geq 0$. The estimate of GMSSLA, H , is then

$$\mathbf{H} = \mathbf{a}^T \mathbf{h} \quad \text{Eq. 17}$$

where \mathbf{h} is the corresponding per-cell vector of cell-month SSLA, each as calculated by Eq. 10.

The uncertainty estimate for the GMSSLA is

$$\mathbf{u}_H = (\mathbf{a}^T \mathbf{S}_h \mathbf{a})^{0.5} = \sqrt{\sum a_i^2 u_{h_i}^2} \quad \text{Eq. 18}$$

where we assume that errors are independent between cells. This is an approximate model for the error correlation, because (i) SST errors may be correlated on scales greater than the cell size, and (ii) some cells have the same Argo profilers contributing data to them in a given month (when the profilers move from one cell to the next within the month).

Overall, three aspects of the uncertainty model are recognized to be potentially optimistic: the modelling of measurement errors as independent between profiles rather than platforms; the use of only 10 years for assessing inter-annual variability; and the assumption of full independence of errors between cells when forming the global average. On the other hand, two assumptions are potentially conservative: measurement errors in salinity and temperature were combined in their worst-case combination; representativity errors in profiles are assumed to be fully correlated vertically, whereas in reality they are likely to decorrelate over large vertical separations. Furthermore, three parameters in the uncertainty model are presently based on expert judgement: the scale factor of 1 between intra-cell and cell-mean inter-annual variability; and the scale parameters for time and space in Eq. 8. Lastly, note that uncertainty in the evaluation of vertical correlations from Argo data in order to condition the climatology are not included in the uncertainty model. In summary, the uncertainty modelling and propagation are largely comprehensive and rigorous, but nonetheless need further development to fully ensure their quantitative realism.

The GMSSLA time series obtained is shown in Figure 3.2. Note how the uncertainty is larger in the earlier years, reflecting the low numbers of Argo profiles at that time, as shown in Figure 3.3. It was noted above that the uncertainty calculation here uses the approximation of independence of error between cells, which is a good approximation later in the record (when the results are dominated by Argo data) and an optimistic approximation earlier in the record (when the results depend more on the conditioned climatology, because the Argo profiles are so few). Therefore, the contrast in uncertainty between 2002 and 2018 is probably underestimated, with uncertainties attributed to 2002 being smaller than they should.

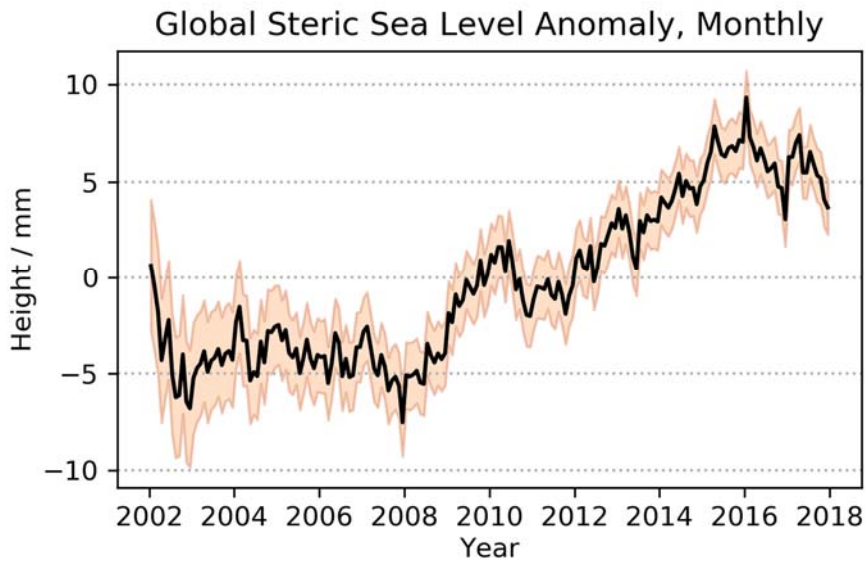


Figure 3.2: Timeseries of global mean steric sea level anomaly, v2.0, monthly resolution and showing the standard (1 sigma) uncertainty

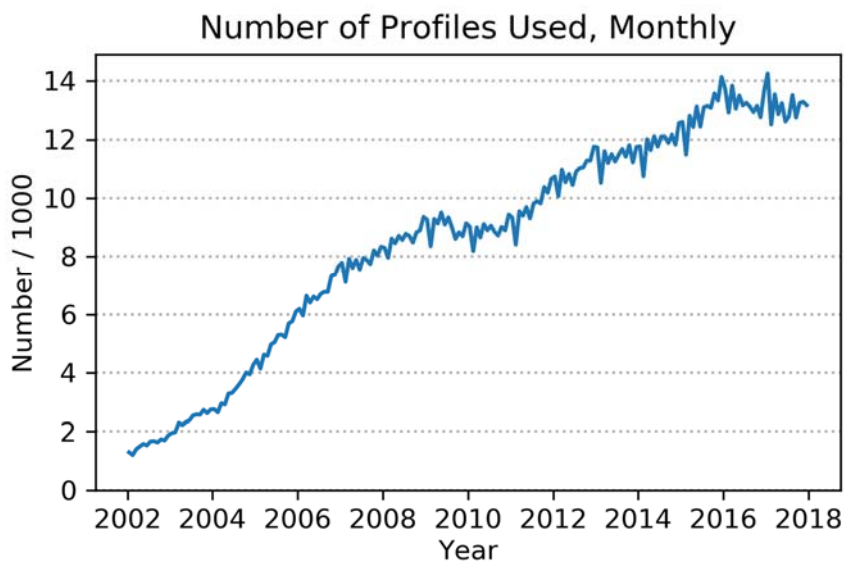


Figure 3.3: Number of Argo profiles per month used for the GMSSLA

An important consideration is to make a judgement regarding when the GMSSLA timeseries is adequately constrained by Argo profile data to constitute useful data for timeseries analysis. At the start of 2002, the number of profiles is a tenth of the number available by 2015 (Figure 3.3) and the earliest years are therefore not adequately constrained. This is clear in Figure 3.4, in that the v1.2 timeseries in the annual mean exhibits larger than expected inter-annual variability over the first three years in particular. These are stabilised in v2.0 by use of the conditioned climatology. Also shown in Figure 3.4 is the ensemble mean of 5 ocean model re-analysis datasets and their spread, from CMEMS. From 2004, the ensemble mean and v2.0 appear qualitatively consistent in the context of their uncertainties. By the end of 2004, the number of profiles per month is a quarter of the 2015 number. Taken together, these observations indicate it is reasonable to use v2.0 from 2004 onwards for timeseries analysis.

Over the period 2004 to 2017, the v2.0 GMSSLA has a mean trend of 0.98 mm/yr (based on weighted least squares regression of the monthly timeseries, using the inverse uncertainty as weight).

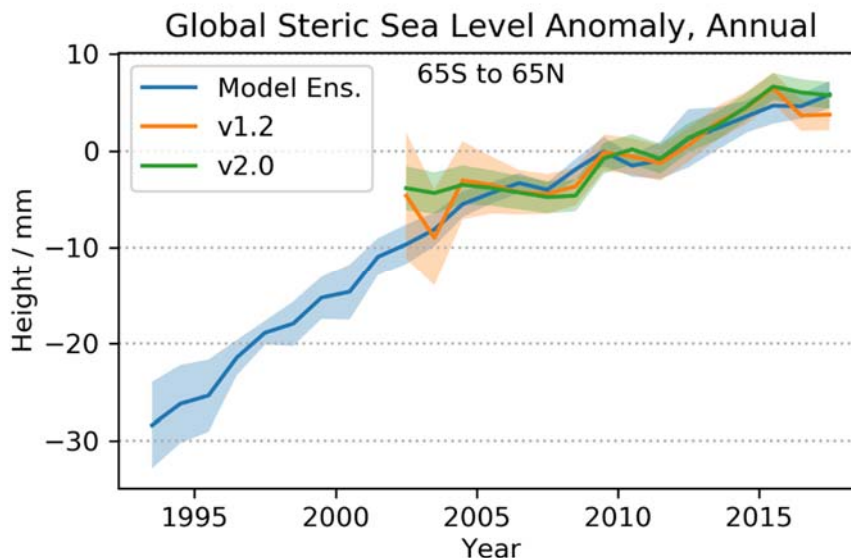


Figure 3.4: Comparison on annual basis of steric sea level in v2.0 with earlier data (v1.2, not using the conditioned climatology) and with the CMEMS model ensemble using the ensemble spread to indicate its standard uncertainty

		CCI Sea Level Budget Closure ESA/ESRIN contract 4000119910/17/I-NB	
		Reference: ESA_SLBC_cci_D2.4.2 Version: v1.2 Date: 18.06.2019 Page: 35 of 116	

3.3 Product Specification

3.3.1 Product geophysical data content

Global timeseries and cell data in one file `steric_r604z.nc`

Geophysical variable	Name in product	Units	Dimensions
Time at middle of month	time	(fractional) calendar year	192 (time)
Calendar year	year	calendar year	(time)
Month of year	month	month of year	(time)
Days since 1993-01-01	day	day	(time)
Global mean steric sea level anomaly (65°S to 65°N)	stericHa	mm	(time)
Uncertainty global mean steric sea level anomaly	stericHa_uncertainty	mm	(time)
Count of profiles used in GMSSLA estimate	nprofiles	none	(time)
Count of cells with one or more profiles	ncells	none	(time)
Latitude of cell centres	lat	degrees north	36 (lat) [5 degree, -87.5 to +87.5]
Longitude of cell centres	lon	degrees east	72 (lon) [5 degree, -177.5 to +177.5]
Latitude bounds of cells	latb	degrees north	37 [5 degree, -90 to +90]
Longitude bounds of cells	lonb	degrees east	73 [5 degree -180 to +180]
Steric sea surface height anomaly	ssla	m	(lon, lat, time)
Uncertainty in height anomaly	ssla_uncertainty	m	(lon, lat, time)
Profile count (number of contributing observation profiles)	n	none	(lon, lat, time)
Area of sea within cell	area	m ²	(lon, lat)
Median depth of sea floor within cell	bathymetry	m	(lon, lat)
Maximum depth of sea floor within cell	bathymetry_max	m	(lon, lat)
Minimum depth of sea floor within cell	bathymetry_min	m	(lon, lat)

		<p>CCI Sea Level Budget Closure</p> <p>ESA/ESRIN contract 4000119910/17/I-NB</p> <p>Reference: ESA_SLBC_cci_D2.4.2</p> <p>Version: v1.2</p> <p>Date: 18.06.2019</p> <p>Page: 36 of 116</p>
---	---	--

3.3.2 Coverage and resolution in time and space

The gridded v2.0 product is available at $5^\circ \times 5^\circ$ monthly resolution, from January 2002 to December 2017. The global average covers the same period. Note: the gridded product is not spatially complete.

3.3.3 Product data format

netCDF4.

3.3.4 Product grid and projection

See 3.3.2.

3.4 Uncertainty Assessment

3.4.1 Sources of error

Uncertainty in measurement of temperature and salinity.

Uncertainty in measurement of sea surface temperature.

Uncertainty in parameters that weight the combination of data, particularly representativity uncertainty assumptions.

Uncertainty from under-sampling geophysical variability.

These sources are estimated, with some approximations and assumptions.

3.4.2 Methodology for uncertainty assessment

See algorithm section, including comments in section 3.2.2.7.

3.4.3 Results of uncertainty assessment

Standard uncertainty for each month's GMSSLA is shown in Figure 3.2. For the gridded product, the mean uncertainty estimate per cell month is shown as Figure 3.5.

3.4.4 Uncertainty documentation in the data products

Refer to section 3.3.1 for how uncertainty is included in the data products.

		CCI Sea Level Budget Closure
		ESA/ESRIN contract 4000119910/17/I-NB Reference: ESA_SLBC_cci_D2.4.2 Version: v1.2 Date: 18.06.2019 Page: 37 of 116

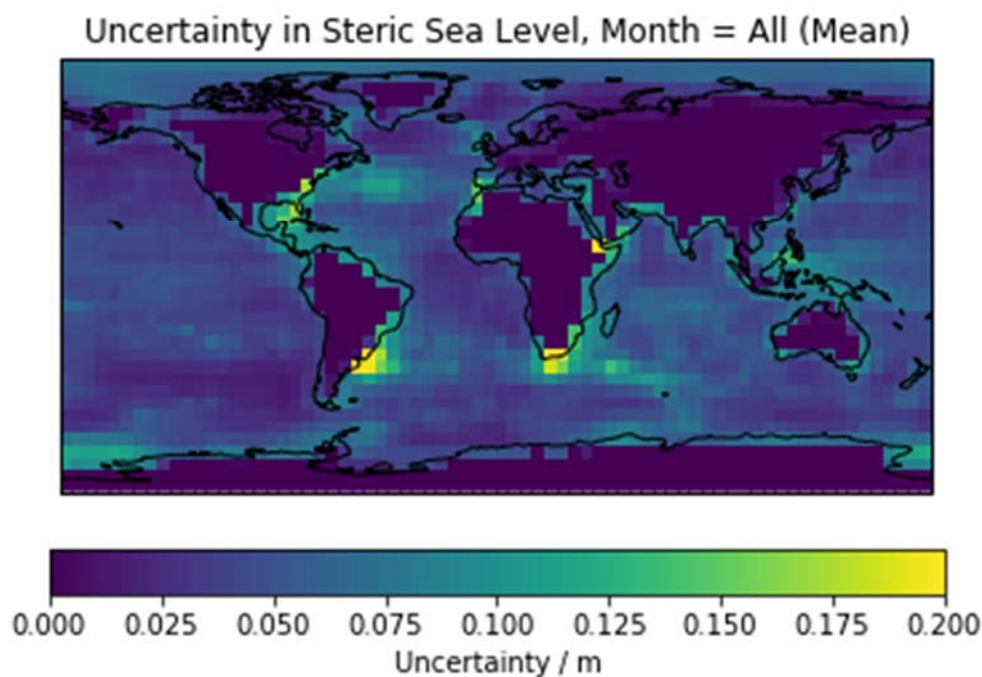


Figure 3.5: Timeseries mean of per-cell-month steric sea level uncertainty

3.5 References

- Cazenave, A., Dominh, K., Guinehut, S., Berthier, E., Llovel, W., Ramillien, G., Ablain M., and Larnicol, G. (2009): Sea level budget over 2003–2008: A reevaluation from GRACE space gravimetry, satellite altimetry and Argo. *Global and Planetary Change*, 65(1), 83-88, doi: [10.1016/j.gloplacha.2008.10.004](https://doi.org/10.1016/j.gloplacha.2008.10.004).
- Leuliette, E. W., and L. Miller (2009): Closing the sea level rise budget with altimetry, Argo, and GRACE, *Geophys. Res. Lett.*, 36, L04608, doi: [10.1029/2008GL036010](https://doi.org/10.1029/2008GL036010).
- Rodgers, C.D. (2000): *Inverse Methods for Atmospheric Sounding, Theory and Practice*. World Scientific Publishing, ISBN 978-981-02-2740-1, doi: [10.1142/3171](https://doi.org/10.1142/3171).
- von Schuckmann K, and Le Traon P-Y (2011): How well can we derive Global Ocean Indicators from Argo data? *Ocean Sci.*, 7:783–791, doi:[10.5194/os-7-783-2011](https://doi.org/10.5194/os-7-783-2011).
- von Schuckmann K, Gaillard F, and Le Traon P-Y (2009): Global hydrographic variability patterns during 2003-2008. *Journal of Geophysical Research*, 114: 1-17, doi:[10.1029/2008JC005237](https://doi.org/10.1029/2008JC005237).
- Willis, J K, Chambers D P, and Nerem S R (2008): Assessing the globally averaged sea level budget on seasonal to interannual timescales. *Journal of Geophysical Research*, 110, C06015, doi: [10.1029/2007JC004517](https://doi.org/10.1029/2007JC004517)

		<p>CCI Sea Level Budget Closure</p> <p>ESA/ESRIN contract 4000119910/17/I-NB</p> <p>Reference: ESA_SLBC_cci_D2.4.2</p> <p>Version: v1.2</p> <p>Date: 18.06.2019</p> <p>Page: 38 of 116</p>
---	---	--

4 Ocean Mass Change

Time-variable ocean mass products and continental mass products are derived from quasi-monthly solutions from the Gravity Recovery And Climate Experiment (GRACE) satellite mission (Tapley et al., 2004). While the processing and inversion approaches of the products involved differ considerably, the common setting is such that mass redistributions in the Earth-/Ocean system cause changes in the gravity field that are observed with the GRACE satellites. Here, these changes are expressed as temporal changes of mass per surface area in kg/m^2 near the Earth's surface, or equivalently, temporal changes of *equivalent water height (EWH)* in millimetres water equivalent (mm w.e.). When given as an equivalent average change distributed over the ocean surface, it may also be expressed as millimetres *sea level equivalent (mm SLE)*. The changes are expressed relative to an arbitrary reference state, e.g. here we use the temporal mean state over the period 01/2006–12/2015. The EWH is a *hypothetical* layer of fresh water which would cause the observed change in gravity at each data point, respectively.

4.1 Data Access and Requirements

SLBC_cci version 2 (v2) products have been derived from ITSG-Grace2018 and GRACE RL06 (CSR, GFZ, JPL) solutions. That is, v2 products are based on new GRACE solution releases, as compared to SLBC_cci v1 products. The following products are considered:

- **ITSG-Grace2018**

SLBC_cci v2 main product Institution: Institut für Geodäsie, TU Graz

Product Source: <https://www.tugraz.at/institute/ifg/downloads/gravity-field-models/itsg-grace2018/>

Data source: ftp://ftp.tugraz.at/outgoing/ITSG/GRACE/ITSG-Grace2018/monthly/monthly_n60

Reference: Mayer-Gürr et al. (2018a,b)

- **CSR / GFZ / JPL RL06**

SLBC_cci v2 supplementary product

GRACE Release 6 (RL06) data from the official GRACE processing centres at CSR Texas, GFZ Potsdam and JPL, CA.

Data source for CSR, GFZ and JPL data: <ftp://podaac.jpl.nasa.gov/allData/grace/L2/{CSR,GFZ,JPL}/RL06/>

- **GSFC Mascons v02.4**

SLBC_cci v2 supplementary product, no change of input data since v1

Institution: Goddard Space Flight Center (NASA)

		<p>CCI Sea Level Budget Closure</p> <p>ESA/ESRIN contract 4000119910/17/I-NB</p> <p>Reference: ESA_SLBC_cci_D2.4.2</p> <p>Version: v1.2</p> <p>Date: 18.06.2019</p> <p>Page: 39 of 116</p>
---	---	--

Product and data source: <https://neptune.gsfc.nasa.gov/gngphys/index.php?section=470>

Reference: Luthcke et al. (2013)

- **Don Chambers' global mean OMC time-series**

SLBC_cci v2 supplementary product, identical to v1. It is an updated version of the file provided in SLBC_cci version 0 (v0). For comparison only; see below. Product Source: Personal communication

Reference: Johnson and Chambers (2013); Chambers and Bonin (2012)

CSR- and GSFC Mascon products of the GRACE Release 6 series as well as products stemming from the GRACE-FO mission were not available at the time of SLBC_cci data processing and are not part of these v2 project deliverables. All RLO6 data at time of the v2 delivery include solutions until August 2016 (for GSFC v2.4 mascons: July 2016).

4.2 Algorithms

4.2.1 Review of scientific background

Global solutions of Earth's gravity field are commonly represented by the coefficients (so-called Stokes coefficients) of a spherical harmonic (SH) expansion up to a specific maximum SH degree (Wahr et al., 1998). GRACE processing centres typically analyse Level-1 GRACE data (including the GRACE K-band ranging data, on-board GPS data and accelerometer data) to estimate a set of Stokes coefficients on a monthly basis ("monthly SH solutions").

Following the "atmospheric and oceanic de-aliasing" (AOD) approach, modelled short-term atmospheric and oceanic mass variations (as well as tidal mass variations) are accounted for as part of the background model within the gravity field estimation procedure (Flechtner et al., 2014; Dobslaw et al., 2013). Therefore, these variations are not included in the monthly solutions. In order to retain the full mass variation effect in the ocean domain, the respective monthly averages of the AOD fields need to be added back to the monthly solutions. These monthly averages are provided by the analysis centres of the GRACE Science and Data System. They have adopted the following nomenclature for those products: GAA products for the atmospheric mass variations, GAB products for the oceanic mass variations, and GAC products for the sum of the two. As an additional series of products, GAD products contain the sum of atmospheric surface pressure effects and ocean mass effects over the ocean domain (advised for comparisons with ocean bottom pressure (OBP) observations). Different options of restoring mass variations in the oceanic domain exist for different oceanic applications of GRACE (compare section "De-aliasing products and ocean-only mascons" in the GSFC mascon description at <https://neptune.gsfc.nasa.gov/gngphys/index.php?section=470>). The SLBC_cci v2 OMC time-series processed from CSR-, GFZ-, JPL- and ITSG-data have the GAD

		<p>CCI Sea Level Budget Closure</p> <p>ESA/ESRIN contract 4000119910/17/I-NB</p> <p>Reference: ESA_SLBC_cci_D2.4.2</p> <p>Version: v1.2</p> <p>Date: 18.06.2019</p> <p>Page: 40 of 116</p>
---	---	--

product consequently restored and the spatial mean of atmospheric surface pressure over the full ocean removed in order to be consistently comparable to steric-corrected altimetry data. (See also ESA_SLBC_cci_D1.2 "Science Requirements Updated and Preliminary Thoughts on Roadmap, Section 3.5.) GSFC v2.4 mascons used for OMC time-series processing in SLBC_cci have the GAD restored and the atmospheric mean removed likewise. JPL RLO6 mascons, in contrast, are only available in a version that is comparable to OBP observations, but technically not to steric- & IB-corrected altimetry. Since the underlying mascons are externally processed products, we do not provide an additional correction for this product as we have accomplished for the SH-based solutions.

GRACE is insensitive to surface mass displacement components of SH degree one (mass exchange between hemispheres). Swenson et al. (2008) have proposed an approach to derive the degree-one components by combining the GRACE information for degree $n \geq 2$ with ocean model output. This approach is widely applied. GRACE has also a reduced sensitivity to the C_{20} component of the gravity field (dynamic flattening term). Therefore, GRACE-based C_{20} components are commonly replaced by results from satellite laser ranging. Specifically, the mascon solution by GSFC as well as the spherical harmonic-based results by D. Chambers and the products generated within SLBC_cci (based on ITSG-Grace2018 and the CSR/GFZ/JPL RLO6 Level-2 products) all follow the approach of adding degree-one terms and replacing C_{20} in the way described here.

Wahr et al. (2015) showed that pole-tide corrections to compensate for the response of the solid Earth and oceans to the Earth's polar motion (affecting coefficients of degree 2 and order 1: C_{21} , S_{21}) are not sufficiently modelled during GRACE RLO5 processing. They recommend an additional correction to be applied to the GRACE RLO5 Level-2 products. This correction is included in the GSFC mascon solution. It is no longer necessary for the GRACE RLO6 / ITSG-Grace2018 products. Hence, we removed this processing step for the v2 mass-change series.

The task of determining changes in the mass distribution from changes of Earth's exterior gravity field has no unique solution. Uniqueness can be enforced by the assumption that the mass redistribution occurs in terms of surface mass changes in a "thin" layer on the Earth's surface, comprising the hydrosphere, atmosphere and cryosphere. In this way, global grids of surface mass variations can be calculated from the temporal variations of the gravity field.

Mass redistribution processes in the Earth interior, in particular glacial isostatic adjustment (GIA) or seismic events, cannot be subsumed in the concept of surface load changes. Therefore, they need to be corrected prior to the conversion of gravity field changes to surface mass changes. This is usually done by using results from geophysical modelling.

Due to the attenuation of short-wavelength (= high SH degree) gravity-field patterns with height, the sensitivity of GRACE rapidly decreases with SH degree. In other words, GRACE

		<p>CCI Sea Level Budget Closure</p> <p>ESA/ESRIN contract 4000119910/17/I-NB</p> <p>Reference: ESA_SLBC_cci_D2.4.2</p> <p>Version: v1.2</p> <p>Date: 18.06.2019</p> <p>Page: 41 of 116</p>
---	---	--

errors increase with SH degree. On top of this general error characteristics, GRACE errors exhibit distinct correlation patterns, which show up as north-south striping features and are related to the orbital geometry. In consequence, GRACE analyses for temporal surface mass change often involve filtering (spatial smoothing) leading to spatial resolutions limited to 300-500 km. Advanced filter approaches (Swenson and Wahr, 2006; Kusche, 2007) account for the complex, non-isotropic GRACE error structure. For the determination of mass change over global-average integration kernels, however, the omission of smoothing filters may prevent leakage effects that would occur otherwise (e.g., Johnson and Chambers, 2013). Extensive internal studies within WP220/310 have confirmed that OMC time-series derived from smoothed GRACE data over the Global Ocean domain give significantly lower trends.

Based on grids of surface mass changes (generated by involving the corrections mentioned above), the total mass change over an area (e.g. the global ocean) is derived by spatial integration with an appropriate weight function. Equivalently, a respective linear functional may be applied in the spherical harmonic domain. The reduced spatial resolution causes leakage effects: Mass changes in coastal regions cannot be uniquely assigned to either the land side or the ocean side of the coastline. Since hydrological (or glaciological) changes on the land side tend to have larger amplitudes than oceanic mass changes on the ocean side, a buffer zone of a few hundred kilometres is typically masked out from the ocean integration kernel (Chambers, 2009). Conversely, for estimating continental water or ice mass changes, a respective buffer zone may be added to the integration kernel. In that case, leakage effects due to oceanic mass changes within the coastal buffer zone need to be considered and corrected.

Mascon approaches are a way to enforce a sharp separation between mass changes on either side of coastlines. Mascons (mass concentrations) are direct parametrisations of (localised) surface mass anomalies. Level-1-based mascon solutions directly estimate mascon magnitudes from the Level-1 GRACE data, without involving global gravity field solutions as an intermediate step. Geographically dependent constraints on the spatio-temporal variance and covariance of mass changes can be employed.

4.2.2 Algorithms

ITSG-Grace2018 based products

ITSG-Grace2018 (Mayer-Gürr et al. 2018a,b) is a series of monthly global SH gravity field solutions. Methodological advancements of the processing by TU Graz include the co-estimation of daily variations (in order to reduce aliasing from short-term variations into the monthly solutions) and the incorporation of temporal instrument error covariances.

RL06- and ITSG-GRACE2018 unconstrained monthly solutions are available in different resolutions between degree 60 and 96, where a higher degree means higher spatial resolution. The model choice is a trade-off between higher resolution and an increased noise level. High

		<p>CCI Sea Level Budget Closure</p> <p>ESA/ESRIN contract 4000119910/17/I-NB</p> <p>Reference: ESA_SLBC_cci_D2.4.2</p> <p>Version: v1.2</p> <p>Date: 18.06.2019</p> <p>Page: 42 of 116</p>
---	---	--

noise levels require smoothing filters, but we found smoothed solutions to be unsuitable for OMC trend determination due to signal dampening (Novotny et al. 2018b, Section 4.2.2; cf. trends of filtered SLBC_cci v0 time series (Tab. 2.2. in Novotny et al. 2018a) which are lower than the trends of the unfiltered SLBC_cci v1 time series (Tab. 2.2 in Horwath et al. 2019). Hence, for reasons of considerable signal-to-noise ratio and consistency with comparable OMC solutions, a lower resolution model (with a corresponding lower noise level) was chosen, that can be integrated over an un-smoothed global ocean kernel. Here we use the series of solutions expanded up to SH degree 60. These SH solutions are further processed at TU Dresden to derive global grids of surface mass changes.

GAD is restored and the mean atmospheric surface pressure effect over the entire Global Ocean is removed according to the considerations outlines in Section 4.2.1. Here, we use the mean of GAD over the ocean area to represent the mean atmospheric surface pressure effect, which is justified as the ocean mass component in the GAD product is mass-conserving. Effectively, adding the GAD change averaged over the global ocean and subtracting the atmospheric effect averaged over the same global ocean surface would cancel each other out. However, due to the application of coastal buffer zones, we treat both effects separately. Calculating the GAD averages only over the buffered area (excluding the 300 km zone) would lead to OMC trends that are on the order of 0.3 mm/yr higher than for our preferred approach (internal analysis for WP222/310). Similar findings are discussed by Uebbing et al. (2019).

GIA is removed using three different GIA modelling results from

- a) A et al. (2013), based on ICE-5Gv2 glaciation history from Peltier (2004),
- b) Peltier et al. (2015, ICE-6G_C, VM5a) and
- c) Caron et al. (2018).

We also provide OMC time-series without GIA effect correction applied as a supplementary product.

Degree one components (centre of mass, geocentre motion) are added from the CSR GRACE RLO6 (60) solution following the approaches of Swenson et al. (2008) and Bergmann-Wolf et al. (2014).

C20 (“flattening” of the Earth) is replaced by results from satellite laser ranging (SLR) after Cheng et al. (2013) (GRACE Technical Note 11).

Different from the version 1 products, for the new RLO6 solutions it is no longer necessary to correct C21/S21 coefficients (pole tide), as suggested by Wahr et al. (2015) for RLO5 products used in v1. Hence we did not apply this correction for SLBC_cci v2 OMC time-series. But it is included in the GSFC mascon data, which belongs to the GRACE RLO5 series.

		<p>CCI Sea Level Budget Closure</p> <p>ESA/ESRIN contract 4000119910/17/I-NB</p> <p>Reference: ESA_SLBC_cci_D2.4.2</p> <p>Version: v1.2</p> <p>Date: 18.06.2019</p> <p>Page: 43 of 116</p>
---	---	--

In the SLBC_cci v2 OMC processing, we use an un-smoothed ocean kernel in order to avoid damping effects from Gauss- and Swenson-filtering. This applies to all v2 integrated OMC time-series and to the ITSG-based $1^{\circ} \times 1^{\circ}$ gridded time-series products. In addition, optional Swenson-filtered (Swenson and Wahr, 2006) and smoothed (Gaussian 300 km) $1^{\circ} \times 1^{\circ}$ gridded time-series are provided as well, but users should be aware that smoothed grids are subject to damping effects and will lead to weaker integrated OMC trends.

Time series of total ocean mass change are derived by the weighted integral of surface mass variations over all oceanic cells. For this integration, a 300 km buffer is applied along the ocean margins to avoid leakage from land mass change. Around islands, the buffer is generally active when the surface area is greater than 20,000 km² (2,000 km² for near-polar latitudes $> \pm 50^{\circ}$). The integral is subsequently scaled by the ratio between total ocean area and the integrated area (i.e. total ocean area minus buffer area), assuming identical mass-change characteristics of the ocean in both parts. The same applies to OMC over the quasi-global ocean restricted to $\pm 65^{\circ}$ in latitude, where we re-scale mass change to the area of the un-buffered ocean between $\pm 65^{\circ}$. For the Arctic Ocean, we re-scale mass change to the un-buffered Arctic Ocean area. Surface areas are given in the OMC files, respectively.

CSR/GFZ/JPL GRACE RL06 based products

The SLBC_cci version 2 OMC integrated time-series include products based on the ‘official’ monthly GRACE Level-2 solutions from Release 6 in the form of spherical harmonic coefficients. The mass change products for SLBC_cci v2 were processed in the same way as described for the ITSG-Grace2018 based deliverable (see above). Concerning GAD corrections, we applied dedicated data sets coming with each solution, respectively. All other corrections as mentioned above are identical. The initial SH solutions are further processed at TU Dresden to derive global grids of surface mass changes, from which the OMC time-series are derived by weighted integration over the 300 km buffered ocean kernel as described above. As for ITSG-Grace2018, solutions were computed for the Global Ocean, for a quasi-global ocean restricted to 65° N/S and for the Arctic Ocean at latitudes greater than 65 degrees.

GSFC Mascons v02.4 (SLA)

The GSFC v02.4 mascon solution (Luthcke et al., 2013) is a global equal area (1 arc-degree) mascon solution based on Level-1 GRACE data. Anisotropic constraints on the signal covariance were applied.

Different versions, w.r.t. GIA corrections and re-addition of signal components are published. For the SLBC_cci v2 purposes, the “GSFC.ocn.200301_201607_v02.4_SLA-GeruoA” version (identical to SLBC_cci v1) is chosen. The following description refers to this version.

Degree-one components are added from the data set based on Swenson et al. (2008) and are freely available at ftp://podaac.jpl.nasa.gov/allData/tellus/L2/degree_1/deg1_coef.txt.

		<p>CCI Sea Level Budget Closure</p> <p>ESA/ESRIN contract 4000119910/17/I-NB</p> <p>Reference: ESA_SLBC_cci_D2.4.2</p> <p>Version: v1.2</p> <p>Date: 18.06.2019</p> <p>Page: 44 of 116</p>
---	---	--

C20 is replaced by results from satellite laser ranging (Cheng et al., 2013).

C21/S21 (“pole-tides”) trends are corrected following Wahr et al. (2015).

GAD is restored and the mean atmospheric pressure removed, i.e. the global ocean average of GAD is subtracted in addition, in order to account for changes of the integrated atmospheric masses over the ocean domain. This makes the GSFC mascon based SLBC_cci v2 product comparable to steric-corrected and IB-corrected sea level anomalies, while currently available OMC time-series derived from CSR(RLO5)- and JPL(RLO6)-mascons are only consistent with ocean bottom pressure measurements instead (thus not part of this deliverable).

The treatment of atmospheric and oceanic background models is complicated by the fact that GSFC uses a different set of background models (namely, ECMWF for the atmosphere and MOG2D for the ocean) than the members of the GRACE Science and Data System CSR and JPL (which use ECMWF for the atmosphere but OMCT for the Ocean). To reach consistency, the difference between the background models was first accounted for by adding ECMWF+MOG2D and subtracting GAC, and subsequently, GAD was restored.

The above mentioned corrections and re-additions are entirely included in the mascon solution provided by GSFC. Time series of total ocean mass change for SLBC_cci v2, however, are derived by TUDr by the weighted integral over all oceanic points using the ocean-land point-set mask provided by GSFC specific to their Mascon solutions. We strictly used the area information provided with the GSFC data set and rescaled the resulting mass change to a standard ocean surface area as given in the version 2 file headers, respectively. Also, as in the other deliverables, the Caspian Sea is not counted as a part of the Global Ocean.

The GSFC mascon product used here is identical to the product used for SLBC_cci version 1, as there has been no update available since.

Chambers’ global ocean mass change time series

Time series result from applying an un-smoothed averaging kernel over the Global Ocean to series of global SH GRACE solutions from the three ‘official’ centres at CSR Texas, GFZ Potsdam and JPL, CA.

Degree one components are added from the data set based on Swenson et al. (2008) and are freely available at ftp://podaac.jpl.nasa.gov/allData/tellus/L2/degree_1/deg1_coef.txt.

C20 is replaced by results from satellite laser ranging (Cheng et al. 2013).

The data are not corrected for pole tides (C21/S21), which may result in Global OMC trends ~0.1 mm/yr higher than with the correction applied (WP220/310 internal analysis).

A 300 km buffer along the coastlines of continents and large islands is applied.

GAD is restored and the mean atmospheric pressure effect has been removed. It is not documented whether the mean atmospheric pressure has been calculated over the entire ocean

		<p>CCI Sea Level Budget Closure</p> <p>ESA/ESRIN contract 4000119910/17/I-NB</p> <p>Reference: ESA_SLBC_cci_D2.4.2</p> <p>Version: v1.2</p> <p>Date: 18.06.2019</p> <p>Page: 45 of 116</p>
---	---	--

or over a buffered ocean area, which is absolutely relevant – see discussion in conjunction with “ITSG-Grace2018-based products”.

We provide the supplementary updated data set “as is” without any further processing by TUDr. The product is identical to the one in SLBC_cci v1.

4.2.3 Algorithms for Continental Mass Change

Time series with GRACE mass change over continents (continental mass change, CMC) without Antarctica and Greenland is provided with the SLBC_cci version 2 release (see Figure 4.1). It comprises ITSG-Grace2018-, CSR_RLO6-, GFZ_RLO6- and JPL_RLO6-based mass-change time-series over continental area (Land-Water-Mask provided by GUF and modified by TUDr).

The data processing is similar to the OMC time-series processing as described above (degree 1 added, C20 replaced, GIA corrected with Caron et al., 2018, but omission of the GAD restore step). As GRACE cannot distinguish between mass changes attributed to hydrology or glaciers, the CMC product is required to be jointly compared with either components together, or the new integrated product of WP253, which combines glacier- and water-storage mass changes.

Following the motivation of the above mentioned leakage problem for OMC determination, an ‘inverse buffering’ principle applies here for the CMC: Leaking signal that is attributed to the land side but appears to occur over the near-coast ocean (in the buffer zone), needs to be integrated with the ‘continental’ surface mass changes together, in order to correctly be counted as part of the continental mass change. We therefore expanded the initial continental Land-Water-Mask by several half-degree grid cells (as a function of latitude) so that the modified part of the mask approximates a 300 km buffer.

The fractional oceanic surface area of grid cells that contain both land and ocean is considered as the total area of a grid cell minus the land surface area as given in the v2 mask by WP253. Mass changes over this fractional area are contained in the integration over the continental grid cells.

However, the mass change derived from integration over fractional cells and over the added buffer cells must not be added without further processing as it also includes the mass change signal of the ocean itself. We developed the following procedure to counteract the superposition. We subtract the monthly mean value of the Global Ocean multiplied by the (fractional) area of the buffer cells, respectively; assuming that the actual ocean mass change therein is adequately close to the global mean OMC. The resulting integrated and corrected signal is attributed to the initial Land-Water-Mask area only and represents the global mean continental mass change from hydrology and ice mass changes, excluding Antarctica and Greenland.

Areas of the 2004/2005 Sumatra/Nias- and the 2011 Tōhoku earthquake show significant signatures of gravity field changes over the combined kernel. They were therefore excluded from the integration. Areal scaling was adjusted accordingly.

A special case arises due to omission of Greenland from the integration, as several additional buffer cells interfere with areas prone to leakage from the GIS and peripheral glaciers. A trade-off had to be made between counting mass changes leaking out from WP253 continents on the one hand, and omitting leakage from Greenland on the other. In this case, the additional buffer is restricted to approximately half distance towards the Greenland coast.

Integration scheme:

$$CMC = \int_{A_C + A_{fO}} EWH \, dA + \int_{A_B} EWH \, d\lambda d\varphi - \frac{A_B + A_{fO}}{A_{bO}} \cdot \int_{A_{bO}} EWH \, d\lambda d\varphi$$

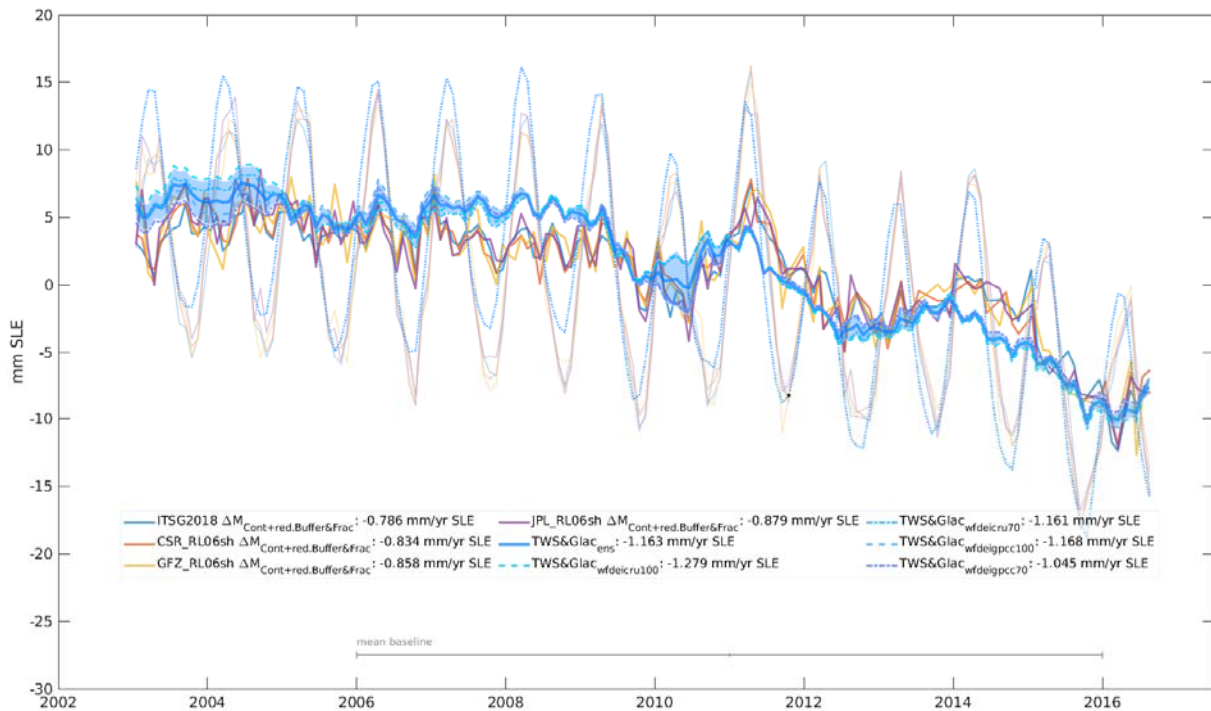


Figure 4.1: Continental mass change (excluding Greenland and Antarctica) from several GRACE RLO6 and ITSG-Grace2018 monthly solutions up to degree 60. In this example, GIA correction after Caron et al. (2018) was applied. The pale coloured curves represent time series including seasonal variation, while the bold curves have the full- and semi-annual cycle removed. Note that there are missing months, in particular towards the end of the time series, despite the graphical representation of the time series by continuous lines. The WP253 combined solution for landwater storage and glaciers mass change is plotted in blue for different forcings together with the shaded band that contains their mean values +- the standard deviation of their spread per month.

with CMC: Continental mass change in kg,

EWH: Equivalent water height from GRACE

dA: area element

A_C : Continental (land surface) area as in WP253

A_{fO} : Fractional ocean area of cells shared by land surface and ocean

AB : Area of 'inverse' leakage buffer extended over the ocean

AbO : Area of the buffered Global Ocean (Global Ocean area minus AB and A_{fO}).

Equivalent mean water height changes over the continental area or over the global ocean can be derived by dividing CMC by A_C or by the Global Ocean area, respectively.

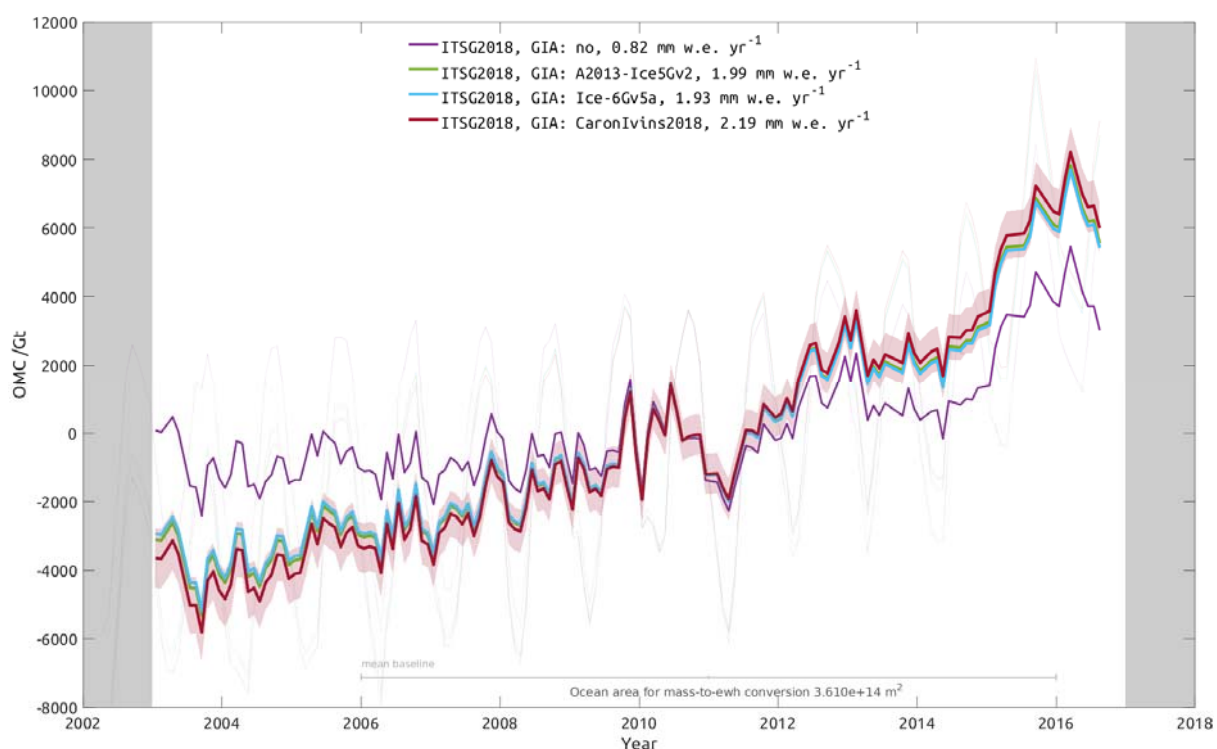


Figure 4.2: Ocean mass change from ITSG-Grace2018 monthly solutions. The four colours represent GIA corrections after A et al. (2013, green), Peltier et al. (2015, blue), Caron et al. (2018, red) and without GIA correction (purple). The pale coloured curves represent the time-series including seasonal variation, while the bold lines have the annual and semi-annual cycle removed. The curve including GIA corrections after Caron et al. (2013) is plotted together with the 1-sigma uncertainty band. Note that there are missing months, in particular towards the end of the time series, despite the graphical representation of the time series by continuous lines. All curves are plotted with respect to their mean value over the baseline interval (2006–2015), which means that differences between the lines get naturally larger at the edges of the observation period as time goes forward/backward from the temporal centre point (2011). The uncertainty band accounts for this effect as it includes trend uncertainties.

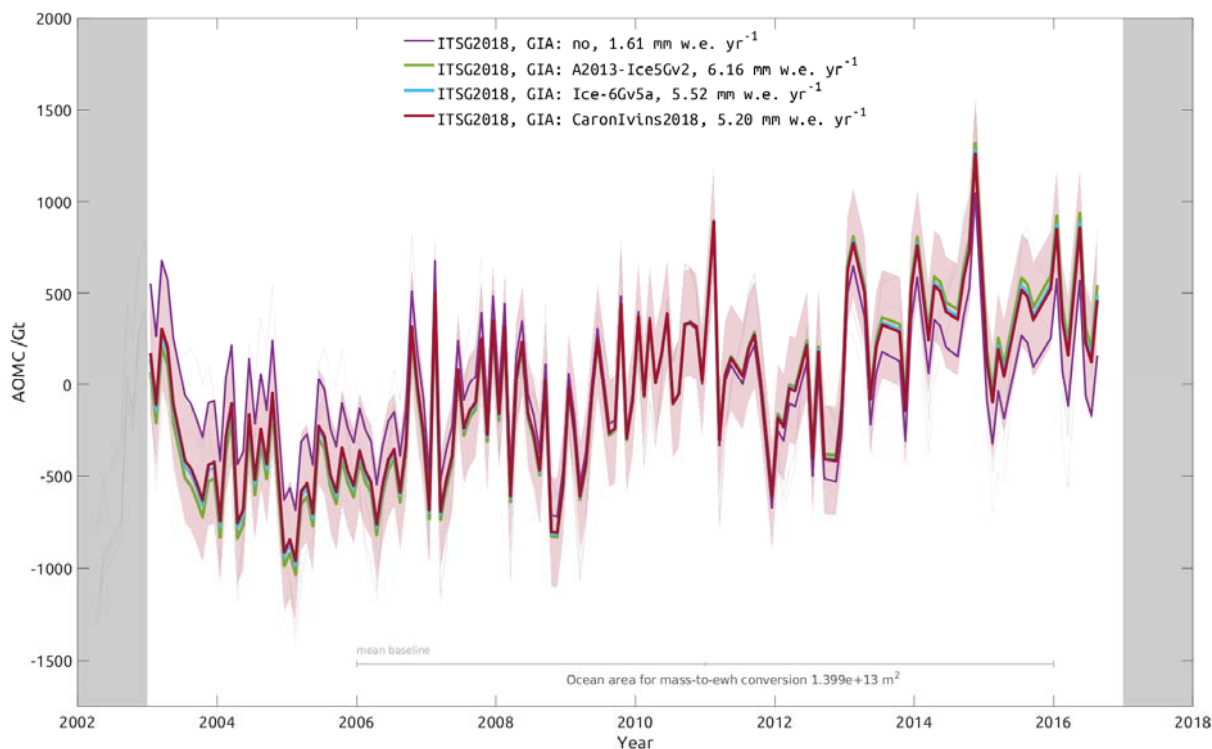


Figure 4.3: Arctic Ocean mass change from ITSG–Grace2018 monthly solutions over the un-smoothed Arctic Ocean integration kernel. The same descriptions as for Figure 4.2 applies.

Further potential for improvement lies in a more consistent treatment of AOD1b background models and a thorough uncertainty estimation.

4.3 Product specification

Time series of OMC are plotted in Figure 4.2 (global ocean) and Figure 4.3 (Arctic Ocean).

4.3.1 Product geophysical data content

OMC time series files

Times series of ocean mass data are provided as text files (comma-separated values, csv) using the following naming scheme:

Files: `[A]OMC[65]ts_SLBCv2.VV_SS_YY_ShFilt-0_c21-0_GAD1-111_GIA-{GG}_R2.csv`

with

- `[A]` ... File for the Arctic Ocean, if present
- `[65]` ... File for the Ocean between 65°N and 65°S
- `VV` ... sub-version number; starts with 'v2.01' for OMC time-series

		CCI Sea Level Budget Closure ESA/ESRIN contract 4000119910/17/I-NB
		Reference: ESA_SLBC_cci_D2.4.2 Version: v1.2 Date: 18.06.2019 Page: 49 of 116

- SS ... Solution source center string, one of {ITSG2018, GSFCm, CSR_RL06sh, GFZ_RL06sh, JPL_RL06sh}
- YY ... Objective SLBC_cci v2 time period to be analysed with this data set (for the mean baseline subtracted please consider the file header)
- GG ... Name of GIA correction applied; one of {A2013-Ice5Gv2, CaronIvins2018, Ice-6Gv5a, no}
- R2 ... The surface mass integration was done over a sphere with an WGS84 ellipsoid equal area radius (so called 'R2')

Several logical switches (1: true, 0: false) have a meaning as follows:

- ShFilt ... smoothing applied
- c21 ... C21/S21 correction applied
- GAD ... GAD restored; with '111' meaning "GAD processing active, GAD was restored and the atmospheric mean subtracted"

The time series are available with A et al. (2013, Ice5Gv2), Ice6Gv5a, or Caron et al. (2018) GIA correction as well as without GIA correction applied. The first column (decimal year) represents the midpoint of an approximately monthly interval of the individual GRACE solutions, respectively.

Content: column description

Please consider using the information given in the file header!

Geophysical Variable	Column in file	Unit
Time	1	decimal year
mass (ocean mass minus mean_OceanMass)	2	Gt

File: CHAMBERS__ocean_mass_orig.txt

Product Source: Pers. comm.

Content: column description

Please note the comments given in the file header.

		CCI Sea Level Budget Closure ESA/ESRIN contract 4000119910/17/I-NB Reference: ESA_SLBC_cci_D2.4.2 Version: v1.2 Date: 18.06.2019 Page: 50 of 116

Geophysical Variable	Column in file	Unit
Time	1	decimal year
Mean ocean mass	.	mm of equivalent mean sea level
CSR	2	
GFZ	3	
JPL	4	
standard error (exact processing and content of error unknown to us)	5	

The first column (decimal year) represents the midpoint of an approximately monthly interval of the GRACE solutions.

Ocean Mass Change Grids SLBCv2

In addition to the OMC time-series CSV files, we provide gridded ocean mass data on 1-by-1 degrees global grids as netCDF files using the following naming scheme:

Files: EWH_OMC-Grid_SSSS_SLBC-v2.VV_RxR[_filt][_bufBB][_GG].nc

with

- SSSS ... GSFCm, ITSG2018
- VV ... sub-version number, starting with 'v2.01' for grids
- RxR ... resolution 1° by 1° (1x1)

and for ITSG

in addition:

- 'filt' ... only present if smoothing was applied
- 'bufBB' ... for the applied leakage buffer, e.g. 300 km: 'buf300'
- 'GG' ... for the GIA correction applied

ITSG-Grace2018 based grids are available with A et al. (2013, Ice5Gv2), Ice6Gv5a, or Caron et al. (2018) GIA correction; as well as with and without smoothing filters applied. The 'time_dec' field in the grid represents the midpoint of an approximately monthly interval of the GRACE solution.

Content (grid files):

Please consider using the information given in the netCDF meta data.

Geophysical Variable	Name in product	Unit
Change in ocean mass (relative to 2006–2015 mean)	EWH	kg/m ² (corresponds to mm w.e.)
Time	time_dec	decimal year
Longitude	lon	degree_east
Latitude	lat	degrees_north

		<p>CCI Sea Level Budget Closure</p> <p>ESA/ESRIN contract 4000119910/17/I-NB</p> <p>Reference: ESA_SLBC_cci_D2.4.2</p> <p>Version: v1.2</p> <p>Date: 18.06.2019</p> <p>Page: 51 of 116</p>
---	---	--

CMC time series files:

Format: comma-separated two-column CSV file. First column is decimal years, second column is mass value in Gt minus the mean between decimal years ≥ 2006.0 and < 2016.0 .

Files: CMCTs_SLBC_cci_v2.VV_SS_YY_F100_GAD-0_GIA-{GG}.csv

with

- VV ... sub-version number; starts with 'v2.00' for CMC time-series
- SS ... Solution source centre string, one of {ITSG2018, CSR_RL06sh, GFZ_RL06sh, JPL_RL06sh}
- YY ... The mean value of this baseline is subtracted
- GG ... Name of GIA correction applied; one of {A2013-Ice5Gv2, CaronIvins2018, Ice-6Gv5a, no}

Several logical switches (1: true, 0: false) have a meaning as follows:

- F100 ... no smoothing applied
- noc5 ... fix part of the file name. (identifier used during product development for the coastal buffering applied as described in Section 4.2.3)
- GAD ... GAD restore; with '0' meaning "GAD processing not active"

The time series are available with A et al. (2013, Ice5Gv2), Ice6Gv5a (Peltier 2015), or Caron et al. (2018) GIA correction as well as without GIA correction applied. The first column (decimal year) represents the midpoint of an approximately monthly interval of the individual GRACE solutions, respectively.

Content: column description

Geophysical Variable	Column in file	Unit
Time	1	decimal year
mass (reduced by mean mass)	2	Gt

4.3.2 Coverage and resolution in time and space

SLBC_cci v2 OMC time-series

- Mass change is given in gigatonnes (Gt, 1 Gt = 10^{12} kg) and refers to an unbuffered standard ocean surface area of 3.6100×10^{14} m² (Global Ocean), 3.3828×10^{14} m² (restricted to $\pm 65^\circ$ in latitude) or 1.3990×10^{13} m² (Arctic Ocean).
- Time is given in decimal years. Each time-stamp gives the mid-time of the function value's epoch. In most cases, this is mid-of-month, but may vary when GRACE

		<p>CCI Sea Level Budget Closure</p> <p>ESA/ESRIN contract 4000119910/17/I-NB</p> <p>Reference: ESA_SLBC_cci_D2.4.2</p> <p>Version: v1.2</p> <p>Date: 18.06.2019</p> <p>Page: 52 of 116</p>
---	---	--

solutions were not processed every consecutive month. Please note that there are ‘missing months’ due to GRACE data gaps.

- Period: second half of 2002 – August 2016, please refer to the individual files. Please consider to use data in the agreed SLBC_cci time period (2003–2016) and compute your own mean-period value reduction if needed. The OMC time-series (except the Chambers file) have already been processed in a way that the mean over the agreed mean baseline 01/2006–12/2015 is subtracted.

SLBC_cci v2 Gridded OMC time-series

GSFC- and ITSG solution series were interpolated onto the grid format defined since SLBC_cci v1:

- EWH given in mm (equivalent to kg/m², assuming a water density of 1000 kg/m³) over the ocean, ‘NaN’ else.
- 1° x 1° geographic grid (pix-reg)
- The grids derived from ITSG-Grace2018 SH have an additional 300 km coastal leakage buffer applied, the GSFC-Mascon based version not.
- Time is given in decimal years.
- Periods are identical to the original data sets. There are ‘missing months’ due to GRACE data gaps. The gridded time-series have already been processed in a way that the mean over the agreed mean baseline 01/2006–12/2015 is subtracted.

As there have been no updates of mascon products that can be considered consistent to steric- and IB-corrected SLA products available (cf. Section 3.5 in Novotny et al. 2018c), the v2 grids derived from GSFC-Mascons are still to be considered the main gridded product for SLBC_cci version 2 analysis. The only difference to the v1 deliverable here is the new reference time frame 2006–2015, the mean of which has been subtracted from the gridded data.

4.3.3 Product data format

Time series of integrated mass changes (global, restricted to +/-65°, and Arctic north of 65°N) are given as ASCII formatted two-column, comma-separated CSV-files. Please consider information given in the file header. Each CSV file’s header ends with the string ‘# EOH’ (end-of-header).

Time series of gridded mass changes are given in the netCDF-4 classic format.

4.3.4 Product grid and projection

SLBC_cci v2 1°x1° global grid, pixel-registration; one grid per time dimension.

		<p>CCI Sea Level Budget Closure</p> <p>ESA/ESRIN contract 4000119910/17/I-NB</p> <p>Reference: ESA_SLBC_cci_D2.4.2</p> <p>Version: v1.2</p> <p>Date: 18.06.2019</p> <p>Page: 53 of 116</p>
---	---	--

4.4 Uncertainty assessment

4.4.1 Sources of error

GRACE errors: Errors in the GRACE observations as well as in the modelling assumptions applied during GRACE processing propagate into GRACE results on surface mass redistribution and in particular into GRACE-based ocean mass change products (“GRACE errors”). GRACE errors need to be damped in some way, either by filtering (in the case of approaches starting from a SH solution) or by applying regularization methods (in the case of mascon approaches). The loss of spatial resolution implied by approaches to reduce GRACE errors causes leakage errors, in turn.

Errors in C_{20} and Degree-1 terms: The GRACE satellites are insensitive to lower degrees coefficients (degree 1 or ‘geocentre motion’, C_{20} or ‘flattening’) of spherical-harmonics representations of the Earth’s gravity field and its changes. These terms are usually derived by employing observations and modelling approaches other than GRACE. Because of their very large scale nature and possible systematic effects (including possible systematic errors in linear trends), errors of these components are particularly important for global ocean mass change applications. The related uncertainties are likely in the order of 0.1 – 0.2 mm/yr (cf. Quinn and Ponte, 2010; Blazquez et al. 2018). As these coefficients are replaced with secondary products during our processing, we account for uncertainties that arise from the low-degree replacements applied to the ITSG-Grace2018 and other SH solutions during the SLBC version 2 processing, accordingly.

Effects of Glacial Isostatic Adjustment (GIA) are known to be a huge source of signal and error for mass change estimates: Post-glacial rebound of the Earth’s crust, flexural effects, viscous back-flow of mantle material and other effects may introduce untargeted mass-change signals in GRACE data and need to be removed from them. GIA effects are usually corrected based on geophysical GIA models. Current models show strong discrepancies. As the models are based on a non-ideal data distribution space- and time-wise, and as the modelling shows considerable variability in its parameter space, the impact of GIA is among the fundamental uncertainties of GRACE-based ocean mass changes. The uncertainty is in the order of up to a few tens of mm/yr, and it is correlated to GIA-based uncertainties of altimetry-based GMSL changes and to GIA-based uncertainties in GRACE based ice sheet mass changes (Quinn and Ponte, 2010; Chambers et al., 2010; Tamisiea, 2011; Rietbroek et al., 2016; , Blazquez et al. 2018).

Leakage errors: Leakage-errors arise from the vanishing sensitivity of GRACE to small spatial scales (high SH degrees) or, respectively, by the necessity to dampen GRACE errors at small spatial scales: For OMC analyses, GRACE data are used only up to a certain spherical-harmonics degree and order (here: 60; ~333 km half-wavelength). At these longer

		<p>CCI Sea Level Budget Closure</p> <p>ESA/ESRIN contract 4000119910/17/I-NB</p> <p>Reference: ESA_SLBC_cci_D2.4.2</p> <p>Version: v1.2</p> <p>Date: 18.06.2019</p> <p>Page: 54 of 116</p>
---	---	--

wavelengths, a significantly large gravity-change signal from the continents (e.g. ice-mass loss of the GIS) leaks into areas over the ocean close to the source and superimposes the actual signal caused by OMC. Hence, leakage errors can be described as errors in correctly assigning gravity field changes to the geographic location of surface mass changes. The problem is aggravated by the fact that surface mass changes on the land side (continental hydrology or continental ice mass changes) are often significantly larger than ocean mass changes. Differences in methods to avoid (or repair) leakage effects can amount to a several tenths of mm w.e./yr in regional OMC estimates (e.g. Kusche et al., 2016).

In order to avoid integrating mass-changes over areas holding such leakage-signals, we make use of an ocean kernel that ‘buffers’ out the closest 300 km surrounding continents, large island (20,000 km²) globally and medium-scale islands (2,000 km²) at high latitudes (>|50°|). The OMC result for the such-derived ‘inner’ ocean is subsequently re-scaled to the standard surface area of the target area (i.e. 3.61e+14 m² for the Global Ocean). Furthermore, users should be aware that potential signal content from fingerprint-effects (i.e. near-coast ocean mass loss through decreasing gravitational acceleration from ice-masses) may partially be omitted in the OMC time-series as a side-effect of the application of coastal buffer zones.

Uncertainty of corrections: Others. Other corrections, with their specific uncertainties, include the correction for rotational feedback effects (polar tides) to long-term mass re-distributions, and corrections for atmospheric mass variations.

4.4.2 Methodology and Results of Uncertainty Assessment

We separate the error into two components distinguished by their temporal characteristics:

- noise, considered temporally uncorrelated, with equal variance for each month
- systematic errors of the linear trend.

We note that this treatment simplifies the situation by not considering autocorrelated errors other than errors that evolve linearly with time.

The standard deviation of the noise is estimated from the OMC time series themselves. For that aim, the de-trended time series, after removal of seasonal signals, are high-pass filtered in the temporal domain. The filtered time series are assumed to be dominated by the high-pass filtered noise. The variance of these filtered time series is calculated. It is subsequently scaled by a factor that accounts for the dampening of white noise variance imposed by the high-pass filtering. The assessed noise component of the uncertainty comprises uncorrelated errors from all sources listed in the previous section, (except for GIA which is considered purely linear in time).

The systematic errors of the linear trends are assumed to originate from the sources Degree-1, C20, GIA, and leakage. The related uncertainties are assessed for each source individually. The analysis of systematic errors of the linear trends follows the same approach as described by

		<p>CCI Sea Level Budget Closure</p> <p>ESA/ESRIN contract 4000119910/17/I-NB</p> <p>Reference: ESA_SLBC_cci_D2.4.2</p> <p>Version: v1.2</p> <p>Date: 18.06.2019</p> <p>Page: 55 of 116</p>
---	---	--

Nagler et al. (2018) for the ESA CCI Antarctica project with GRACE Mass Balance derived changes over Antarctica (cf. Section 6 and the Comprehensive Error Characterisation Report, Nagler et al., 2018).

For example, our GIA correction chooses one GIA model out of a small sample of possible GIA model options. The uncertainty assessment is based on this small sample of GIA correction options. The standard deviation of the sample of options is taken as the standard uncertainty of the GIA correction. Note that this is not the same as trying to determine the uncertainty of the mean value, or expectation value, of all GIA correction options. We do not assume such an expectation value to represent the truth. A t-factor modification of Student's distribution due to small sample sizes was not applied, which is equivalent to applying t_{∞} at a confidence level of 68.3%).

The same approach as described in the previous paragraph for GIA is applied for the Degree one uncertainty and for the C20 uncertainty and the leakage error uncertainty.

Specifically, for the v2 products based on ITSG-Grace2018 (and CSR/GFZ/JPL) spherical harmonics the uncertainty is done as follows. Results are summarized in Table 4.1.

- Degree-1 errors have been assessed through an intercomparison of different degree-1 time-series and the distribution of their effect on the OMC trend. The assessed standard uncertainty for degree 1 is **0.136 mm/yr** for the Global OMC trend, **0.141 mm/yr** for the Global OMC trend restricted to +/-65° latitude, and **1.233 mm/yr** for the Arctic OMC trend (north of 65°N).
- C20 uncertainties have been assessed through an intercomparison of different C20 time-series and the distribution of their effect on the OMC trend. The assessed standard uncertainties are **0.049 mm/yr** for the Global OMC trend, **0.074 mm/yr** for the Global OMC trend restricted to +/-65° latitude, and **0.665 mm/yr** for the Arctic OMC trend, respectively.
- In order to estimate uncertainties that arise from GIA corrections, we analysed the distribution of OMC trends with different GIA models from A et al. (2013, ICE-5G-VM2), Peltier et al. (2015, ICE-6G_C-VM5a) and Caron et al. (2018). The assessed standard uncertainties for GIA corrections in SLBC_cci version 2 are **0.135 mm/yr** for the Global OMC trend, **0.173 mm/yr** for the Global Ocean trend restricted to +/-65° latitude, and **0.489 mm/yr** for the Arctic OMC trend, respectively.

In order to estimate the error that arises from leakage-buffering and rescaling during processing, we performed an extensive study based on synthetic mass change data, namely the updated ESA Earth System Model (ESM; Dobslaw et al., 2015). Synthetic data of the ESM was processed according to the settings of the SLBC_cci v2 OMC time-series setting (pseudo-observed) and then compared with the full-resolution ESM data (pseudo-true) over the identical target area and time, respectively. The weighted RMS of misfits between pseudo-observed and pseudo-true OMC trends for a set of different

		CCI Sea Level Budget Closure ESA/ESRIN contract 4000119910/17/I-NB	
		Reference: ESA_SLBC_cci_D2.4.2 Version: v1.2 Date: 18.06.2019 Page: 56 of 116	

9–12 years long time frames gives us the estimate of the leakage error. The re-assessed standard uncertainty for v_2 coming from this effect is **0.097 mm/yr** for the Global OMC trend, **0.092 mm/yr** for the Global OMC trend restricted to $\pm 65^\circ$ latitude, and **0.480 mm/yr** for the Arctic OMC trend.

Table 4.1: Estimated OMC standard uncertainties for different trend solutions

Error Component	Estimation procedure	Assessed Standard Uncertainty (Global)	Assessed Standard Uncertainty (LAT $\pm 65^\circ$)	Assessed Standard Uncertainty (Arctic)
Noise	Estimation of STD of white noise component of time series			
GRACE solution:				
ITSG		1.645 mm (593.8 Gt)	1.770 mm (598.8 Gt)	20.91 mm (292.5 Gt)
CSR		1.681 mm (607.0 Gt)	1.815 mm (613.9 Gt)	21.65 mm (302.9 Gt)
GFZ		1.826 mm (659.0 Gt)	1.955 mm (661.4 Gt)	22.68 mm (317.3 Gt)
JPL		1.726 mm (623.2 Gt)	1.883 mm (637.0 Gt)	21.68 mm (303.3 Gt)
Trend uncertainty Degree 1	Intercomparison of different degree-1 time-series	0.136 mm/yr 48.9 Gt/yr	0.141 mm/yr 47.8 Gt/yr	1.233 mm/yr 17.3 Gt/yr
Trend uncertainty C_{20}	Intercomparison of different C_{20} time-series	0.049 mm/yr 17.8 Gt/yr	0.074 mm/yr 25.1 Gt/yr	0.665 mm/yr 9.3 Gt/yr
Trend uncertainty GIA	Intercomparison of different models	0.135 mm/yr 48.8 Gt/yr	0.173 mm/yr 58.7 Gt/yr	0.489 mm/yr 6.8 Gt/yr
Trend uncertainty Leakage	Synthetic model data analysis (ESM)	0.097 mm/yr 35.0 Gt/yr	0.092 mm/yr 31.2 Gt/yr	0.480 mm/yr 6.7 Gt/yr
Combined trend Uncertainty	Root Sum Square	0.220 mm/yr 79.5 Gt/yr	0.253 mm/yr 85.6 Gt/yr	1.559 mm/yr 21.8 Gt/yr

		CCI Sea Level Budget Closure	
		ESA/ESRIN contract 4000119910/17/I-NB Reference: ESA_SLBC_cci_D2.4.2 Version: v1.2 Date: 18.06.2019 Page: 57 of 116	

Uncertainties of the CMC time series have been derived in the same way as described for the OMC and are to be used accordingly. Table 4.2 summarises the assessed uncertainties for continental mass change.

Table 4.2: Estimated CMC standard uncertainties for different trend solutions

Error Component	Estimation procedure	Assessed Standard Uncertainty (Global)
Noise GRACE solution: ITSG CSR GFZ JPL	Estimation of STD of white noise component of time series	1.403 mm (506.6 Gt) 1.361 mm (491.2 Gt) 1.786 mm (644.9 Gt) 1.582 mm (571.0 Gt)
Trend uncertainty Degree 1	Intercomparison of different degree-1 time-series	X mm/yr X Gt/yr
Trend uncertainty C ₂₀	Intercomparison of different C ₂₀ time-series	X mm/yr X Gt/yr
Trend uncertainty GIA	Intercomparison of different models	0.120 mm/yr 43.3 Gt/yr
Trend uncertainty Leakage	Synthetic model data analysis (ESM)	X mm/yr X Gt/yr
Combined trend Uncertainty	Root Sum Square	X mm/yr X Gt/yr

		<p>CCI Sea Level Budget Closure</p> <p>ESA/ESRIN contract 4000119910/17/I-NB</p> <p>Reference: ESA_SLBC_cci_D2.4.2</p> <p>Version: v1.2</p> <p>Date: 18.06.2019</p> <p>Page: 58 of 116</p>
---	---	--

4.4.3 Uncertainty documentation in the data products

Detailed information about the uncertainty characterisation is placed in the header of each self-processed OMC time-series file. Specifically, the noise component (in Gt and mm) and the systematic uncertainty of the linear trend (in Gt/yr and mm/yr) are given individually for all assessed uncertainty components. [Due to automated processing, this is also the case for supplementary files without GIA correction applied, but can be ignored in that case]. The file header specifically describes to combine the uncertainties in the form of

$$\sigma^2_{\text{total}}(t) = \sigma^2_{\text{noise}}(t) + (\sigma_{\text{trend}} * (t-t_0))^2$$

for time-series of mass change $m(t)-m(t_0)$ with respect to a reference time t_0 .

The Global OMC time-series data file from Chambers has a standard error given in the last (5th) column for each epoch. It is not to be confused with standard uncertainties from our processing.

4.5 References

- A, G., Wahr, J., and Zhong, S. (2013): Computations of the viscoelastic response of a 3-D compressible Earth to surface loading: an application to Glacial Isostatic Adjustment in Antarctica and Canada. *Geophysical Journal International*, 192(2), 557-572. doi: 10.1093/gji/ggs030.
- Bergmann-Wolf, I., Zhang, L. & Dobslaw, H. (2014). Global Eustatic Sea-Level Variations for the Approximation of Geocenter Motion from Grace. *Journal of Geodetic Science*, 4(1), doi:10.2478/jogs-2014-0006
- Blazquez, A., Meyssignac, B., Lemoine, J. M., Berthier, E., Ribes, A., & Cazenave, A. (2018). Exploring the uncertainty in GRACE estimates of the mass redistributions at the Earth surface: implications for the global water and sea level budgets. *Geophysical Journal International*, 215(1), 415-430.
- Caron, L., Ivins, E. R., Larour, E., Adhikari, S., Nilsson, J., and Blewitt, G. (2018): GIA model statistics for GRACE hydrology, cryosphere, and ocean science. *Geophysical Research Letters*, 45, 2203–2212. doi: 10.1002/2017GL076644.
- Chambers, D. P. (2009): Calculating trends from GRACE in the presence of large changes in continental ice storage and ocean mass, *Geophysical Journal International*, 176(2), 415–419. doi: 10.1111/j.1365-246X.2008.04012.x.
- Chambers, D. P., and J. A. Bonin (2012): Evaluation of Release-05 GRACE time-variable gravity coefficients over the ocean, *Ocean Sci.*, 8, 859–868, doi: 10.5194/os-8-859-2012.
- Chambers, D. P., J. Wahr, M. E. Tamisiea, and R. S. Nerem (2010): Ocean mass from GRACE and glacial isostatic adjustment, *J. Geophys. Res.*, 115, B11415, doi: 10.1029/2010JB007530.
- Cheng, M.K., B. D. Tapley, and J. C. Ries(2013): Deceleration in the Earth's oblateness, *Jour. Geophys. Res.*, V118, 1-8, doi: 10.1002/jgrb.50058, 2013.
- Dobslaw, H., Bergmann-Wolf, I., Dill, R., Forootan, E., Klemann, V., Kusche, J., and Sasgen, I. (2015): The updated ESA Earth System Model for future gravity mission simulation studies, *Journal of Geodesy*, 89, 5, 505–513, doi: 10.1007/s00190-014-0787-8.
- Dobslaw, H., Flechtner, F., Bergmann-Wolf, I., Dahle, C., Dill, R., Esselborn, S., ... , and Thomas, M. (2013): Simulating high-frequency atmosphere-ocean mass variability for dealiasing of satellite

		<p>CCI Sea Level Budget Closure</p> <p>ESA/ESRIN contract 4000119910/17/I-NB</p> <p>Reference: ESA_SLBC_cci_D2.4.2</p> <p>Version: v1.2</p> <p>Date: 18.06.2019</p> <p>Page: 59 of 116</p>
---	---	--

gravity observations: AOD1B RL05. *Journal of Geophysical Research: Oceans*, 118(7), 3704–3711. doi: 10.1002/jgrc.20271.

Flechtner, F., Dobslaw, H., and Fagiolini, E. (2014): *AODIB product description document for product release 05 (Rev. 4.2, May 20, 2014)*. Technical Note, GFZ German Research Centre for Geosciences Department, 1.

Horwath, M.; Novotny, K.; Cazenave, A.; Palanisamy, H.; Marzeion, B.; J.-H. Mallet; Paul, F.; Döll, P.; Cáceres, D.; Hogg, A.; Shepherd, A.; Ootosaka, I.; Forsberg, R.; Barletta, V.R.; Andersen, O.B.; Rannald, H.; Johannessen, J.; Nilsen, J.E.; Gutknecht, B.D.; Merchant, Ch.J.; von Schuckmann, K.: ESA Climate Change Initiative (CCI) Sea Level Budget Closure (SLBC_cci). Product Description Document D3.2: SLBC Assessment Report 2 based on version 1 data. Version 1.1, 08 March 2019.

Johnson, G. C., and D. P. Chambers (2013): Ocean bottom pressure seasonal cycles and decadal trends from GRACE Release-05: Ocean circulation implications, *J. Geophys. Res. Oceans*, 118, 4228–4240, doi: 10.1002/jgrc.20307.

Kusche, J. (2007): Approximate decorrelation and non-isotropic smoothing of time-variable GRACE-type gravity field models. *Journal of Geodesy*, 81(11), 733–749, doi: 10.1007/s00190-007-0143-3.

Kusche, J., Uebbing, B., Rietbroek, R., Shum, C. K., and Khan, Z. H. (2016): Sea level budget in the Bay of Bengal (2002–2014) from GRACE and altimetry. *Journal of Geophysical Research: Oceans*, 121, 1194–1217, doi: 10.1002/2015JC011471.

Luthcke, S. B., Sabaka, T. J., Loomis, B. D., Arendt, A. A., McCarthy, J. J., and Camp, J. (2013): Antarctica, Greenland and Gulf of Alaska land-ice evolution from an iterated GRACE global mascon solution. *J. Glac.*, 59(216), 613–631. doi: 10.3189/2013JoG12J147.

Mayer-Gürr, T., Behzadpour, S., Ellmer, M., Klinger, B., Kvas, A., Strasser, S., & Zehentner, N. (2018a). ITSG-Grace2018: The new GRACE time series from TU Graz. *Abstract from GRACE / GRACE-FO Science Team Meeting 2018*, Potsdam, Germany.

Mayer-Gürr, T.; Behzadpur, S.; Ellmer, M.; Kvas, A.; Klinger, B.; Strasser, S.; Zehentner, N. (2018b): ITSG-Grace2018 - Monthly, Daily and Static Gravity Field Solutions from GRACE. *GFZ Data Services*. <http://doi.org/10.5880/ICGEM.2018.003>

Nagler et al. (2018): ST-UL-ESA-AISCCI-CECR-001_v3.0.pdf: *Comprehensive Error Characterisation Report (CECR)*. An update for the GMA part is given under https://data1.geo.tu-dresden.de/ais_gmb/source/ST-UL-ESA-AISCCI-CECR-Draft_GMB.pdf.

Novotny, K.; Horwath, M.; Cazenave, A.; Palanisamy, H.; Marzeion, B.; Paul, F.; Döll, P.; Cáceres, D.; Hogg, A.; Shepherd, A.; Forsberg, R.; Sørensen, L.; Barletta, V.R.; Andersen, O.B.; Rannald, H.; Johannessen, J.; Nilsen, J.E.; Gutknecht, B.D.; Merchant, Ch.J.; MacIntosh, C.R., von Schuckmann, K. (2018a): ESA Climate Change Initiative (CCI) Sea Level Budget Closure (SLBC_cci) Sea Level Budget Closure Assessment Report D3.1. Version 1.1, 07.05.2018.

Novotny, K.; Horwath, M.; Cazenave, A.; Palanisamy, H.; Marzeion, B.; Paul, F.; Döll, P.; Cáceres, D.; Hogg, A.; Shepherd, A.; Ootosaka, I.; Forsberg, R.; Barletta, V.R.; Andersen, O.B.; Rannald, H.; Johannessen, J.; Nilsen, J.E.; Gutknecht, B.D.; Merchant, Ch.J.; MacIntosh, C.R.; Old, Ch.; von Schuckmann, K. (2018b): ESA Climate Change Initiative (CCI) Sea Level Budget Closure (SLBC_cci). Product Description Document D2.3.2: Version 1 data sets and uncertainty assessments. Version 1.2, 22 Nov 2018.

Novotny, K.; Horwath, M.; Cazenave, A.; Palanisamy, H.; Marzeion, B.; Paul, F.; Döll, P.; Cáceres, D.; Hogg, A.; Shepherd, A.; Forsberg, R.; Sørensen, L.; Barletta, V.R.; Andersen, O.B.; Rannald, H.; Johannessen, J.; Nilsen, J.E.; Gutknecht, B.D.; Merchant, Ch.J.; MacIntosh, C.R.; Old, Ch.; von Schuckmann, K. (2018c): ESA Climate Change Initiative (CCI) Sea Level Budget Closure (SLBC_cci) Science Requirements Updated and Preliminary Thoughts on Roadmap. Version 1.0, 05.06.2018.

		<p>CCI Sea Level Budget Closure</p> <p>ESA/ESRIN contract 4000119910/17/I-NB</p> <p>Reference: ESA_SLBC_cci_D2.4.2</p> <p>Version: v1.2</p> <p>Date: 18.06.2019</p> <p>Page: 60 of 116</p>
---	---	--

- Peltier, W. R. (2004): Global glacial isostasy and the surface of the ice-age Earth: the ICE-5G (VM2) model and GRACE. *Annu. Rev. Earth Planet. Sci.*, 32, 111-149, doi: 10.1146/annurev.earth.32.082503.144359.
- Peltier, W. R., Argus, D. F., and Drummond, R. (2015): Space geodesy constrains ice age terminal deglaciation: The global ICE-6G_C (VM5a) model: Global Glacial Isostatic Adjustment. *J. Geophys. Res. Solid Earth*, 120(1), 450–487. doi: 10.1002/2014JB011176.
- Quinn, K.J, and Ponte, R.M. (2010): Uncertainty in ocean mass trends from GRACE. *Geophys J In*, 181 (2): 762-768. doi: 10.1111/j.1365-246X.2010.04508.x.
- Rietbroek, R, Brunnabend, S-E, Kusche, J, Schröter, J, and Dahle, C (2016):-Revisiting the contemporary sea-level budget on global and regional scales. *PNAS* 2016 113 (6) 1504-1509, doi: 10.1073/pnas.1519132113.
- Swenson, S., and Wahr, J. (2006): Post-processing removal of correlated errors in GRACE data. *Geophysical Research Letters*, 33(8), doi: 10.1029/2005GL025285.
- Swenson S., Chambers D., and Wahr J. (2008): Estimating geocenter variations from a combination of GRACE and ocean model output. *Journal of Geophysical Research: Solid Earth*, 113(B8), doi: 10.1029/2007JB005338.
- Tamisiea, M.E. (2011): Ongoing glacial isostatic contributions to observations of sea level change. *Geophys J Int.*, 186 (3): 1036-1044. doi: 10.1111/j.1365-246X.2011.05116.x.
- Tapley, B. D., Bettadpur, S., Watkins, M., and Reigber, C. (2004): The gravity recovery and climate experiment: Mission overview and early results. *Geophys. Res. Lett.*, 31, L09607. doi: 10.1029/2004GL019920.
- Uebbing, B. , J. Kusche, R. Rietbroek, and F. W. Landerer (2019): Processing choices affect ocean mass estimates from GRACE. *JGR Oceans*, doi: 10.1029/2018JC014341.
- Wahr, J., M. Molenaar, and F. Bryan (1998): Time variability of the Earth's gravity field: Hydrological and oceanic effects and their possible detection using GRACE, *J. Geophys. Res.*, 103(B12), 30205–30229, doi:10.1029/98JB02844.
- Wahr, J., Nerem, R. S., and Bettadpur, S. V. (2015): The pole tide and its effect on GRACE time-variable gravity measurements: Implications for estimates of surface mass variations. *Journal of Geophysical Research: Solid Earth*, 120(6), 4597-4615, doi: 10.1002/2015JB011986.

		<p>CCI Sea Level Budget Closure</p> <p>ESA/ESRIN contract 4000119910/17/I-NB</p> <p>Reference: ESA_SLBC_cci_D2.4.2</p> <p>Version: v1.2</p> <p>Date: 18.06.2019</p> <p>Page: 61 of 116</p>
---	---	--

5 Glacier Contribution to Sea Level Change

5.1 Data Access and Requirements

The glacier evolution model used to calculate glacier mass changes and their contribution to sea level (Marzeion et al. 2012) requires (1) global glacier outlines, (2) atmospheric boundary conditions, and (3) measured mass balances (for calibration and validation) as an input. These datasets are freely available from the following sites: Glacier outlines are taken from the Randolph Glacier Inventory (RGI) version 6.0 (updated from Pfeffer et al. 2014) that provides an initial extent for each of the world's glaciers and is available from glims.org/RGI.

Atmospheric boundary conditions were obtained from 7 different global reanalysis products/gridded observational data sets:

- CRU gridded climate data version 4.01 (updated from Harris et al. 2014) that are available from http://browse.ceda.ac.uk/browse/badc/cru/data/cru_ts/ in combination with the spatially higher resolved climatological dataset CRU CL 2.0 (updated from New et al. 2002) that can be obtained from <https://crudata.uea.ac.uk/cru/data/hrg/tmc/> and is available up to 2016.
- The 20th Century Reanalysis version 2 (20CRv2, Compo et al., 2011) that is available from https://www.esrl.noaa.gov/psd/data/20thC_Rean/. Only anomalies were taken from this dataset, the climatology was obtained from the spatially higher resolved CRU CL 2.0 data set mentioned above. Since this reanalysis only includes data up to 2014, the remaining years were filled using CRU TS version 4.01 (see above).
- The Climate Forecast System Reanalysis (CFSR, Saha et al., 2014) that is available from <https://rda.ucar.edu/datasets/ds093.2/>. Only anomalies were taken from this dataset, the climatology was obtained from the spatially higher resolved CRU CL 2.0 data set mentioned above. Since this reanalysis only includes data between 1979 and 2011, the remaining years were filled using CRU TS version 4.01 (see above).
- The ERA-20C reanalysis (ERA20C, Poli et al., 2016) that is available from <http://apps.ecmwf.int/datasets/data/era20c-mod4/levtype=sfc/type=an/>. Only anomalies were taken from this dataset, the climatology was obtained from the spatially higher resolved CRU CL 2.0 data set mentioned above. Since this reanalysis only includes data up to 2010, the remaining years were filled using CRU TS version 4.01 (see above).
- The ERA-Interim reanalysis (ERA-Interim, Dee et al., 2011) that is available from <http://apps.ecmwf.int/datasets/data/interim-full-mod4/levtype=sfc/>. Only anomalies were taken from this dataset, the climatology was obtained from the spatially

		<p>CCI Sea Level Budget Closure</p> <p>ESA/ESRIN contract 4000119910/17/I-NB</p> <p>Reference: ESA_SLBC_cci_D2.4.2</p> <p>Version: v1.2</p> <p>Date: 18.06.2019</p> <p>Page: 62 of 116</p>
---	---	--

higher resolved CRU CL 2.0 data set mentioned above. Since this reanalysis only includes data starting in 1979, the remaining years were filled using CRU TS version 4.01 (see above).

- The Japanese 55-year reanalysis (JRA55, Kobayashi et al., 2015) that is available from <https://rda.ucar.edu/datasets/ds628.1/>. Only anomalies were taken from this dataset, the climatology was obtained from the spatially higher resolved CRU CL 2.0 data set mentioned above. Since this reanalysis only includes data between 1958 and 2014, the remaining years were filled using CRU TS version 4.01 (see above).
- The Modern-Era Retrospective analysis for Research and Applications, Version 2 (MERRA-2, Gelaro et al., 2017) that is available from <https://disc.gsfc.nasa.gov/datasets?keywords=%22MERRA-2%22&page=1&source=Models%2FAnalyses%20MERRA-2>. Only anomalies were taken from this dataset, the climatology was obtained from the spatially higher resolved CRU CL 2.0 data set mentioned above. Since this reanalysis only includes data starting in 1980, the remaining years were filled using CRU TS version 4.01 (see above).

The model is calibrated and validated using observations of glacier mass balance from the collections of the World Glacier Monitoring Service (WGMS, 2016) that are available from wgms.ch.

5.2 Algorithms

5.2.1 Review of scientific background

The objective of model-based estimates of glacier mass change is to complement observations of glaciers with observations of the state of the atmosphere and physical understanding of glacier mass balance. While there is a growing number of glacier models being developed and used for projecting future glacier change, there is currently only one that allows to reconstruct past and reproduce current glacier change on the global scale, while also accounting for glacier geometry change (Marzeion et al., 2012). We will use this model for all calculations, as a specific aim of this project is also the globally consistent reconstruction of former glacier extents and their contribution to sea level. Special constraints such as storage of water in endorheic basins or potential future lakes forming in overdeepenings (e.g. Haeberli and Linsbauer 2013) of currently still glacier covered glacier beds have to be considered separately.

5.2.2 Algorithms

The model uses global fields of temperature and precipitation rates to estimate the glacier mass balance. Changes in glacier geometry are modeled following an area-volume-time scaling approach, enabling the model to account for various feedbacks between glacier geometry and

		<p>CCI Sea Level Budget Closure</p> <p>ESA/ESRIN contract 4000119910/17/I-NB</p> <p>Reference: ESA_SLBC_cci_D2.4.2</p> <p>Version: v1.2</p> <p>Date: 18.06.2019</p> <p>Page: 63 of 116</p>
---	---	--

mass balance. Glacier geometries obtained through remote sensing (from the RGI) are used to initiate the model, as well as validate results and obtain error characteristics. From the time of initialization, the model is run forward by using volume changes obtained from the mass balance module to calculate changes in glacier area, length, and terminus altitude. Glacier changes prior to the time of initialization are obtained using an iterative process: the model is also run forward during the time preceding the initialization. However, to find the correct starting conditions, the model iteratively searches for that state of the glacier at the beginning of the model run, which results in the observed state of the glacier at the time of glacier observation (i.e., at the time the glacier outlines were obtained). A detailed description of the model is found in Marzeion et al. (2012).

The procedure described above was repeated for all seven forcing data sets, as well as their mean, in order to obtain an ensemble estimate of the glacier mass change. Local (i.e., glacier-specific) parameters were re-calibrated and cross-validated following the procedure described in Marzeion et al. (2012). Global parameters were optimized following a multi-objective optimization routine as described below.

For each of the eight forcing data sets described above, 900 calibration/cross-validation runs of the model were performed, varying the following global parameters:

1. the air temperature above which melt of the ice surface is assumed to occur;
2. the temperature threshold below which precipitation is assumed to be solid;
3. the vertical precipitation gradient used in the model to capture local precipitation patterns not resolved in the forcing data set;
4. a precipitation multiplication factor used in the model to account for effects from (among other things) wind-blown snow and avalanching, not resolved in the forcing data set.

The model performance of each of these in total 7200 model runs was validated employing the leave-one-glacier-out cross validation routine described in 5.4.2. The optimal model configuration (i.e., forcing data set and global parameter set) was then chosen based on the assessment of three criteria:

1. the temporal correlation between modeled and observed mass balances, with a higher correlation indicating a generally higher ability of the model to represent observed glacier mass change;
2. the ratio of the temporal variance of modeled and observed mass balances, with a ratio close to one indicating a realistic sensitivity of the model to climate variability and change;

- the bias (or mean absolute error) of the model, with a bias close to zero indicating a negligible artificial trend in the modeled glacier mass change.

Note that the root mean square error (RMSE) of the model was deliberately not included among the objectives of the optimization, since it can be derived as a combination of the three objectives listed above, and is thus not an independent additional measure of model performance.

Figure 5.1 shows the optimal model run (i.e., results obtained using the optimal parameter set) for each of the eight atmospheric forcings. It turned out that the model forced by the mean of the seven atmospheric data sets performed best. All the results presented below are thus based on the optimal model run forced by the ensemble mean.

Figure 5.2 shows the resulting v2 time series of monthly accumulated glacier contribution in comparison with former v1 and v1 time series. The validation results of the multi-objective optimization are discussed in section 5.4.3.

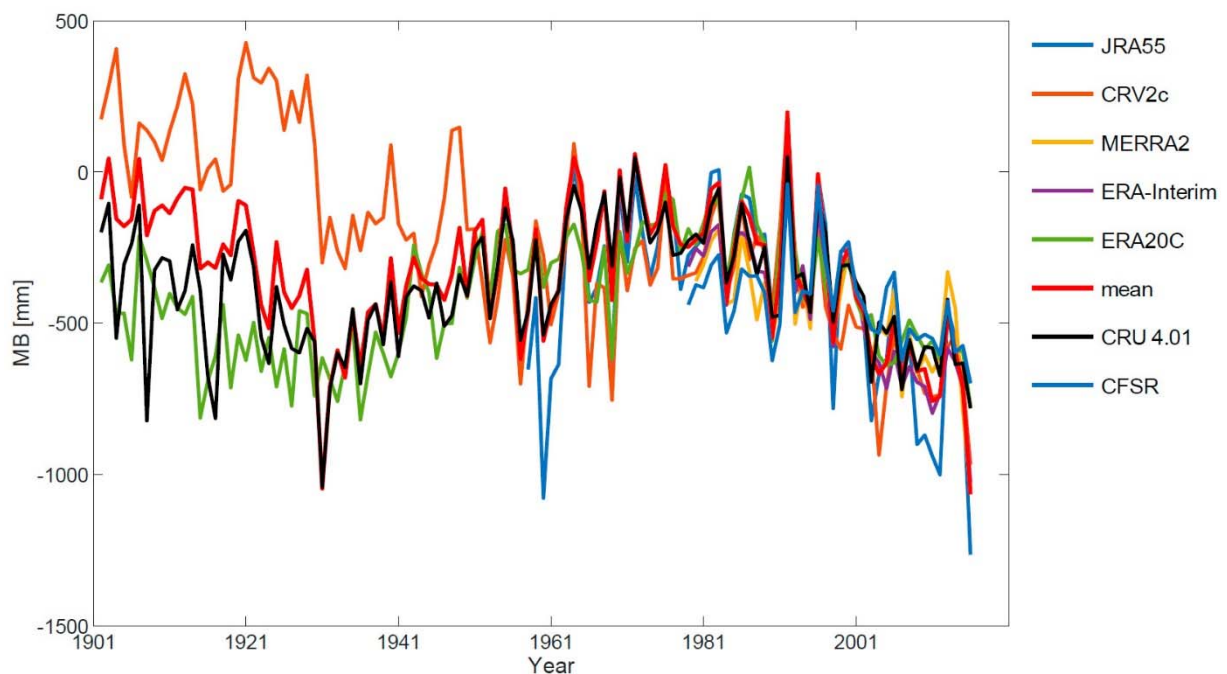


Figure 5.1: Ensemble of reconstructed annual global mean glacier mass balance showing the entire period for each of the eight atmospheric forcing data sets. For each atmospheric data set, the results using the optimal parameter set are shown. The mean forcing (red line) corresponds to the v2 data product.

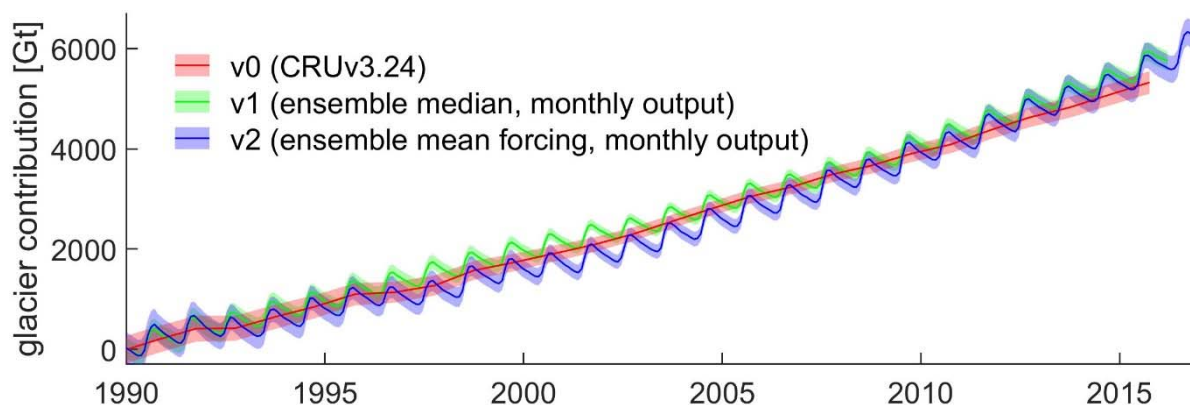


Figure 5.2: Comparison of the temporally accumulated contribution of glaciers to sea-level change of data product version 0, version 1, and final version 2.

5.3 Product Specification

5.3.1 Product geophysical data content

Four variables are given:

1. Glacier mass change is calculated in the unit m water equivalent (w.e.) and multiplied with glacier area (in m^2) and water density (1000 kg m^{-3}) to obtain the mass of water in Gt. This is the temporally accumulated mass contribution of glaciers within each grid cell to sea-level change. Mass loss of glaciers is counted positive (see Figure 5.1). Regional or global values of glacier mass change can be obtained by summing over the region of interest.
2. Uncertainties of glacier mass change are originally also in the unit m w.e. and are converted to Gt. These uncertainties are obtained from the cross-validation of the model using annual values. To obtain the monthly values, it is assumed that each month of the mass balance year contributes equally to the annual uncertainty. The uncertainties are accumulated temporally forward and backward from the initialization year of each glacier, and then accumulated spatially for all glaciers contained within each grid cell. The value from 1. (see above) \pm this uncertainty indicates the 5th to 95th percentile of the uncertainty band. Regional or global values of the uncertainty can be obtained by taking the square root of the sum of the squares of these uncertainties over the region of interest. To convert the given uncertainties to standard uncertainties, the numbers have to be divided by 1.645. The underlying assumption of a normal distribution of errors is supported by the uncertainty assessment.

		CCI Sea Level Budget Closure ESA/ESRIN contract 4000119910/17/I-NB
		Reference: ESA_SLBC_cci_D2.4.2 Version: v1.2 Date: 18.06.2019 Page: 66 of 116

While the global datasets exclude the Greenland peripheral glaciers, separate datasets for these glaciers are also given. In this way, Greenland peripheral glaciers can be excluded or included in the OGGM assessment, depending on whether they are included or excluded within the Greenland Ice Sheet assessment.

Data are provided with the files

glaciers_rgi_v6_monthly.nc and glaciers_rgi_v6_monthly_greenland_periphery.nc

Geophysical Variable	Name in product	Unit
Time	time	decimal year
Latitude	latitude	degrees north
Longitude	longitude	degrees east
Glacier mass change	accumulated glacier mass loss [Gt]	Gt
Uncertainty of glacier mass change (half-width of 90% confidence interval)	uncertainty of accumulated glacier mass loss [Gt]	Gt

glaciers_rgi_v6_annually.nc and glaciers_rgi_v6_annually_greenland_periphery.nc

Geophysical Variable	Name in product	Unit
Time	time	year
Latitude	latitude	degrees north
Longitude	longitude	degrees east
Glacier mass change rate	glacier mass loss rate [Gt yr ⁻¹]	Gt/yr
Uncertainty of glacier mass change rate (half-width of 90% confidence interval)	uncertainty of glacier mass loss rate [Gt yr ⁻¹]	Gt/yr
Glacier mass change	accumulated glacier mass loss [Gt]	Gt
Uncertainty of glacier mass change (half-width of 90% confidence interval)	uncertainty of accumulated glacier mass loss [Gt]	Gt

5.3.2 Coverage and resolution in time and space

Data coverage is global, but excluding peripheral glaciers in Greenland and Antarctica. Data are provided starting 1948 through to 2017. Note that since only three forcing data sets are available for 2017, the forcing for the final year is based on a smaller ensemble, and the uncertainties given are based on the assumption that they remain unaffected by the change in ensemble size. The resolution in space is half a degree and the resolution in time is one month.

		<p>CCI Sea Level Budget Closure</p> <p>ESA/ESRIN contract 4000119910/17/I-NB</p> <p>Reference: ESA_SLBC_cci_D2.4.2</p> <p>Version: v1.2</p> <p>Date: 18.06.2019</p> <p>Page: 67 of 116</p>
---	---	--

The time axis in the annual file is based on mass balance years, which also form the basis for the validation data. This implies that, e.g., the year “2014” refers to the mass change over the period October 2013 to September 2014 in the Northern Hemisphere, and April 2013 to March 2014 in the Southern Hemisphere. This time shift in the annual file between the hemispheres (and relative to the calendar year) is unavoidable, since the objective of providing annual data is to provide uncertainties for the rates of mass change, and these uncertainties are derivable only for mass balance years, based on which observations are reported.

In the monthly file, time stamps are centered in each month, and values indicate the mass change during that month.

5.3.3 Product data format

The data are provided in netcdf4 format.

5.3.4 Product grid and projection

Data are provided on a rectangular grid. Latitude and longitude values of the grid correspond to the center of the grid cell. Each glacier is assigned to that grid cell that contains its center point (as given in the RGIv6.0), even if the glacier stretches across several grid cells.

5.4 Uncertainty assessment

5.4.1 Sources of error

The most relevant sources of error are:

1. uncertainty in the initialization data set (i.e., errors in glacier outlines);
2. simplification of physics in the model (concerning both the mass balance module and the simple representation of ice dynamics);
3. uncertainty in the forcing data (i.e., scarce observations of temperature and precipitation near glaciers that impact the aggregated climate data as well as the reanalysis data used),
4. uncertainty in the observations of glacier mass balance used to calibrate the model,
5. uncertainty in the model calibration.

Uncertainties increase forward and backward in time relative to the year of model initialization, which is typically around the year 2000 (but differs for glaciers individually), since then the model's results depend on the modeled rather than observed glacier geometries, which become more uncertain. This increasing uncertainty is included in the error propagation. On considerably larger time scales, particularly time periods preceding the

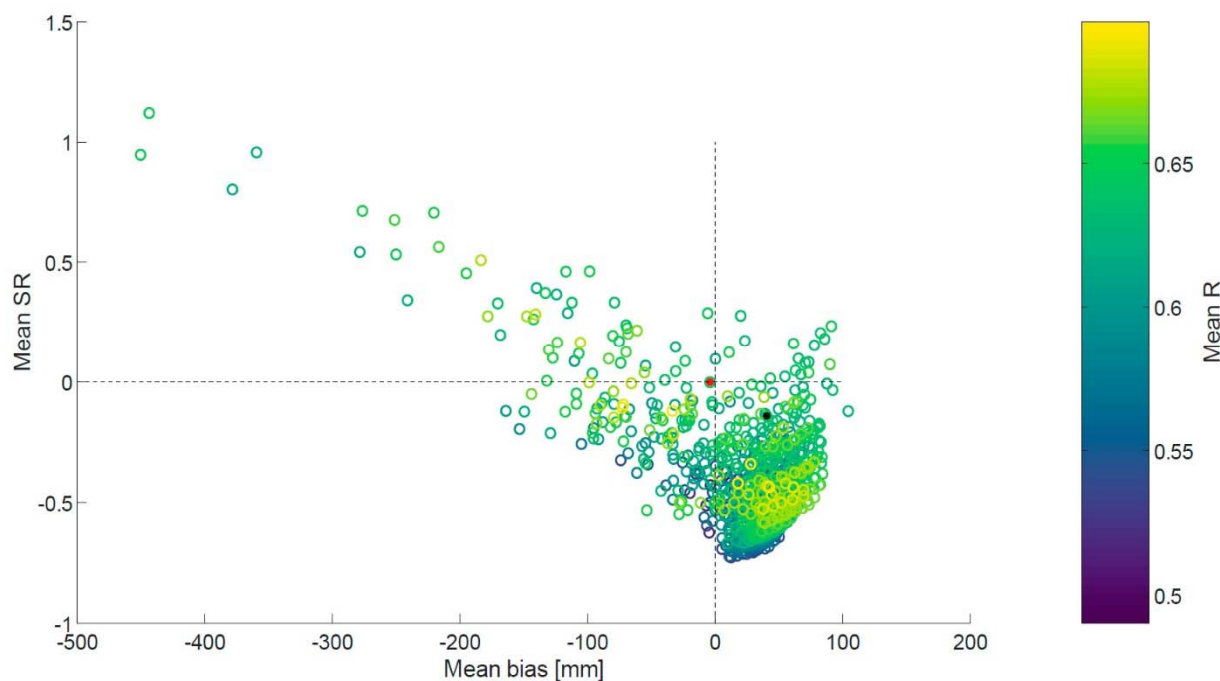


Figure 5.3: Result of the optimization of the glacier model. Vertical axis (SR = standard deviation ratio) shows the normalized ratio of the temporal variance of modeled and observed mass balances (zero is optimal), horizontal axis the model bias (zero is optimal), color the correlation (one is optimal); the colored dots indicate the validation results of the 900 model runs forced by the ensemble mean atmospheric data set. Black dot indicates the results using the standard parameter set. Red dot indicates the optimized parameter set, on which the data product v2 is based.

satellite era, the uncertainty of the atmospheric data used as boundary conditions for the glacier model increases. In principle, this increased uncertainty should be detectable during the validation, but since there are very few validation data points (i.e., in situ glacier mass balance observations) available preceding the satellite era, there is no robust signal of an increased uncertainty detectable. However, we don't believe this unquantified uncertainty is a significant contributor during the period considered here 1979 to 2016, and if so, only in the first few years.

5.4.2 Methodology for uncertainty assessment

The total uncertainty of the resulting glacier mass change estimates is determined using a leave-one-glacier-out cross validation of the glacier model. In this procedure, the out-of-sample uncertainties of the model are measured by:

1. calibrating the model based on glacier observations, but withholding from the calibration all observations from one glacier;
2. running the model for that glacier and determine model error;
3. repeat the above two steps for all glaciers with available mass balance observations.

		<p>CCI Sea Level Budget Closure</p> <p>ESA/ESRIN contract 4000119910/17/I-NB</p> <p>Reference: ESA_SLBC_cci_D2.4.2</p> <p>Version: v1.2</p> <p>Date: 18.06.2019</p> <p>Page: 69 of 116</p>
---	---	--

A total of 255 glaciers with 3997 observed mass balance years was used in this procedure.

As uncertainties in the estimated mass balance feed back to the modeled glacier geometry, these uncertainty estimates were then propagated through the entire model chain, forward and backward in time relative to the year of model initialization. The obtained uncertainty estimates of temporally integrated glacier area and volume change were then validated once more using observations of glacier area and volume change.

5.4.3 Results of uncertainty assessment

Compared to version 0 and the preliminary version 1 of the data product, we now use an ensemble approach, particularly to reduce – as far as possible – error source 3 listed above. The glacier-specific model parameters were recalibrated for each of the ensemble members in each of the 7200 optimization runs.

The multi-objective optimization lead to the following changes in uncertainty measures:

1. the temporal correlation between observed and modeled mass balances was increased from 0.60 (v1) to 0.64 (v2);
2. the ratio of the temporal variance of modeled and observed mass balances was improved from 0.83 (v1) to 1.00 (v2);
3. the model bias was changed from 5 mm w.e. (v1) to -4 mm w.e. (v2, both values statistically indistinguishable from zero).

As a result, the mean RMSE of modeled mass balances for individual glaciers increased from 736 mm w.e. (v1) to 745 mm w.e. (v2). Despite this slight increase in RMSE, our confidence in the model results has grown, most critically by the improved capability of the model to accurately represent the observed variability of mass balance of individual glaciers. The model errors are spatially and temporally uncorrelated. While the model results for any given individual glacier are therefore quite uncertain (RMSE of a similar order of magnitude as the typical annual mass balance), the relative error becomes smaller for ensembles of glaciers (e.g. all glaciers within a grid cell, on a mountain range, or globally).

Since errors grow forward and backward relative to the time of model initialization, and since model initialization occurs at different years for different glaciers (depending on the year the glacier geometry was observed), the uncertainties of rates of mass change are not trivially to derive from the uncertainties of accumulated glacier mass changes. Since validation is only possible of mass balances accumulated within a year, we only provide the uncertainty of accumulated mass balances in the data file of monthly values. Uncertainties in mass change rates are included in the annual data file.

		<p>CCI Sea Level Budget Closure</p> <p>ESA/ESRIN contract 4000119910/17/I-NB</p> <p>Reference: ESA_SLBC_cci_D2.4.2</p> <p>Version: v1.2</p> <p>Date: 18.06.2019</p> <p>Page: 70 of 116</p>
---	---	--

5.4.4 Uncertainty documentation in the data products

The delivered data files contains gridded data of the uncertainty for temporally accumulated mass change (in Gt) on monthly and annual time scale, and for the mass change rates (in Gt/yr) on the annual time scale. See Section 5.3.1.

5.5 References

- Compo, G.P., J.S. Whitaker, P.D. Sardeshmukh, N. Matsui, R.J. Allan, X. Yin, B.E. Gleason, R.S. Vose, G. Rutledge, P. Bessemoulin, S. Brönnimann, M. Brunet, R.I. Crouthamel, A.N. Grant, P.Y. Groisman, P.D. Jones, M. Kruk, A.C. Kruger, G.J. Marshall, M. Maugeri, H.Y. Mok, Ø. Nordli, T.F. Ross, R.M. Trigo, X.L. Wang, S.D. Woodruff, and S.J. Worley (2011): The Twentieth Century Reanalysis Project. *Quarterly J. Roy. Meteorol. Soc.*, 137, 1-28.
- Dee, D. P., Uppala, S. M., Simmons, A. J., Berrisford, P., Poli, P., Kobayashi, S., ... and Bechtold, P. (2011): The ERA-Interim reanalysis: Configuration and performance of the data assimilation system. *Quarterly Journal of the royal meteorological society*, 137(656), 553-597.
- Gelaro, R., McCarty, W., Suárez, M. J., Todling, R., Molod, A., Takacs, L., ... and Wargan, K. (2017): The modern-era retrospective analysis for research and applications, version 2 (MERRA-2). *Journal of Climate*, 30(14), 5419-5454.
- Haeberli, W. and Linsbauer, A. (2013): Brief communication: Global glacier volumes and sea level – small but systematic effects of ice below the surface of the ocean and of new local lakes on land, *The Cryosphere*, 7, 817-821.
- Harris, I. P. D. J., Jones, P. D., Osborn, T. J., and Lister, D. H. (2014): Updated high-resolution grids of monthly climatic observations—the CRU TS3. 10 Dataset. *International Journal of Climatology*, 34(3), 623-642.
- Kobayashi, S., Ota, Y., Harada, Y., Ebata, A., Moriya, M., Onoda, H., ... and Miyaoka, K. (2015): The JRA-55 reanalysis: General specifications and basic characteristics. *Journal of the Meteorological Society of Japan*. Ser. II, 93(1), 5-48.
- Marzeion, B.; Jarosch, A. H.; Hofer, M. (2012): Past and future sea-level change from the surface mass balance of glaciers. *The Cryosphere* 6 (6), 1295–1322, doi: 10.5194/tc-6-1295-2012.
- New, M., Lister, D., Hulme, M., and Makin, I. (2002): A high-resolution data set of surface climate over global land areas. *Climate Research*, 21(1), 1-25, doi: 10.3354/cr021001.
- Pfeffer, W. T., Arendt, A. A., Bliss, A., Bolch, T., Cogley, J. G., Gardner, A. S., ... and Miles, E. S. (2014). The Randolph Glacier Inventory: a globally complete inventory of glaciers. *Journal of Glaciology*, 60(221), 537-552.
- Poli, P., Hersbach, H., Dee, D. P., Berrisford, P., Simmons, A. J., Vitart, F., ... and Trémolet, Y. (2016): ERA-20C: An atmospheric reanalysis of the twentieth century. *Journal of Climate*, 29(11), 4083-4097.
- Saha, S., Moorthi, S., Wu, X., Wang, J., Nadiga, S., Tripp, P., ... and Ek, M. (2014): The NCEP climate forecast system version 2. *Journal of Climate*, 27(6), 2185-2208.
- WGMS (2016): *Fluctuations of Glaciers Database*. World Glacier Monitoring Service, Zurich, Switzerland. DOI: 10.5904/wgms-fog-2016-08. Online access: <http://dx.doi.org/10.5904/wgms-fog-2016-08>.

		CCI Sea Level Budget Closure ESA/ESRIN contract 4000119910/17/I-NB Reference: ESA_SLBC_cci_D2.4.2 Version: v1.2 Date: 18.06.2019 Page: 71 of 116
---	---	---

6 Ice Sheets Contribution to Sea Level Change

Time series for the Greenland Ice Sheet (GrIS) and for the Antarctic Ice Sheet (AIS) are provided. Most of the ice sheet methods and data are documented in the respective ESA CCI Greenland Ice Sheet and Antarctica Ice Sheet documentation.

6.1 Data access and requirements

(1) Greenland Ice Sheet mass changes from GRACE

The data set described here is the time series of mass changes of the Greenland Ice Sheet derived from GRACE data. The product is publicly available as one of the ECVs of the Greenland Ice Sheet CCI, and hence is described in depth in the various documents (deliverables) of this programme. Therefore, it will not be described as thoroughly here. The summary here is based on the reference documents from the Greenland Ice Sheet CCI.

The GRACE-derived time series for Greenland is available for free download at <http://products.esa-icesheets-cci.org/products/downloadlist/GMB/> (for product specifications see Sørensen et al., 2017).

At this site, four products are available: two generated by TU Dresden and two by DTU Space. The data submitted here are the ones derived by DTU Space.

GRACE data are available from different processing centres, in particular the GIS CCI products are available for the release RLO6 provided by CSR and the ITSG-Grace2016 release provided by TU Graz (www.tugraz.at/institute/ifg/downloads/gravity-field-models/itsg-grace2016). The v2 data is identical to the v1 data. It makes use of the CSR, which includes spherical harmonic coefficients up to degree $l_{max}=96$.

(2) Greenland Ice Sheet mass changes from radar altimetry

The data set described here is the annual mean mass loss for the GrIS in the period of ESA radar altimetry (1992-2017). The data are calibrated using the 2003-2009 data from ICESat laser altimetry and snow/firn modelling to both account for firn changes and radar penetration. The combined radar volume change data-series is published in Simonsen and Sørensen (2017) and Sørensen et al. (2018). This document explains the basic information and highlights updates in the conversion of radar volume change to mass change, for details regarding the volume change estimates we refer to the two publications above.

(3) Antarctic Ice Sheet mass changes from GRACE

The data set described here is the time series of mass changes of the Antarctic Ice Sheet derived from GRACE data. The product is publicly available as one of the ECVs of the Antarctic Ice Sheet CCI, and hence is described in depth in the various documents (deliverables) of this

		<p>CCI Sea Level Budget Closure</p> <p>ESA/ESRIN contract 4000119910/17/I-NB</p> <p>Reference: ESA_SLBC_cci_D2.4.2</p> <p>Version: v1.2</p> <p>Date: 18.06.2019</p> <p>Page: 72 of 116</p>
---	---	--

project. The relevant documents are available at ftp://anon-ftp.ceda.ac.uk/neodc/esacci/ice_sheets_antarctica/docs/, namely

- ST-UL-ESA-AISCCI-ATBD-001_v1.0.pdf: Algorithm Theoretical Baseline Document (ATBD)
- ST-UL-ESA-AISCCI-CECR-001_v1.1.pdf: Comprehensive Error Characterisation Report (CECR)
- ST-UL-ESA-AISCCI-PSD-001_v1.1.pdf: Product Specification Document (PSD)
- ST-UL-ESA-AISCCI-PUG-001_v1.2.pdf: Product User Guide (PUG)

The datasets are available from ftp://anon-ftp.ceda.ac.uk/neodc/esacci/ice_sheets_antarctica/data/gravimetric_mass_balance/. In addition, the datasets and the documentation can be obtained at the interactive geodetic data portal of TU Dresden at https://data1.geo.tu-dresden.de/ais_gmb/index.html.

(4) Antarctic Ice Sheet mass changes from altimetry

The data set described here is the time series of ice mass loss for the East Antarctic Ice Sheet (EIAS), the West Antarctic Ice Sheet (WAIS) and the Antarctic Peninsula (AP) for the time period 1992-2016 derived from radar altimetry and a time evolving ice density mask. Data for the 2010-2016 interval is published in McMillan et al. (2014), and the full 25 year time series is in the publication process. This document explains the basic information about the dataset, for details of the plane fit method, please refer to McMillan et al. (2014).

The mass change time series is derived from surface elevation change generated by processing Level 2 elevation measurements provided by ESA, and acquired by multiple radar altimetry satellite missions, ERS-1, ERS-2, ENVISAT and CryoSat-2. The lateral limit used for both the Greenland and Antarctic ice sheet CCI can be found at <http://imbie.org/imbie-2016/>, and this has been provided to the Glaciers and Ice Caps CCI project team.

6.2 Algorithms

6.2.1 Review of scientific background

Ice Sheet mass changes from GRACE (Greenland and Antarctica)

The GRACE mission has two identical space crafts flying about 220 km apart in a near-polar orbit originally at 480 km above the Earth. GRACE maps the Earth's gravity field by making accurate measurements of the distance between the two satellites, using GPS and a microwave ranging system. GRACE-derived solutions of the Earth's time variable gravity field are

		<p>CCI Sea Level Budget Closure</p> <p>ESA/ESRIN contract 4000119910/17/I-NB</p> <p>Reference: ESA_SLBC_cci_D2.4.2</p> <p>Version: v1.2</p> <p>Date: 18.06.2019</p> <p>Page: 73 of 116</p>
---	---	--

available from different processing facilities like CSR, GFZ or JPL. With a typical temporal resolution of one month, GRACE Level-2 products allow the investigation of seasonal and inter-annual variations in addition to long-term changes (Horwath et al., 2012). A comprehensive review of scientific background is found in Khvorostovsky et al. (2016).

Greenland Ice Sheet mass changes from radar altimetry

Satellite radar altimetry is used to derive elevation changes of the GrIS for the given time period. The elevation changes are interpolated to cover the entire ice sheet. The elevation changes are corrected for any elevation change signal that is not associated with ice mass loss (GIA, elastic uplift and changes in firn compaction), by calibrating the radar mass change series by the observations from ICESat.

Antarctic Ice Sheet mass changes from altimetry

The scientific background is described in the Antarctic Ice Sheet Climate Change Initiative (AIS_CCI) Algorithm Theoretical Basis Document (ATBD) (Nagler et al., 2018a).

6.2.2 Algorithms

Greenland Ice Sheet mass changes from GRACE

Methods used for the inference of ice sheet mass changes from GRACE data is an inversion approach as in Barletta et al. (2013). The mass inversion method has been adopted for the GMB product generation, within the GIS_CCI.

A detailed description of the method and associated algorithms is provided in Sect. 6.3.1 of Khvorostovsky et al. (2016).

Greenland Ice Sheet mass changes from radar altimetry

Elevation change method:

The volume change method is derived following Simonsen and Sørensen (2017) and Sørensen et al. (2018).

Conversion from Volume to Mass, including the appropriate corrections:

The mass change estimate is derived in a three-step procedure:

- 1) The coverage of the radar altimetry is limited to ice sheets slopes less than 1.5 degrees. To estimate the volume change of the entire GrIS, the volume change is extrapolated using nearest-neighbor interpolation. This will underestimate the volume change in the fast losing areas for GrIS and is in need of calibration.
- 2) Following the methodology of Sørensen et al. (2011) the volume change is converted into mass change by the appropriate density.

- 3) As the radar volume shown in Figure 6.1, is not accounting for the correction terms given above and the radar also are biased by changing scattering horizon in the firm column (Nilsson et al., 2015) it was decided to account for all of the terms at once by calibrating the mass change rate during the ICESat era.

Antarctic Ice Sheet mass changes from GRACE

The Antarctic Ice Sheet GMB products are derived from the spherical harmonic monthly solution series by ITSG-Grace2016 by TU Graz (Klinger et al., 2016; Mayer-Gürr et al., 2016) following a regional integration approach with tailored integration kernels that account for both the GRACE error structure and the information on different signal variance levels on the ice sheet and on the ocean (Horwath and Groh, 2016).

Antarctic Ice Sheet mass changes from altimetry

The algorithm for elevation changes is described in the Antarctic Ice Sheet Climate Change Initiative (AIS_CCI) Algorithm Theoretical Basis Document (ATBD) (Nagler et al., 2018a) and is summarized here.

Elevation change method

Several methods for deriving elevation changes from repeat laser altimetry exist. Here, we have employed the plane fit method (McMillan et al., 2014). The plane fit method is an adaption of the along track method which can be applied to satellites which operate in both short 27-35 day orbit repeat periods (such as the main operational periods of Envisat, ERS-1,2 and Sentinel-3A,B) and long 369 day repeat periods where measurements do not exactly repeat within monthly time scales such as CryoSat-2.

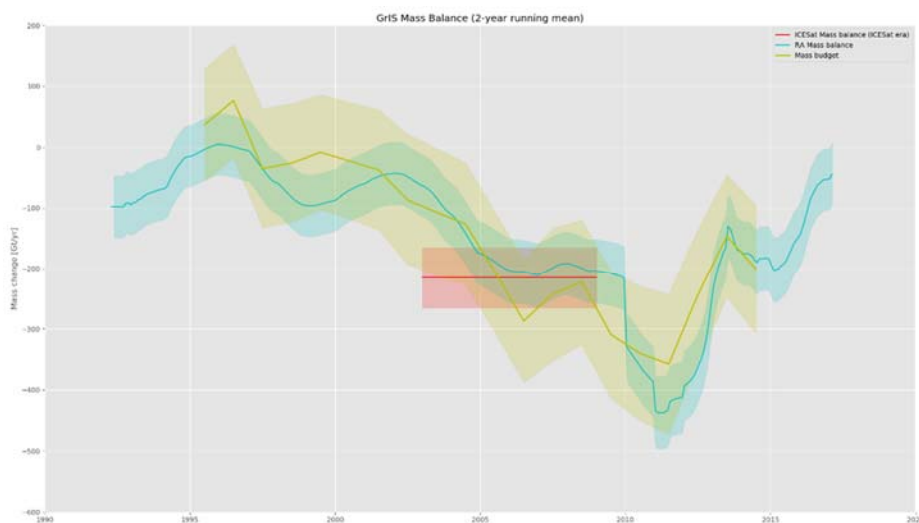


Figure 6.1: Cyan: GrIS volume change estimates from radar altimetry have been converted into mass by scaling to a known mass change field. Here, the “known” field is based on the laser altimetry mass change (Sørensen et al., 2011) (in red). The yellow line indicates an independent mass balance estimate from the bass budget method (Colgan et al., 2019).

		<p>CCI Sea Level Budget Closure</p> <p>ESA/ESRIN contract 4000119910/17/I-NB</p> <p>Reference: ESA_SLBC_cci_D2.4.2</p> <p>Version: v1.2</p> <p>Date: 18.06.2019</p> <p>Page: 75 of 116</p>
---	---	--

The plane fit method grids both ascending and descending measurements in a regular polar stereographic grid instead of gridding separately along track. It derives a surface elevation change estimate at the center of each grid cell by applying a surface model to the measurements within that cell and has been shown in the CCI round robin experiments (Nagler et al. 2018a) to perform as well or better than other along track methods for all missions (except Envisat's drifting phase from Oct 2010- Apr 2012, where special techniques are required for all methods) and hence is the primary along track method chosen for the Antarctic CCI. Another advantage of the plane fit method is that surface elevation change (SEC) results are produced on the same grid as the SEC output product and hence do not require re-gridding which can introduce an additional error and reduce accuracy.

Correction for Glacial Isostatic Adjustment

A post-glacial rebound (PGR) correction was applied to all the residual heights in each selected cell. The correction used was the IJ05_R2 correction, from Ivins and James et al, 2013.

Treatment of unobserved areas

New methods of estimating the SEC of the unobserved regions of the ice sheets have been developed, both between a satellite's ground tracks and beyond the latitude limits of the satellite's orbit.

- Polar hole filling: beyond the orbit limits, SEC is estimated from an annular region, 80°S-81°S. Most drainage basins within that region are treated together but Zwallybasin 18 is a special case: its snow area is treated separately, and its ice area, which includes the Kamb Ice Stream, is used to estimate all unobserved ice, since the unobserved ice area is continuous.
- Between-tracks: the between-track estimates are based on spatially-limited triangulation, followed by a velocity-guided interpolation (using BISICLES) on the ice sheet margins, i.e. within 100km of the coast, and mean estimates elsewhere

Derivation of Height Time Series

Time series calculations used values for elevation change, dz , and time difference, dt , retained after the model-fitting stage and aggregated in 140-day epochs, which were only calculated for grid cells that were observed by satellite. Time series can be calculated over any region. In each case, unobserved grid cells had to be filled.

Inter-Mission Cross Calibration

The previous calculations produced a time series of changes in height per mission. To produce a continuous dataset, biases had to be added between missions. The biasing method used is applied to each grid cell individually, which is known as pixel cross-calibration. In each case,

		<p>CCI Sea Level Budget Closure</p> <p>ESA/ESRIN contract 4000119910/17/I-NB</p> <p>Reference: ESA_SLBC_cci_D2.4.2</p> <p>Version: v1.2</p> <p>Date: 18.06.2019</p> <p>Page: 76 of 116</p>
---	---	--

the biasing aimed to bring ERS1, ERS2 and CryoSat-2 data onto the same baseline as the Envisat data.

Conversion from Volume to Mass

As radar altimeters penetrate some (unknown) depth into the snow surface, direct application of a firm correction to the elevation change measurement, and then derivation of mass at the density of ice from the residual signal, has known issues in Antarctica. Therefore we use a time-evolving density mask to delimit the region where we convert volume to mass at the density of snow (350kg/m³) and ice (917kg/m³). To derive mass change, grid cells are identified as containing changing amounts of either snow or ice, using a time-dependent density mask. In this study the density mask was derived from the pixel cross-calibrated timeseries and the Berkeley Ice Sheet Initiative for Climate Extremes (BISICLES) ice velocity map (Cornford et al, 2013).

Down sampling of mass change time series at annual temporal resolution

The mass change time series is provided with an epoch of 140 day and we additionally provide the mass change time series at annual temporal resolution. The annual estimates are computed by taking the total accumulation at the end of each year from the 140 day timeseries.

6.3 Product Specification

6.3.1 Product geophysical data content

Greenland Ice Sheet mass changes from GRACE

Ice mass changes for the entire ice sheet (Figure 6.2) and for the single basins (cf. Figure 6.3) are estimated and provided. The drainage basins used are an aggregation of those described by Zwally et al. (2012). The mass change is the mass anomaly in Gt (relative to a chosen zero level) with the associated errors (see Forsberg et al., 2013).

The time series for the entire ice sheet is constructed so that the estimate also includes the signal from outlying Glaciers and ice caps, while the individual basin estimates are derived in a way that aims at leaving those out of the solution. Therefore, there is a difference between the mass balance derived from the total time series and the sum of the individual basins. For further information on how ice sheet and the surrounding glaciers and ice caps are separated see Khvorostovsky et al. (2016).

Files provided are stored in a zipped file (CCI_GMB_RL06_time_series_NO_GIA.zip)

and are named: GIS**_grace.dat

where ** denotes the number of the basin (see Figure 6.3), "00" stands for the entire GrIS.

		CCI Sea Level Budget Closure ESA/ESRIN contract 4000119910/17/I-NB
		Reference: ESA_SLBC_cci_D2.4.2 Version: v1.2 Date: 18.06.2019 Page: 77 of 116

Geophysical Variable	Column in file	Unit
Time	1	decimal year
Mass change	2	Gt
Error on mass change	3	Gt
Start epoch for estimating the monthly mean mass change	4	decimal year
End epoch for estimating the monthly mean mass change	5	decimal year

Greenland Ice Sheet mass changes from radar altimetry

We provide a grid of mass change rates at 100x100 km² resolution. Figure 6.2 shows the resulting mass change estimate for the main Greenland ice sheet, excluding weakly-connected ice and peripheral glaciers.

Content of file SLBC_GrIS_RA_MB_vers2.1.nc

Geophysical Variable	Name in product	Unit
Cartesian x-coordinate - easting	x	m
Cartesian y-coordinate - northing	y	m
Time	t	year (decimal)
Latitude	lat	degrees_north
Longitude	lon	degrees_east
Ice sheet mass change rate	mass_change_rate	Gt/year
Uncertainty of mass change rate	mass_change_rate_uncertainty	Gt/year
Ice sheet area in cell	Ice_area	km ²
Projection Type (Name of projection and parameters used)	grid_projection	-

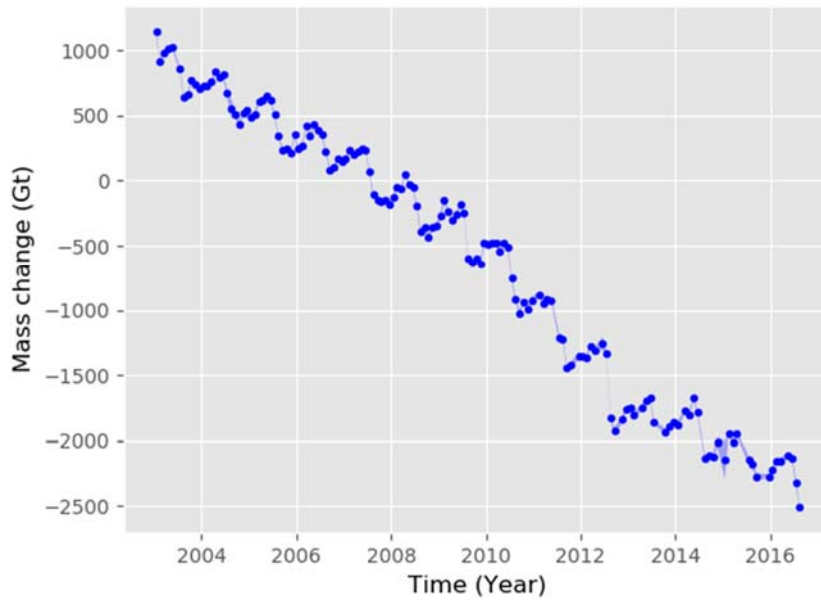



Figure 6.2: GrIS GMB ice mass change time series derived by DTU Space



Figure 6.3: Eight main Greenland Ice Sheet basins (Zwally et al., 2012) colour-coded. Glaciers and ice caps marked with dark blue.

		CCI Sea Level Budget Closure
		ESA/ESRIN contract 4000119910/17/I-NB Reference: ESA_SLBC_cci_D2.4.2 Version: v1.2 Date: 18.06.2019 Page: 79 of 116

Antarctic Ice Sheet mass changes from GRACE

Mass change time series are provided for a number of drainage basins, based on the boundary definitions by Zwally et al. (2012). They describe the evolution of ice mass relative to a modelled reference value. This reference value is defined to be the GRACE-derived mass as of 2009-01-01. Respective time series are also derived for the total areas of the West Antarctic Ice Sheet, the East Antarctic Ice Sheet, the Antarctic Peninsula and the Antarctic Ice Sheet as a whole.

The gridded changes are given in millimetres of equivalent water height (mm w.e., or kg/m²). The applied algorithm is consistent with the one used for the GMB Basin Product.

The file AIS_GMB_basin.dat is an ASCII file that gives GRACE-derived time series of basin-averaged Antarctic ice mass changes in the form

Geophysical Variable	Column in file	Unit
time	1	decimal year
time	2	modified julian data
Mass change (dm) basin1	3	kg
Uncertainty of mass change (sigma dm) basin1	4	kg
dm, sigma dm basin2	5, 6	kg
...	...	
dm, sigma dm basin30	31, 32	kg

The file AIS_GMB_trend.dat gives information, per basin, on the linear trend over the entire time series, on the uncertainties of the linear trends (cf. Section 6.4) and on the GIA correction. This allows, for example, to undo the GIA correction and apply a GIA correction according to a different model. The format is

		CCI Sea Level Budget Closure ESA/ESRIN contract 4000119910/17/I-NB
		Reference: ESA_SLBC_cci_D2.4.2 Version: v1.2 Date: 18.06.2019 Page: 80 of 116

Variable	Column in file	Unit
Basin number	1	
Mass trend	2	kg / yr
Total standard uncertainty of mass trend	3	kg/year
Applied GIA correction	4	kg/year
Basin area	5	m ²

In addition, gridded AIS mass changes from GRACE are given as a grid file in netCDF format. The NetCDF-4 classic file follows the Climate and Forecast (CF) conventions in version 1.6. Changes in ice mass are stored in the NetCDF variable *dm* [kg/m²]. Beside the projected x- and y-coordinates of the grid cell centres, corresponding ellipsoidal latitudes (*lat*) and longitudes (*lon*) are also given. In addition, each grid cell's area (*area*) on the ellipsoid is provided. Times are indicated in two different formats: modified Julian date (*time*) and decimal years (*time_dec*). Additional information on the product and the generating institution are stored in the global attributes.

Content of AIS_GMB_grid.nc

Geophysical Variable	Name in product	Unit
x-coordinate, y-coordinate	x, y	m
Modified Julian Date	time	days
Decimal year	time_dec	year
Longitude, Latitude	lon, lat	degrees_east, degrees_north
Change in ice mass	dm	kg/m ²
Grid cell area on the ellipsoid	area	m ²
Projection Type (Name of projection and parameters used)	crs	-

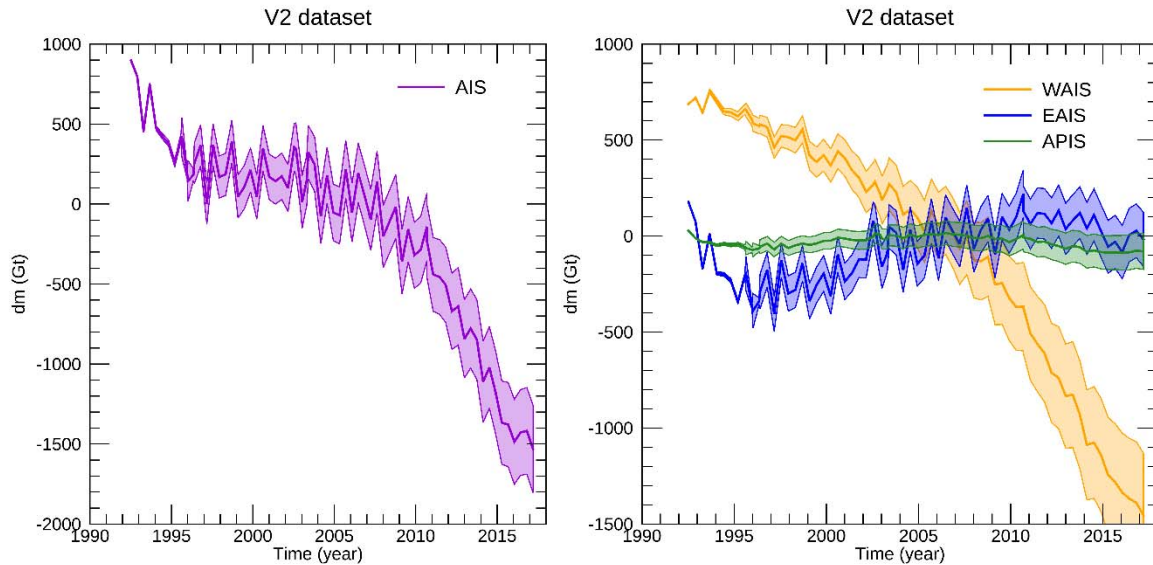


Figure 6.4: Mass change time series from Antarctic Ice sheet derived from radar altimetry by CPOM Leeds

Antarctic Ice Sheet mass changes from altimetry

We provide mass change time series for West Antarctica, East Antarctica and the Antarctic Peninsula as well as for the whole continent. This data is delivered as a comma separated text file for each region, with columns containing information on time, cumulative mass balance, and the measurement uncertainty respectively. Figure 6.4 shows the resulting mass change estimate for the Antarctic ice sheet. The time series are provided with two temporal resolutions, namely with an epoch of 140 days and with annual values.

The 140-day mass change time series are provided in CSV text files

`<NNN>_timeseries_and_uncertainty_varying_err_dens.csv`

where `<NNN>` specifies the region covered:

- AIS ... (entire) Antarctic Ice Sheet
- APIS ... Antarctic Peninsula
- EAIS ... East Antarctic Ice Sheet
- WAIS ... West Antarctic Ice Sheet

Geophysical Variable	Column in file	Unit
Year	1	Decimal year
Cumulative mass change	2	Gt
Uncertainty associated to mass change	3	Gt

		CCI Sea Level Budget Closure	
		ESA/ESRIN contract 4000119910/17/I-NB Reference: ESA_SLBC_cci_D2.4.2 Version: v1.2 Date: 18.06.2019 Page: 82 of 116	

The mass change time series down sampled at annual resolution are provided in CSV text files for the three different subregions. Time series of mass change are provided by the files:

slbc_<NNN>_1yr_epoch.csv

where <NNN> specifies the region covered:

- APIS ... Antarctic Peninsula
- EAIS ... East Antarctic Ice Sheet
- WAIS ... West Antarctic Ice Sheet

For the new annual estimates, the time stamp should be placed at the end of the year (e.g for 1992, it refers to the last day of 1992).

Geophysical Variable	Column in file	Unit
Year (Time of epoch = last day of year)	1	year (integer)
mass change	2	Gt
uncertainty of mass change (σ_{dm})	3	Gt

In the datasets delivered (140-day epoch and 1-yr epoch), the error estimates are cumulative estimates referenced at the start of the timeseries in 1992. We also provide estimates of the non-cumulative error for both the 140-day and 1-yr epoch datasets by the files:

slbc_error_<NNNN>_<TT>_epoch_noncumul.csv

where <NNN> specifies the region covered (see above) and <TT> specifies the temporal resolution (140d, 1yr).

Geophysical Variable	Column in file	Unit
Time of epoch	1	Decimal year ($TT = 140d$) Year ($TT = 1yr$)
Non-cumulative uncertainty associated	2	Gt

		<p>CCI Sea Level Budget Closure</p> <p>ESA/ESRIN contract 4000119910/17/I-NB</p> <p>Reference: ESA_SLBC_cci_D2.4.2</p> <p>Version: v1.2</p> <p>Date: 18.06.2019</p> <p>Page: 83 of 116</p>
---	---	--

6.3.2 Coverage and resolution in time and space

Greenland Ice Sheet mass changes from GRACE

The temporal coverage is constrained by the data availability (2003-2016 for the CSR RL06 solution), and is continuously extended as data become available. The temporal resolution is monthly estimates (some months are missing due to missing data.)

The spatial coverage for the ice mass balance estimate from GRACE are both the entire ice sheet and basins as shown in Figure 6.3.

Greenland Ice Sheet mass changes from radar altimetry

The spatial coverage for the yearly mass change rates is the entire ice sheet with a resolution of 100x100 km². The temporal coverage is from 1992 to 2017.

Antarctic Ice Sheet mass changes from GRACE

AIS mass changes from GRACE cover the entire ice sheet and the period 2002-2016.

Antarctic Ice Sheet mass changes from altimetry

The altimetry time series provided cover West Antarctica (WAIS), East Antarctica (EAIS) and the Antarctic Peninsula (AP) mass change from 1992 to 2017.

Temporal resolution of the time series is 140 days. In addition, annual time series are provided.

6.3.3 Product data format

Greenland Ice Sheet mass changes from GRACE

The data provided here are given in a simple ASCII format.

Greenland Ice Sheet mass changes from radar altimetry

The mass change grid is given in NetCDF4-format at 100x100 km² resolution.

Antarctic Ice Sheet mass changes from GRACE

AIS ice mass changes and mass change trends are given for a number of drainage basins in the ASCII files AIS_GMB_basin.dat and AIS_GMB_trend.dat.

In addition, gridded AIS mass changes from GRACE are given as a grid file in netCDF format (AIS_GMB_grid.nc).

Antarctic Ice Sheet mass changes from altimetry

The mass change time series are provided in CSV text files.

		<p>CCI Sea Level Budget Closure</p> <p>ESA/ESRIN contract 4000119910/17/I-NB</p> <p>Reference: ESA_SLBC_cci_D2.4.2</p> <p>Version: v1.2</p> <p>Date: 18.06.2019</p> <p>Page: 84 of 116</p>
---	---	--

6.3.4 Product grid and projection

Greenland Ice Sheet mass changes from GRACE

No grid definitions apply, since integrated mass changes are provided.

Greenland Ice Sheet mass changes from radar altimetry

The data product is given in EPSG:3413, at 100x100 km² grid.

The mass changes are provided on the ice-sheet covered areas of Greenland, as defined by the ice sheet definition (#4) in the grid¹, the grid resolution is 5x5 km². Counting the 5 x5 km² grid-cells within the 100x100 km² grid gives the estimate of ice sheet area within the given grid-resolution.

Antarctic Ice Sheet mass changes from GRACE

For the map projection utilized for the GMB gridded product a polar stereographic projection with reference latitude at 71°S, reference meridian at 0°, and based on the ellipsoid WGS84 (EPSG3031) is used.

Antarctic Ice Sheet mass changes from altimetry

No grid definitions apply, since integrated mass changes are provided.

6.4 Uncertainty Assessment

For the Greenland Ice Sheet mass changes the uncertainty assessment is described in the Greenland Ice Sheet CCI Comprehensive Error Characterisation Report (CECR) (Forsberg et al., 2013).

For the Antarctic Ice Sheet mass changes the uncertainty assessment is described in the Antarctic Ice Sheet CCI CECR (Nagler et al., 2018b).

6.4.1 Sources of error

Ice Sheet mass changes from GRACE

The error characterization of the GRACE product is provided in detail in Forsberg et al. (2013). Errors in GRACE-derived mass changes have several origins. The three major contributions arise from:

1. GRACE errors in the monthly solutions,
2. Leakage errors due to the limited spatial resolution achieved by GRACE,

¹ available at http://websrv.cs.umt.edu/isis/index.php/Present_Day_Greenland

		CCI Sea Level Budget Closure
		ESA/ESRIN contract 4000119910/17/I-NB Reference: ESA_SLBC_cci_D2.4.2 Version: v1.2 Date: 18.06.2019 Page: 85 of 116

- Errors in models used to reduce superimposed mass signals.

Ice Sheet mass changes from altimetry

The sources of errors are

- Uncertainty in the interpolation of elevation change point estimates into volume change,
- error in the firn compaction,
- error in bedrock movement,
- error from neglecting basal melt and possible ice build-up above the Equilibrium Line Altitude (ELA).
- (5.) Radar altimetry has in addition an error source from changing radar penetration of the firn column.

6.4.2 Methodology for uncertainty assessment

Greenland Ice Sheet mass changes from GRACE

We derive the uncertainties which are related to the data errors provided directly with the GRACE monthly models by using a Monte-Carlo-like approach in which 200 simulations are performed. The simulations are created from Stokes coefficients drawn from normal distributions with zero mean, and the standard deviation provided with the GRACE level-2 data.

In order to give an estimate at basin scale of the effect of the outer glaciers leakage effect, we compute two solutions which represent an upper and lower bound for the mass loss and find that this leakage error is between 4% and 10% of the mass trend.

Table 6.1: Sources and ranges of errors in GrIS GMB

Error source	Estimation procedure	Expected range
GRACE solutions	Propagation of the scaled standard deviation	3.2Gt/yr
GIA model	Intercomparison of different models	7.2Gt/yr
Leakage	Analysis of use of different SA	3.2Gt/yr
Degree one	Intercomparison of different degree one time series	3 Gt/yr
Total	Individual components summed in quadrature	9Gt/yr

		<p>CCI Sea Level Budget Closure</p> <p>ESA/ESRIN contract 4000119910/17/I-NB</p> <p>Reference: ESA_SLBC_cci_D2.4.2</p> <p>Version: v1.2</p> <p>Date: 18.06.2019</p> <p>Page: 86 of 116</p>
---	---	--

The GIA error is meaningful only for the linear trends in mass changes. For the entire GrIS we used the value in Barletta et al. (2013) (Table 6.1). For our best value we chose to use the A et al. (2013) model, which is an ICE5g-VM2 compressible model with rotational feedback. This GIA contribution for Greenland is **-5.4 Gt/yr** and the uncertainty is up to +/- 7.2 Gt/yr. Note that the GIA contribution in the submitted v1 time series is not included.

The results of a thorough (mass trend) uncertainty investigation (Forsberg et al., 2103) revealed the numbers provided in Table 6.2. The error source, estimation procedure and expected range in trend values are provided.

Greenland Ice Sheet mass changes from radar altimetry

Following the error sources above the uncertainty is given as a conservative estimate based on converting the radar altimetry volume error into mass by ascribing ice densities to all grid cells. This estimate is assumed to be slightly overestimating the combined error of the five error sources, however as seen in Figure 6.1 the estimated uncertainty reconciles the radar altimetry mass balance with the GRACE estimate.

Antarctic Ice Sheet mass changes from GRACE

The uncertainty assessment is described in detail in the Antarctic_Ice_Sheet_cci CECR (Nagler et al., 2016), updated under https://data1.geo.tu-dresden.de/ais_gmb/source/ST-UL-ESA-AISCCI-CECR-Draft_GMB.pdf and are analogous to the assessment described in Section 4. Table 6.2 summarizes the uncertainty assessment for the entire Antarctic Ice Sheet.

		CCI Sea Level Budget Closure	
		ESA/ESRIN contract 4000119910/17/I-NB Reference: ESA_SLBC_cci_D2.4.2 Version: v1.2 Date: 18.06.2019 Page: 87 of 116	

Table 6.2: Error components contributing to the overall error budget of the final GMB products for the entire AIS.

Error source	Estimation procedure	standard uncertainty
<u>Basin averaged mass change time series</u>		
Noise	assessed uncorrelated noise level in the GRACE time series	65 Gt
Total		65 Gt
<u>linear trend uncertainty</u>		
GRACE solutions	Propagation of the scaled error rms	2 Gt/yr
GIA model	Intercomparison of different models	32 Gt/yr
Leakage AIS	Analysis of dominant patterns of dynamic mass changes	6 Gt/yr
Leakage non-AIS	Analysis of a global trend pattern (excluding AIS) derived from GRACE	1 Gt/yr
Degree one	Intercomparison of different degree one time series	16 Gt/yr
C20	Intercomparison of different C20 time series	10 Gt/yr
Total	Individual components summed in quadrature	38 Gt/yr

Antarctic Ice Sheet mass changes from altimetry

The uncertainty in mass change is estimated by summing in quadrature the uncertainty associated with our elevation change measurements (taking into account systematic errors, time-varying errors and errors associated with the calculation of inter-satellite biases) and the snowfall variability uncertainty to account for the additional error associated to the identification of ice dynamical imbalance. The total uncertainty is then converted to an equivalent mass change with the density of ice (917 kg m^{-3}) or snow (250 kg m^{-3}) based on our map of ice dynamic imbalance areas.

In response to a request from the project team for the version 2 dataset UoL produced a non-cumulative error estimate for both the annual and 140 day timeseries. The mission cross calibration error was modified, very slightly changing the errors on the SLBC v1 files that were previously provided. Due to this modification, if using the cumulative error the best option is still to use the original files, as the modification of the cross calibration error to get the non-cumulative error was a work around. This will be improved upon in future iterations.

In order to calculate the total AIS non-cumulative error please combine the data from all three sub-regions, i.e. AP, WAIS and EAIS.

		<p>CCI Sea Level Budget Closure</p> <p>ESA/ESRIN contract 4000119910/17/I-NB</p> <p>Reference: ESA_SLBC_cci_D2.4.2</p> <p>Version: v1.2</p> <p>Date: 18.06.2019</p> <p>Page: 88 of 116</p>
---	---	--

6.4.3 Results of uncertainty assessment

See the individual produce releases.

6.4.4 Uncertainty documentation in the data products

Greenland Ice Sheet mass changes from GRACE

Monthly mass change time series per basin are provided with an average monthly error estimate.

Greenland Ice Sheet mass changes from radar altimetry

The uncertainty is provided in the data product as the standard deviation of the elevation change converted into mass as ice densities.

Antarctic Ice Sheet mass changes from GRACE

Uncertainties of monthly values for the basin products are part of the products.

Uncertainties of linear trends are given in the CECR (Nagler et al., 2016) and updated in Table 6.2.

Antarctic Ice Sheet mass change from altimetry

The uncertainty is provided in the data product per epoch as the standard deviation of the error of cumulated mass change.

6.5 References

- A, G., Wahr, J., and Zhong, S. (2013): Computations of the viscoelastic response of a 3-D compressible Earth to surface loading: an application to Glacial Isostatic Adjustment in Antarctica and Canada. *Geophysical Journal International*, 192(2), 557-572.
- Barletta, V. R., Sørensen, L. S., and Forsberg, R. (2013): Scatter of mass changes estimates at basin scale for Greenland and Antarctica. *The Cryosphere*, 7(5), 1411-1432
- Colgan, W., K. Mankoff, K. Kjeldsen, A. Bjørk, J. Box, S. Simonsen, L. Sørensen, S. Khan, A. Solgaard, R. Forsberg, H. Skourup, L. Stenseng, S. Kristensen, S. Hvidegaard, M. Citterio, N. Karlsson, X. Fettweis, A. Ahlstrøm, S. Andersen, D. van As and R. Fausto. (In press): Greenland Ice Sheet mass balance assessed by PROMICE (1995-2015). *Geological survey of Denmark and Greenland Bulletin*, Vol 43.
- Cornford, S. L., Martin, D. F., Graves, D. T., Ranken, D. F., Le Brocq, A. M., Gladstone, R. M., Payne, A. J., Ng, E. G and Lipscomb, W. H. (2013): Adaptive mesh, finite volume modeling of marine ice sheets. *Journal of Computational Physics*, 232(1), 529-549. doi:10.1016/j.jcp.2012.08.037.
- Forsberg, R., L. Sørensen, et al. (2013): *Comprehensive Error Characterisation Report for the Ice_Sheets_cci project of ESA's Climate Change Initiative*, version 1.2, 06 June 2013.
- Horwath, M., and Groh, A. (2016): The GRACE mass change estimators developed for ESA's CCI ice sheet mass balance products. Proc. GRACE Science Team Meeting 2016, Potsdam, 5-7 November 2016. <http://www.gfz-potsdam.de/en/section/global-geomonitoring-and-gravity-field/topics/>

		<p>CCI Sea Level Budget Closure</p> <p>ESA/ESRIN contract 4000119910/17/I-NB</p> <p>Reference: ESA_SLBC_cci_D2.4.2</p> <p>Version: v1.2</p> <p>Date: 18.06.2019</p> <p>Page: 89 of 116</p>
---	---	--

developmentoperation-and-analysis-of-gravity-field-satellite-missions/grace/gstm/gstm-2016/proceedings/.

- Horwath, M., Tranchant, J.-B., van den Broeke, M., Legrésy, B. (2012): Evaluation of GRACE monthly solutions of Release 5 versus Release 4, with an ice sheet perspective. *Proc. GRACE Science Team Meeting*, September 2012, Potsdam, Germany.
- Ivins E., James T., Wahr J., Schrama E., Landerer F., and Simon K. (2013): Antarctic contribution to sea level rise observed by GRACE with improved GIA correction. *J. Geophys. Res.: Solid Earth*, 118(6), 3126-3141, doi:doi.org/10.1002/jgrb.50208.
- Khvorostovsky, et al. (2016): *Algorithm Theoretical Baseline Document (ATBD) for the Greenland_Ice_Sheet_cci project of ESA's Climate Change Initiative*, version 3.1 (ST-DTU-ESA-GISCCI-ATBD-001), 09 Sep 2016.
- Klinger, B., Mayer-Gürr, T., Behzadpour, S., Ellmer, M., Kvas, A., and Zehentner, N. (2016): The new ITSG-Grace2016 release. *Geophys. Res. Abstr.*, 18, EGU2016-11547.
- Mayer-Gürr, T., Behzadpour, S., Ellmer, M., Kvas, A., Klinger, B., and Zehentner, N. (2016): ITSG-Grace2016 - Monthly and Daily Gravity Field Solutions from GRACE. *GFZ Data Services*. doi: 10.5880/icgem.2016.007.
- McMillan, M., Shepherd, A., Sundal, A., Briggs, K., Muir, A., Ridout, A., Hogg, A., Wingham, D. (2014): Increased ice losses from Antarctica detected by CryoSat-2. *Geophysical Research Letters* 41(11), doi: 10.1002/2014GL060111.
- Nagler, T., et al. (2016): *Comprehensive Error Characterisation Report (CECR). Antarctic_Ice_Sheet_cci project, ESA's Climate Change Initiative*, version 1.1, 01 May 2016, Available from: <http://www.esa-icesheets-antarctica-cci.org/>.
- Nagler, T., D. Floricioiu, A. Groh, M. Horwath, A. Kusk, A. Muir, J. Wuite (2018a): *Algorithm Theoretical Basis Document (ATBD) for the Antarctic_Ice_Sheet_cci project of ESA's Climate Change Initiative*, version 2.1, 05 July 2018. Available from: <http://www.esa-icesheets-antarctica-cci.org/>.
- Nagler, T., et al. (2018b): *Comprehensive Error Characterisation Report (CECR). Antarctic_Ice_Sheet_cci project, ESA's Climate Change Initiative*, version 2.1, 05 July 2018. Available from: <http://www.esa-icesheets-antarctica-cci.org/>.
- Nilsson, J., Vallelonga, P., Simonsen, S.B., Sørensen, L.S., Forsberg, R., Dahl-Jensen, D., Hirabayashi, M. (2015): Greenland 2012 Melt Event Effects on CryoSat-2 Radar Altimetry. *Geophysical Research Letters* 42 (10): 3919-26. doi:10.1002/2015GL063296.
- Simonsen, S. B., and Sørensen, L.S: (2017): Implications of Changing Scattering Properties on Greenland Ice Sheet Volume Change from Cryosat-2 Altimetry. *Remote Sensing of Environment* 190 (March). Elsevier Inc.: 207-16. doi:10.1016/j.rse.2016.12.012.
- Sørensen L.S., et al. (2017): *Product Specification Document (PSD) for the Greenland_Ice_Sheet_cci project of ESA's Climate Change Initiative*, version 2.3 (ST-DTU-ESA-GISCCI-PSD-001), 20 March 2017.
- Sørensen, L. S., Simonsen, S. B., Nielsen, K., Lucas-Picher, P., Spada, G., Adalgeirsdóttir, G., ... Hvidberg, C. S. (2011): Mass balance of the Greenland ice sheet (2003-2008) from ICESat data - the impact of interpolation, sampling and firn density. *The Cryosphere*, 5(1), 173-186. <http://doi.org/10.5194/tc-5-173-2011>.
- Sørensen L. S., Simonsen, S.B., Forsberg, R., Khvorostovsky, K., Meister, R., and Engdahl, M. E.. (2018): 25 Years of Elevation Changes of the Greenland Ice Sheet from ERS, Envisat, and CryoSat-2 Radar Altimetry. *Earth and Planetary Science Letters* 495. Elsevier B.V.: 234-41. doi:10.1016/j.epsl.2018.05.015.

		<p>CCI Sea Level Budget Closure</p> <p>ESA/ESRIN contract 4000119910/17/I-NB</p> <p>Reference: ESA_SLBC_cci_D2.4.2</p> <p>Version: v1.2</p> <p>Date: 18.06.2019</p> <p>Page: 90 of 116</p>
---	---	--

Zwally, H. J., M. B. Giovinetto, M. A. Beckley, J. L. Saba (2012): *Antarctic and Greenland Drainage Systems*, GSFC Cryospheric Sciences Laboratory, at http://icesat4.gsfc.nasa.gov/cryo_data/ant_grn_drainage_systems.php.

		<p>CCI Sea Level Budget Closure</p> <p>ESA/ESRIN contract 4000119910/17/I-NB</p> <p>Reference: ESA_SLBC_cci_D2.4.2</p> <p>Version: v1.2</p> <p>Date: 18.06.2019</p> <p>Page: 91 of 116</p>
---	---	--

7 Total Land Water Storage Change

7.1 Data Access and Requirements

Global and gridded time series of total land water storage anomalies (TWSA) were obtained with the global hydrological model WaterGAP2.2d, which is currently applied and developed at the Institute of Physical Geography of the University of Frankfurt. This model version includes improvements over WaterGAP2.2c (used for data products version 1) that will be discussed in the following section.

7.2 Algorithms

7.2.1 Review of scientific background

The latest version of the WaterGAP Global Hydrology Model, WaterGAP2.2d (description paper currently in preparation, submission planned for February 2019), includes a series of model enhancements which differentiate it from the previous version, WaterGAP2.2c. These enhancements are listed below:

- Integration of historic development of irrigated grid cells (1900-2005)
- New standard semi-arid/arid mask
- Modification of groundwater recharge algorithm in semi-arid regions; in case of precipitation below the critical value, the water that does not become groundwater recharge now remains in the soil instead of running off, which increases the soil water content and evapotranspiration
- New consistent river velocity algorithm based on river storage, with adjustment of roughness coefficient to avoid overestimation of velocity
- Elimination of inconsistent (too high) values of domestic and manufacturing water use in coastal areas as defined by the WATCH-CRU ocean land mask
- Elimination of inconsistent negative values of actual consumptive water use; net groundwater abstraction is adjusted when not all net surface water abstraction can be satisfied, and thus return flows from irrigation with surface water are smaller (and net groundwater abstraction therefore larger)

Figure 7.1 (corresponding to forcing WFDEI-GPCC) and Figure A 3 (corresponding to forcing WFDEI-CRU, see Appendix) show that, in terms of globally averaged TWSA over the altimetry era (1992-2016), WaterGAP2.2c standard and WaterGAP2.2d standard only vary slightly for

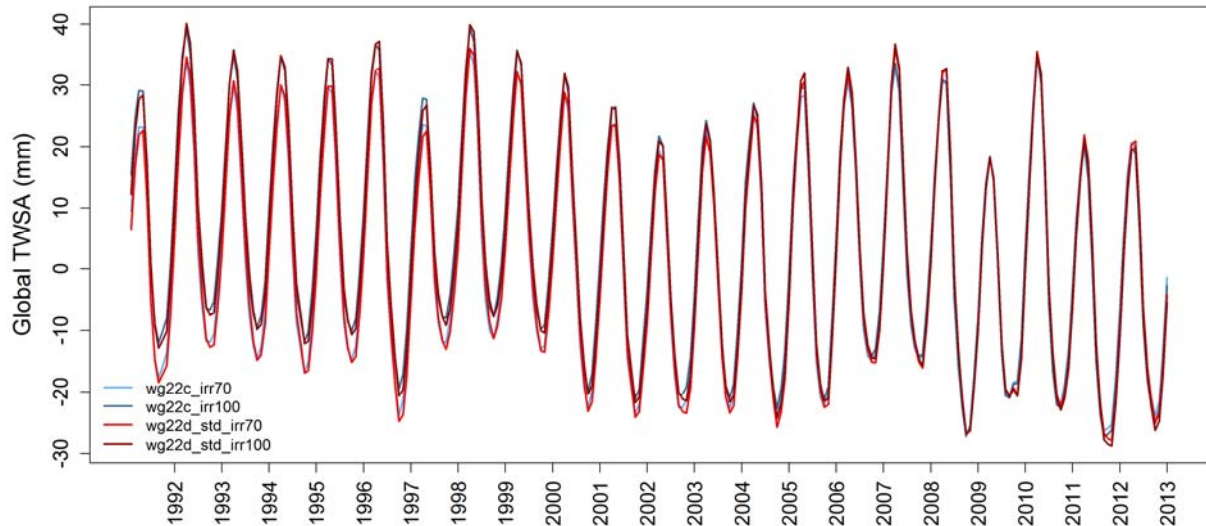


Figure 7.1: Comparison of globally averaged TWSA in mm with respect to the global continental area (except Greenland and Antarctica) as computed by WaterGAP2.2c standard (blue curves) and by WaterGAP2.2d standard (red curves) forced with WFDEI-GPCC for two irrigation variants, either 70% deficit (irr70) irrigation in groundwater depletion areas or optimal (irr100) irrigation. Anomalies are relative to the mean of 2006–2013.

both the 70% deficit irrigation variant and the optimal irrigation variant (for more details on the irrigation variants, please refer to the data description document version 1).

7.2.2 Algorithms

Glacier storage. WaterGAP2.2d standard (hereafter “wg22d_std”) does not include a glacier water storage compartment, and thus the effect of variations in this compartment on the continental water balance is not represented explicitly. However, in order to account for the latter, monthly 0.5° gridded time series of glacier area, glacier mass loss and precipitation on glacier area (provided by WP230) have been implemented in a non-standard version of WaterGAP2.2d (hereafter “wg22d_gl”).

The original data files provided by WP230 are listed below:

- “glacier_area_mean_rgi_v6.nc”; gridded annual glacier area in km^2
- “glacier_mass_mean_rgi_v6_monthly.nc”; gridded monthly cumulated glacier mass loss in Gt
- “model_precipitation_mean.nc”; precipitation (solid plus liquid) on glacier area in km^3

The monthly time series of cumulated glacier mass loss were computed by the Global Glacier Model (hereafter “GGM”) of Marzeion et al. (2012). Note that the model is conceived to output these data for each individual glacier. WaterGAP2.2d has a 0.5° spatial resolution; consequently, the original GGM output data per individual glacier was adapted to be provided

as a 0.5° grid covering the entire globe. In the gridded GGM time series, the mass loss of a glacier that in reality may be spread over several grid cells is assigned to the grid cell where the center of the glacier is located. This also applies to the gridded glacier area and precipitation on glacier area time series.

In order to implement the mentioned glacier-related data sets into WaterGAP2.2d, a number of pre-processing steps had to be applied to the GGM gridded data. As a first step, the GGM grid cells with glacier data (hereafter “glacierized cells”) had to be assigned to the corresponding grid cells of the WaterGAP2.2d grid, defined by the WATCH-CRU ocean-land mask, in terms of geographical location. As a consequence, 49 grid cells from the gridded GGM data were excluded, as they were outside of the boundaries of the mentioned ocean-land mask (see Figure A 1 and Figure A 2 in Appendix). As a reference, the global glacier mass loss over 1948-2016 from the original gridded GGM data amounts to 5730.626 Gt; after the exclusion of the 49 cells, it amounts to 5715.808 Gt (99.7% of 5730.626 Gt) (Figure 7.2). The monthly glacier mass loss and precipitation time series were disaggregated to daily time series to fit the internal computational time step of WaterGAP2.2d. GGM data format was internally transformed from NetCDF to UNF format (WaterGAP-defined binary data format).

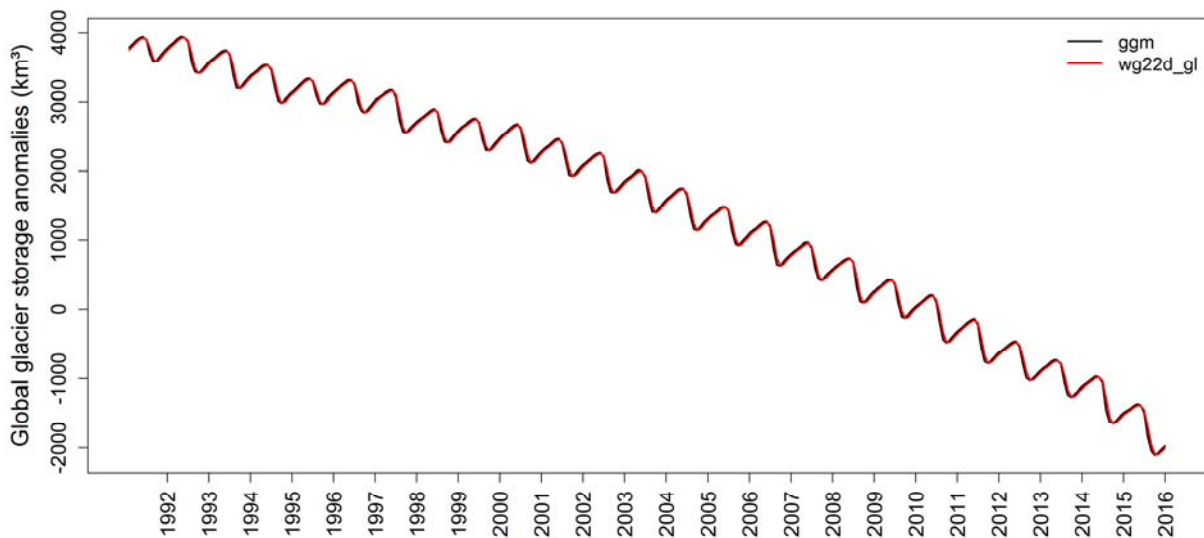


Figure 7.2: Comparison between global glacier water storage anomalies from GGM (black curve) and from the WaterGAP2.2d variant including glaciers explicitly (red curve) in km³. Glacier water storage anomalies from GGM were computed after excluding the grid cells outside of the boundaries of the WATCH-CRU ocean-land mask. All anomalies are relative to the mean of 2006-2015.

		<p>CCI Sea Level Budget Closure</p> <p>ESA/ESRIN contract 4000119910/17/I-NB</p> <p>Reference: ESA_SLBC_cci_D2.4.2</p> <p>Version: v1.2</p> <p>Date: 18.06.2019</p> <p>Page: 94 of 116</p>
---	---	--

In addition, a series of code adaptations were implemented in WaterGAP2.2d. A glacier water storage compartment, assumed to increase with incoming precipitation on glacier area and decrease with outgoing glacier runoff (see Equation 7.1), was included, described by

$$\frac{dS_{gl}}{dt} = P_{gl} - R_{gl} \quad (\text{Equation 7.1})$$

where $\frac{dS_{gl}}{dt}$ are temporal glacier water storage variations, P_{gl} is precipitation on glacier area and R_{gl} is glacier runoff.

$\frac{dS_{gl}}{dt}$ is equal to the glacier mass variations computed by GGM. This is illustrated in Figure 7.2. P_{gl} is also supplied by GGM, and Equation 7.1 is used to compute daily glacier runoff. Moreover, the land area of each WaterGAP grid cell was reduced by the glacier area. The purpose of this reduction was to limit the hydrological processes computed by WaterGAP2.2d (runoff generation, evapotranspiration, infiltration, etc.) to the fraction of continental area without glacier(s). Furthermore, the grid cell precipitation was adapted by adding the precipitation on glacier area (from WP230) to the precipitation from the input forcing corresponding to the fraction of continental area without glacier(s) (see Equation 7.2). For reference, as a result from the adaptation of precipitation in glacierized cells, the global precipitation increased by 657 km³/year on average between 1992 and 2016.

$$P_{cell} = P_{gl} * A_{gl} + P_{rest} * A_{rest} \quad (\text{Equation 7.2})$$

where P_{cell} is grid cell precipitation, P_{gl} is precipitation on glacier area (from WP230), A_{gl} is glacier area, P_{rest} is precipitation on continental area without glacier(s) (from input forcing) and A_{rest} is continental area minus glacier area. Glacier runoff was added to the grid cell fast runoff, which partly flows directly into the river and partly flows to the surface water bodies. It was assumed that glacier runoff does not recharge the groundwater.

Figure 7.3 (corresponding to WFDEI-GPCC forcing) and Figure A 4 (corresponding to WFDEI-CRU forcing, see Appendix) show the difference between global TWSA from wg22d_std and from wg22d_gl (for two irrigation variants). Due to introducing the strongly decreasing glacier storage volume into WaterGAP, the TWSA of the two wg22d_gl variants shows a much stronger decreasing trend over time than wg22d_std, which does not include simulation of glacier mass variations.

In Figure 7.4 (corresponding to WFDEI-GPCC forcing) and Figure A 5 (corresponding to WFDEI-CRU forcing, see Appendix), we can see a comparison of global TWSA as observed by GRACE as provided by WP220 (version 1) and TWSA simulated by different WaterGAP

variants. Inclusion of glacier mass storage anomalies into WaterGAP strongly improves the fit to GRACE TWSA, with the overall interannual variability fitting very well. Performance indicator values (Nash-Sutcliffe Efficiency and correlation coefficient) increase significantly (Table 7.1). Still, before 2008, all WaterGAP results show a phase shift as compared to GRACE, with WaterGAP being approximately one month early. From 2007 to 2010 the lowest GRACE values are underestimated by WaterGAP. Furthermore, we can notice that the magenta curves (anomaly of the sum of TWS from wg22d_std and glacier mass variations from GGM) and the green curves (wg22d_gl) give very similar results throughout the whole period, indicating the land area fraction of the standard version of WaterGAP (without glacier compartment) did not lose a significant amount of water e.g. due to a decrease of snow cover over time. However, as shown in Table 7.1, the wg22d_gl solutions are the best fit to GRACE in terms of Nash-Sutcliffe Efficiency and correlation coefficient; these solutions are plotted against GRACE in Figure 7.5.

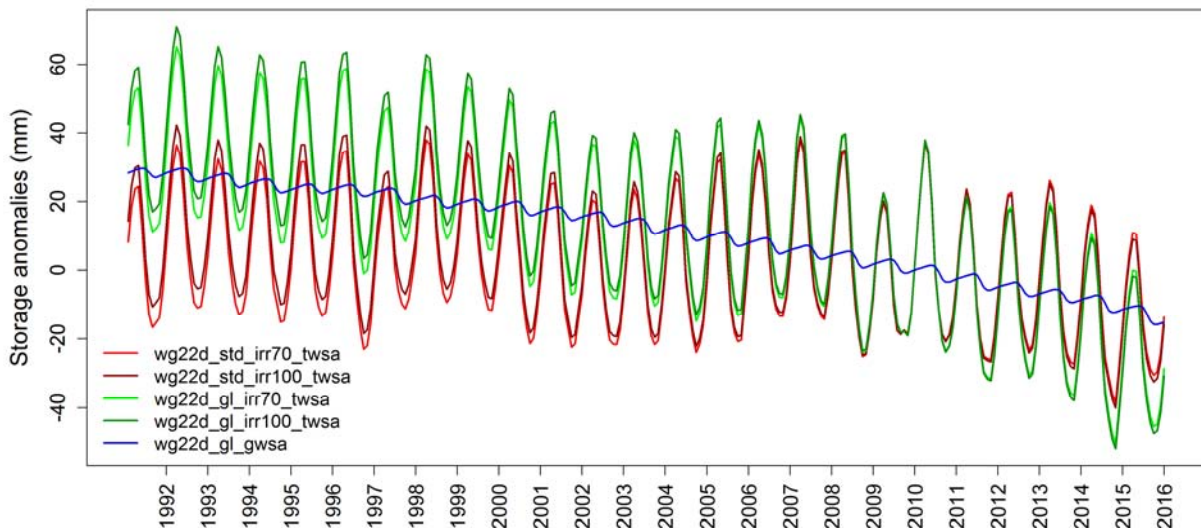


Figure 7.3: Effect of adding a glacier water storage compartment on global TWSA in mm with respect to the global continental area (except Greenland and Antarctica) from WaterGAP2.2d forced with WFDEI-GPCC for two irrigation variants (70% deficit and optimal irrigation variants). Red curves: TWSA from WaterGAP2.2d standard, green curves: TWSA from WaterGAP2.2d variant including glaciers explicitly, blue curve: glacier water storage anomalies from WaterGAP2.2d variant including glaciers explicitly. All anomalies are relative to the mean of 2006-2015.

Table 7.1: Performance indicators values derived from comparison between GRACE-derived (solution provided by WP220 version 1) and modeled TWSA for global land area (except Greenland and Antarctica). The first two rows correspond to WaterGAP2.2d standard, rows 3 and 4 correspond to the WaterGAP2.2d variant including glaciers. Rows 5 and 6 correspond to the TWSA derived from the sum of TWS from WaterGAP2.2d standard and glacier water storage from GGM. All modeling solutions are given for the 70% deficit and the optimal irrigation variants. NSE: Nash-Sutcliffe efficiency, r: Pearson product-moment correlation coefficient.

WFDEI-GPCC	NSE	r	WFDEI-CRU	NSE	r
wg_std_ir70	0.7208	0.8522	wg_std_ir70	0.7703	0.8837
wg_std_ir100	0.7611	0.8762	wg_std_ir100	0.8025	0.9023
wg_gl_ir70	0.8715	0.9379	wg_gl_ir70	0.8777	0.9417
wg_gl_ir100	0.8685	0.9382	wg_gl_ir100	0.8687	0.9392
ggm_wg22d_std_ir70	0.8627	0.9345	ggm_wg22d_std_ir70	0.8706	0.9392
ggm_wg22d_std_ir100	0.8594	0.9354	ggm_wg22d_std_ir100	0.8606	0.9371

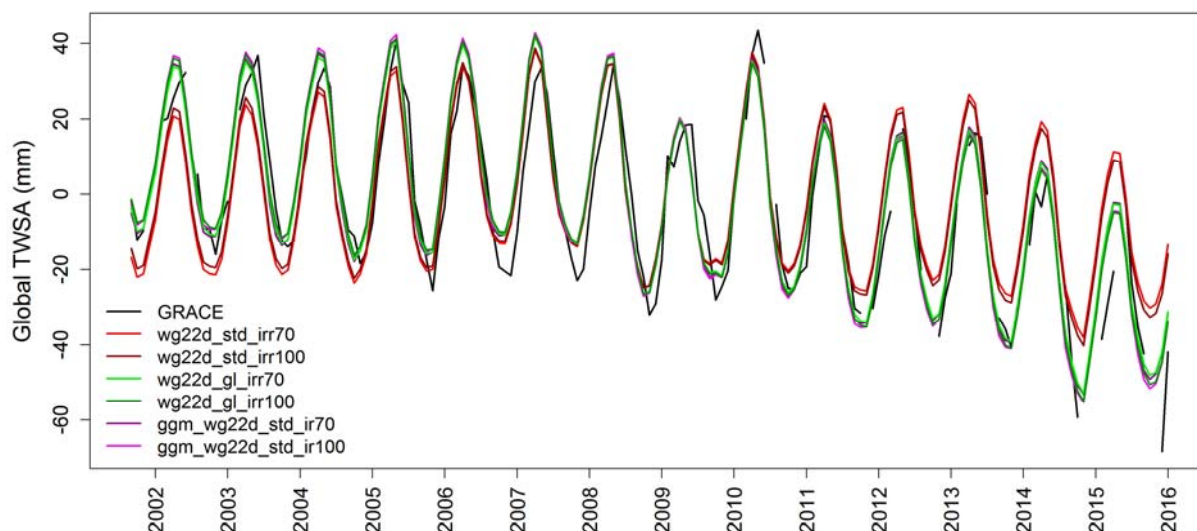


Figure 7.4: Comparison between global TWSA in mm with respect to the global continental area (except Greenland and Antarctica) from GRACE (solution provided by WP220 version 1) and from modeling (WFDEI-GPCC) for two irrigation variants (70% deficit and optimal irrigation variants). Black curve: GRACE, red curves: WaterGAP2.2d standard, green curves: WaterGAP2.2d variant including glaciers explicitly. The magenta curves were obtained by summing TWS from WaterGAP2.2d standard and glacier water storage from GGM, and deriving anomalies. All anomalies are relative to the mean of January 2003 – January 2016.

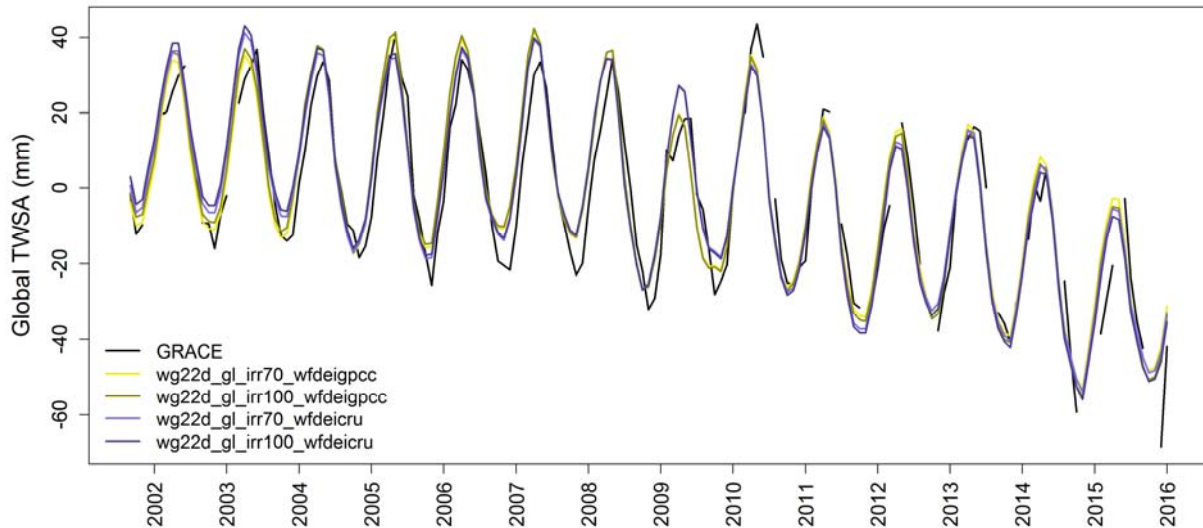


Figure 7.5: Comparison between global TWSA in mm with respect to the global continental area (except Greenland and Antarctica) from GRACE (solution provided by WP220 version 1) and from WaterGAP2.2d for two irrigation variants (70% deficit and optimal irrigation variants). Black curve: GRACE, yellow curves: WaterGAP2.2d variant including glaciers explicitly forced with WFDEI-GPCC, blue curves: WaterGAP2.2d variant including glaciers explicitly forced with WFDEI-CRU. All anomalies are relative to the mean of January 2003 January 2016.

7.3 Product Specification

7.3.1 Product geophysical data content

Two versions of WaterGAP2.2d (wg22d_std and wg22d_gl) were run with two irrigation variants (70% deficit irrigation variant and optimal irrigation variant) and two state-of-the-art climate forcings:

- daily WFDEI (“WATCH Forcing Data methodology applied to ERA-Interim data”) dataset (Weedon et al. 2014) with precipitation bias-corrected using GPCC monthly precipitation sums (Schneider et al. 2015) (WFDEI-GPCC)
- daily WFDEI dataset with precipitation bias-corrected using CRU TS 3.23 monthly precipitation sums (Harris et al. 2014) (WFDEI-CRU)

Eight gridded datasets (2 model versions * 2 climate forcings * 2 irrigation variants) of TWSA are provided. As complementary information, a gridded dataset with continental area information for each grid cell is provided (see Table 7.4 and Table 7.5). Time series of globally averaged TWSA (relative to the mean of 2006-2015) are provided as text files and are described in Table 7.2 and Table 7.3.

		CCI Sea Level Budget Closure ESA/ESRIN contract 4000119910/17/I-NB
		Reference: ESA_SLBC_cci_D2.4.2 Version: v1.2 Date: 18.06.2019 Page: 98 of 116

Table 7.2: Files of globally averaged data provided for sea level budget assessment version 2.

Geophysical Variable	Unit	Time step	Period	File name
Total water storage anomalies (WFDEI-GPCC)	mm	monthly and annual	1992-2016	twsa_WaterGAP22d_std_wfdeigpcc_mm_irr70_version2_month1992_2016.txt twsa_WaterGAP22d_std_wfdeigpcc_mm_irr70_version2_year1992_2016.txt twsa_WaterGAP22d_std_wfdeigpcc_mm_irr70_version2_yearinmonth1992_2016.txt twsa_WaterGAP22d_std_wfdeigpcc_mm_irr100_version2_month1992_2016.txt twsa_WaterGAP22d_std_wfdeigpcc_mm_irr100_version2_year1992_2016.txt twsa_WaterGAP22d_std_wfdeigpcc_mm_irr100_version2_yearinmonth1992_2016.txt twsa_WaterGAP22d_gl_wfdeigpcc_mm_irr70_version2_month1992_2016.txt twsa_WaterGAP22d_gl_wfdeigpcc_mm_irr70_version2_year1992_2016.txt twsa_WaterGAP22d_gl_wfdeigpcc_mm_irr70_version2_yearinmonth1992_2016.txt twsa_WaterGAP22d_gl_wfdeigpcc_mm_irr100_version2_month1992_2016.txt twsa_WaterGAP22d_gl_wfdeigpcc_mm_irr100_version2_year1992_2016.txt twsa_WaterGAP22d_gl_wfdeigpcc_mm_irr100_version2_yearinmonth1992_2016.txt
Total water storage anomalies (WFDEI-CRU)	mm	monthly and annual	1992-2016	twsa_WaterGAP22d_std_wfdeicru_mm_irr70_version2_month1992_2016.txt twsa_WaterGAP22d_std_wfdeicru_mm_irr70_version2_year1992_2016.txt twsa_WaterGAP22d_std_wfdeicru_mm_irr70_version2_yearinmonth1992_2016.txt twsa_WaterGAP22d_std_wfdeicru_mm_irr100_version2_month1992_2016.txt twsa_WaterGAP22d_std_wfdeicru_mm_irr100_version2_year1992_2016.txt twsa_WaterGAP22d_std_wfdeicru_mm_irr100_version2_yearinmonth1992_2016.txt twsa_WaterGAP22d_gl_wfdeicru_mm_irr70_version2_month1992_2016.txt twsa_WaterGAP22d_gl_wfdeicru_mm_irr70_version2_year1992_2016.txt twsa_WaterGAP22d_gl_wfdeicru_mm_irr70_version2_yearinmonth1992_2016.txt twsa_WaterGAP22d_gl_wfdeicru_mm_irr100_version2_month1992_2016.txt twsa_WaterGAP22d_gl_wfdeicru_mm_irr100_version2_year1992_2016.txt twsa_WaterGAP22d_gl_wfdeicru_mm_irr100_version2_yearinmonth1992_2016.txt

Table 7.3: Geophysical data content of globally averaged files.

File name	Geophysical Variable	Name in product	Unit
month.txt	Time	month	month counted with reference epoch 1992-01
	TWSA (globally averaged per month)	value_mm	mm over global continental area (sum of grid cell continental areas from contarea_wghm_wlm.nc)
year.txt	Time	year	year (integer)
	TWSA (globally averaged per year)	value_mm	mm over global continental area
yearinmonth.txt	Time	year	month counted with reference epoch 1992-01
	TWSA (globally averaged per year)	value_mm	mm over global continental area, annual mean which is given as value for each month

		CCI Sea Level Budget Closure ESA/ESRIN contract 4000119910/17/I-NB
		Reference: ESA_SLBC_cci_D2.4.2 Version: v1.2 Date: 18.06.2019 Page: 99 of 116

Table 7.4: Files of monthly gridded data provided for sea level budget assessment version 2.

Geophysical Variable	Name in product	Unit	Period	File name
Total water storage anomalies (WFDEI-GPCC)	twsa	mm	1992-2016	twsa_WaterGAP22d_std_WFDEI_GPCC_mm_irr70_version2.nc twsa_WaterGAP22d_std_WFDEI_GPCC_mm_irr100_version2.nc twsa_WaterGAP22d_gl_WFDEI_GPCC_mm_irr70_version2.nc twsa_WaterGAP22d_gl_WFDEI_GPCC_mm_irr100_version2.nc
Total water storage anomalies (WFDEI-CRU)	twsa	mm	1992-2016	twsa_WaterGAP22d_std_WFDEI_CRU_mm_irr70_version2.nc twsa_WaterGAP22d_std_WFDEI_CRU_mm_irr100_version2.nc twsa_WaterGAP22d_gl_WFDEI_CRU_mm_irr70_version2.nc twsa_WaterGAP22d_gl_WFDEI_CRU_mm_irr100_version2.nc
Continental area	contarea	km ²	-	contarea_wghm_wlm.nc

Table 7.5: Geophysical data content of gridded files.

File name	Geophysical Variable	Name in product	Unit
all files	Latitude	lat	degrees north
	Longitude	lon	degrees east
twsa_*.nc	Time	time	months since 1992-01-01
	total water storage anomalies (excluding Greenland)	twsa	mm (over grid cell continental area, see contarea_wghm_wlm.nc)
contarea_*.nc	Time	time	not used
	continental area (excluding Greenland)	contarea	km ²

7.3.2 Coverage and resolution in time and space

Gridded time series are given for the global continental area, with the exception of Antarctica and Greenland. For the globally averaged time series, an area-weighted average was used. Weighting areas are so-called “continental areas” that in case of coastal cells exclude the part of the 0.5° grid cell that is ocean.

7.3.3 Product data format

Gridded time series of TWSA as well as of continental area are provided in a NetCDF format. Globally averaged time series of TWSA are provided in a text format (see Table 7.2 and Table 7.4).

		<p>CCI Sea Level Budget Closure</p> <p>ESA/ESRIN contract 4000119910/17/I-NB</p> <p>Reference: ESA_SLBC_cci_D2.4.2</p> <p>Version: v1.2</p> <p>Date: 18.06.2019</p> <p>Page: 100 of 116</p>
---	---	---

7.3.4 Product grid and projection

The WATCH-CRU ocean-land mask, covering 67420 $0.5^{\circ} \times 0.5^{\circ}$ grid cells, was used for the simulations.

7.4 Uncertainty Assessment

7.4.1 Sources of error

For data products version 2, the uncertainty in simulated TWSA due to spatially distributed climate input data and to the modeling approach with respect to, on the one hand, the explicit simulation of glaciers and, on the other hand, the irrigation water use in groundwater depletion regions (choice between two irrigation variants) was considered by running different model variants.

7.4.2 Methodology for uncertainty assessment

In order to assess the uncertainty due to the three sources of error mentioned above, the following model variants were used to compute monthly time series of TWS and derive TWSA relative to the mean of 2006-2015:

- Wg22d_std, 70% deficit irrigation, WFDEI-GPCC forcing
- Wg22d_std, 70% deficit irrigation, WFDEI-CRU forcing
- Wg22d_std, optimal irrigation, WFDEI-GPCC forcing
- Wg22d_std, optimal irrigation, WFDEI-CRU forcing
- Wg22d_gl, 70% deficit irrigation, WFDEI-GPCC forcing
- Wg22d_gl, 70% deficit irrigation, WFDEI-CRU forcing
- Wg22d_gl, optimal irrigation, WFDEI-GPCC forcing
- Wg22d_gl, optimal irrigation, WFDEI-CRU forcing

The two irrigation variants are considered equally plausible.

7.4.3 Results of uncertainty assessment

Figure 7.6 shows that global TWSA is not very dependent on climate forcing. The impact of using different irrigation variants (70% deficit variant and optimal variant) is also rather small at the global scale. This can be partly explained by the fact that the two irrigation variants differ only at the scale of groundwater depletion regions, not at the scale of the global land area. The impact is larger at the scale of individual grid cells.

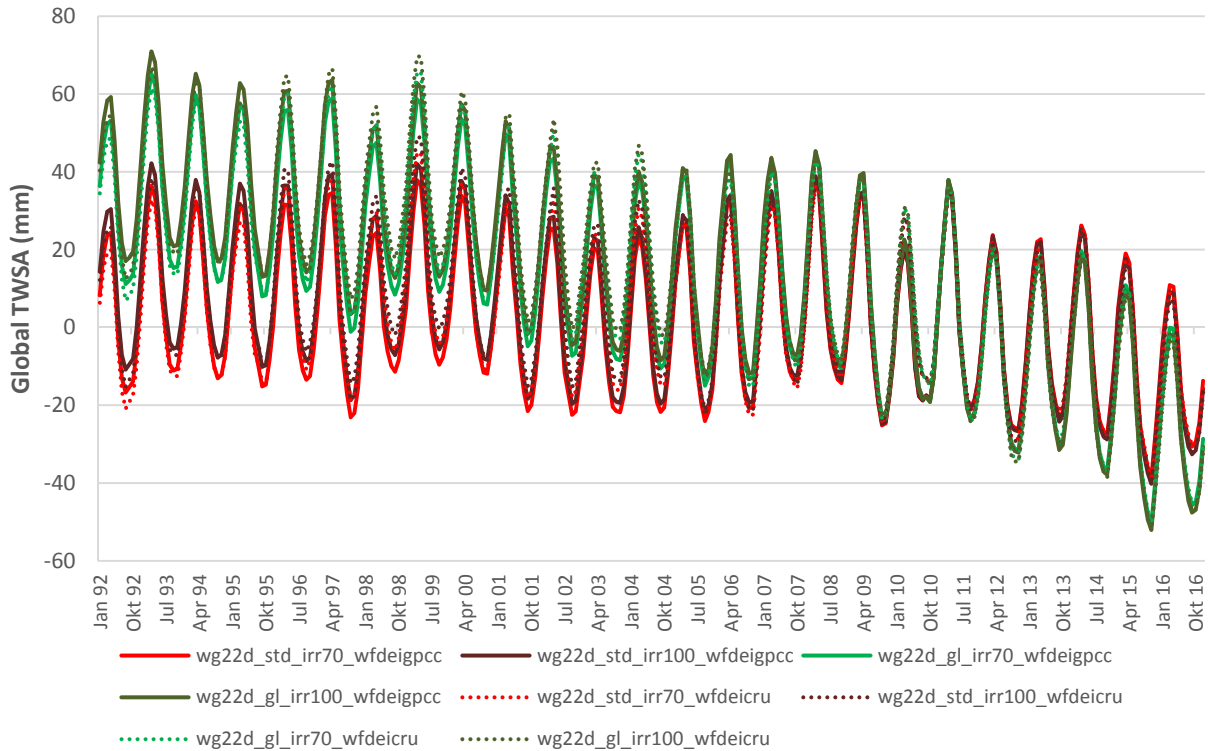


Figure 7.6: Comparison between global TWSA in mm with respect to the global continental area (except Greenland and Antarctica) from WaterGAP2.2d for two irrigation variants (70% deficit and optimal irrigation variants). Solid red curves: WaterGAP2.2d standard forced with WFDEI-GPCC, solid green curves: WaterGAP2.2d variant including glaciers explicitly forced with WFDEI-GPCC, dotted red curves: WaterGAP2.2d standard forced with WFDEI-CRU, dotted green curves: WaterGAP2.2d variant including glaciers explicitly forced with WFDEI-CRU. All anomalies are relative to the mean of 2006-2015.

Furthermore, Figure 7.6 also shows that the differences between `wg22d_std` (standard version) and `wg22d_gl` (inclusion of glaciers) are considerable and constitute the largest part of the uncertainty; overall, `wg22d_gl` shows a more negative trend than `wg22d_std` due to globally decreasing glacier storage volume.

7.4.4 Uncertainty documentation in the data products

No uncertainty ranges are provided in the data products.

		<p>CCI Sea Level Budget Closure</p> <p>ESA/ESRIN contract 4000119910/17/I-NB</p> <p>Reference: ESA_SLBC_cci_D2.4.2</p> <p>Version: v1.2</p> <p>Date: 18.06.2019</p> <p>Page: 102 of 116</p>
---	---	---

7.5 References

- Harris, I.; Jones, P.D; Osborn, T.J; and Lister, D.H (2014): Updated high-resolution grids of monthly climatic observations - the CRU TS3.10 dataset. *Int. J. Climatol.* 34 (3), pp. 623–642. DOI: 10.1002/joc.3711.
- Marzeion, B.; Jarosch, A. H.; and Hofer, M. (2012): Past and future sea-level change from the surface mass balance of glaciers. *The Cryosphere* 6 (6), pp. 1295–1322. DOI: 10.5194/tc-6-1295-2012.
- Schneider, U.; Becker, A.; Finger, P.; Meyer-Christoffer, A.; Rudolf, B.; and Ziese, M. (2015): GPCP Full Data Reanalysis Version 7.0 at 0.5°: Monthly Land-Surface Precipitation from Rain-Gauges built on GTS-based and Historic Data. *Research Data Archive at the National Center for Atmospheric Research, Computational and Information Systems Laboratory, Boulder, Colo.* (Updated irregularly.). DOI: 10.5676/DWD_GPCP/FD_M_V7_050.
- Weedon, G. P.; Balsamo, G.; Bellouin, N.; Gomes, S.; Best, M. J.; and Viterbo, P. (2014): The WFDEI meteorological forcing data set. WATCH Forcing Data methodology applied to ERA-Interim reanalysis data. *Water Resour. Res.* 50 (9), pp. 7505–7514. DOI: 10.1002/2014WR015638.

		<p>CCI Sea Level Budget Closure</p> <p>ESA/ESRIN contract 4000119910/17/I-NB</p> <p>Reference: ESA_SLBC_cci_D2.4.2</p> <p>Version: v1.2</p> <p>Date: 18.06.2019</p> <p>Page: 103 of 116</p>
---	---	---

8 Arctic Sea Level Change

For the Arctic, sea level heights from satellite altimetry as well as sea level heights and steric sea level from the TOPAZ4 model are provided and described in the following sections. Note, that the sea level heights from the TOPAZ4 model are updated till 2017.

8.1 Data Access and Requirements

The altimetric sea level anomaly (SLA) record is obtained from ERS-2, Envisat, and CryoSat-2 data north of 65°N to 81.2°N. The SLA is obtained by measuring the range between the satellite altimeter and the underlying surface. Measuring the range between the satellite altimeter and the underlying sea surface yields the sea surface height, which then is referenced to a mean sea surface to obtain SLA. The more homogenous the underlying surface is, the easier it is to estimate the correct range from the altimeter waveform. Large parts of the Arctic Ocean have a permanent or seasonal sea ice cover, which makes accurate range estimation difficult.

In addition, data on both sea level change and steric sea level change are also obtained from the TOPAZ4 data assimilation system operated at NERSC. This system represents the Arctic Marine Forecasting Center of the Copernicus Marine Services (<http://marine.copernicus.eu/>). The system delivers routinely products and information used for analyses, forecast (up to 10 days) and reanalyses.

8.2 Algorithms

8.2.1 Review of scientific background

DTU Arctic Altimetric Sea Level Record: To obtain the altimetric SLA record, ERS-2 and Envisat data have been retracked using the Adaptive Leading Edge Subwaveform (ALES+) retracker. The ALES+ (Passaro et al., 2018) retracker is similar to the original ALES retracker (Passaro et al., 2014), but has been adjusted to fit waveform returns from all types of water surfaces, i.e. not only open ocean, but also coastal areas, lakes and rivers, and sea ice covered areas. 1 Hz CryoSat-2 data in LRM and SAR mode were taken from the Radar Altimetry Database System (RADS, Scharoo et al., 2013). However, 20 Hz CryoSat-2 SAR and SARIn data have been retracked by the Lars Advanced Retracking System (LARS) system (Stenseng, 2011), since RADS is not able to handle 20 Hz data, which is necessary in order to retrieve height estimates from leads in-between sea ice.

The retracking methods used for the v2 data have been chosen due to the need for a better height retrieval in the Arctic Ocean, where traditional retrackers are not sufficient for extracting accurate height estimates in sea ice leads. In addition, not only a higher quality of

		<p>CCI Sea Level Budget Closure</p> <p>ESA/ESRIN contract 4000119910/17/I-NB</p> <p>Reference: ESA_SLBC_cci_D2.4.2</p> <p>Version: v1.2</p> <p>Date: 18.06.2019</p> <p>Page: 104 of 116</p>
---	---	---

data is needed, but definitely also a higher quantity of data. At the moment, most data are acquired during the late summer season, where peaky waveforms from melt ponds on top of sea ice might be mistaken for the desired waveforms stemming from sea ice leads.

Using the ALES+ retracker as well as utilizing the retracking of CryoSat-2 SAR and SARIn data in the LARS system at DTU Space will provide a higher quality and quantity of data compared to standard ocean retracking.

NERSC TOPAZ4: NERSC TOPAZ4 is a coupled ocean and sea ice data assimilation system for the North Atlantic and the Arctic Ocean that is based on the Hybrid Coordinate Ocean Model (HYCOM) and the Ensemble Kalman Filter data assimilation (Sakov et al., 2012). HYCOM is using 28 hybrid z-isopycnal layers at a horizontal resolution varying from 16 km in North Atlantic to 12 km in the Arctic Ocean. The TOPAZ4 system is forced by the ECMWF ERA Interim reanalysis and assimilates most available measurements including along-track altimetry data, sea surface temperatures, sea ice concentrations and sea ice drift from satellites along with in-situ temperature and salinity profiles from Argo floats and research cruises. For validation results and more details see Sakov et al. (2012) and Xie et al. (2017).

8.2.2 Algorithms

ALES+

ALES+ is a subwaveform retracking algorithm that takes into account the sea state and the slope of the trailing edge. The retracking algorithm itself is based on the Brown-Hayne model (Brown, 1977; Hayne, 1980) and contains a preliminary step in order to estimate the most appropriate length of the trailing edge contained by the subwaveform. For very specular waveforms, the trailing edge is much shorter, which is taken into account during the fitting of the procedure if the waveform is found to be a “non-standard” ocean waveform. Non-standard ocean waveforms are detected by identifying waveforms with a pulse peakiness (PP) higher than 1 (PP>1). The PP value is determined as defined by Peacock and Laxon (2004):

$$PP = 31.5 \frac{p_{max}}{\sum_{i=5}^{64} p_i},$$

where pmax is the maximum power of the waveform and p_i is the power in range bin number i . More on the retracking algorithms can be found in Passaro et al. (2014) and Passaro et al. (2018).

LARS

For 20 Hz SAR and SARIn data from LARS we are only including waveforms retrieved over ice leads. Within the LARS database, the waveforms are retracked using a simple threshold retracker. Ice lead waveforms are then found to be those with a PP higher than 0.35 for SAR and 0.25 for SARIn, and a stack standard deviation lower than 4. For the CryoSat-2 SAR and SARIn data, PP is defined as in Armitage and Davidson (2014):

		<p>CCI Sea Level Budget Closure</p> <p>ESA/ESRIN contract 4000119910/17/I-NB</p> <p>Reference: ESA_SLBC_cci_D2.4.2</p> <p>Version: v1.2</p> <p>Date: 18.06.2019</p> <p>Page: 105 of 116</p>
---	---	---

$$PP = \frac{p_{max}}{\sum_{i=1}^N p_i} ,$$

where p_{max} is the maximum power of the waveform, N is the number of range bins in the waveform (128 for SAR, 512 for SARIn), and p_i is the power in bin number i .

Intermission bias

To make a seamless transition between the three satellite missions, the intermission biases were estimated and minimized. In this step a difference from v1 to v2 is that v2 is resampling data directly to monthly instead of diurnal medians. The following steps were completed to handle the intermission biases:

1. Monthly medians were calculated for each mission for the entire region covered by the data set.
2. For overlapping mission pairs (either ERS-2 and Envisat, or Envisat and CryoSat-2), coinciding days were detected and extracted.
3. The trend was removed for each data set containing coinciding monthly medians.
4. For each data set, the median was determined.
5. For each overlapping pair, the median difference was calculated and the data sets were aligned.
6. The data sets were corrected corresponding to the RADS reference (TOPEX/Poseidon).

For CryoSat-2, RADS and LARS data have been adjusted by looking at individual satellite tracks.

The raw but inter-satellite bias corrected satellite data are divided into months filtered and gridded with a resolution of 0.50 x 0.25 (longitude x latitude). For more information, see Rose et al. (in preparation).

A time series showing the monthly median SLA for the entire Arctic region is shown in Figure 8.1. The time series has been constructed by taking a weighted average of each monthly mean grid from the netCDF file. The weights were derived from the inverse of the uncertainty, e , multiplied by cosine of the latitude, for each grid point, i , out of all N grid points:

$$w_i = \frac{\cos(lat_i)}{\sum_i^N \cos(lat_i)}$$

		<p>CCI Sea Level Budget Closure</p> <p>ESA/ESRIN contract 4000119910/17/I-NB</p> <p>Reference: ESA_SLBC_cci_D2.4.2</p> <p>Version: v1.2</p> <p>Date: 18.06.2019</p> <p>Page: 106 of 116</p>
---	---	---

The average SLA for each month, t , was then found to be:

$$SLA_t = \sum_i^N w_i * SLA_i$$

The time series from 1996 to 2019 have a mean trend of 2.43 ± 0.42 mm/year for the entire Arctic region and with the GIA correction applied the trend is 2.58 ± 0.77 mm/year. The spatial distribution of the trend can be seen in Figure 8.2.

8.3 Product Specification

8.3.1 Product geophysical data content

DTU Arctic Altimetric Sea Level Record: The data con SLA record was corrected for all geophysical corrections and is referenced to the DTU18MSS (Andersen et al., 2018). This is a change from v1, where we used the DTU15MSS (Andersen et al., 2016). The new MSS is constructed to improve the central Arctic. The ocean tides are from FES2014 (Carrere et al., 2016b). The dynamic atmospheric correction (DAC) applied is the DAC-ERA (Carrere et. al, 2016a) for the ERS-2 and Envisat periods, where MOG2d is used for CryoSat. The DAC can be very large in the Arctic (in the level of the SLA) and very noisy in sea ice covered regions. Therefore, errors in the DAC can introduce large errors in the SLA. There exist two SLA products one with and one without the DAC correction.

For the comparison altimetry vs. TG data, the reference range and geophysical corrections are consistently applied (Andersen and Scharroo, 2011). No DAC/IB correction have been applied in the comparison with tide gauges.

Monthly mean SLA covering the region from 65°N-81-5°N and 180°W-180°E are provided for the period January 1996 and October 2018 with the file

ARCTIC_SLA_xx_v2.nc

xx corresponds to dac or nodac

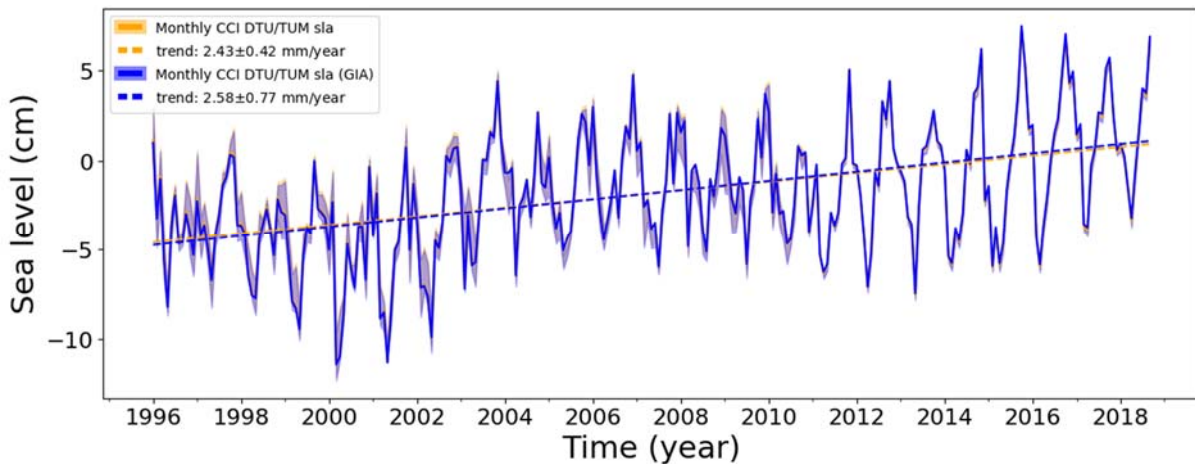


Figure 8.1: Monthly ESA CCI DTU/TUM Arctic sea level anomaly record including GIA_Caron2018.

Geophysical Variable	Name in product	Unit
Longitude	longitude	degrees east
Latitude	latitude	degrees north
Date of monthly mean SLA estimate	date	YY-MM-DD
SLA above DTU18MSS	sea_level_anomaly	m
2.5% confidence level	P2.5	m
97.5% confidence level	P97.5	m
95% confidence level range	95_confidence_range	m
Standard deviation of SLA	standard_deviation	m

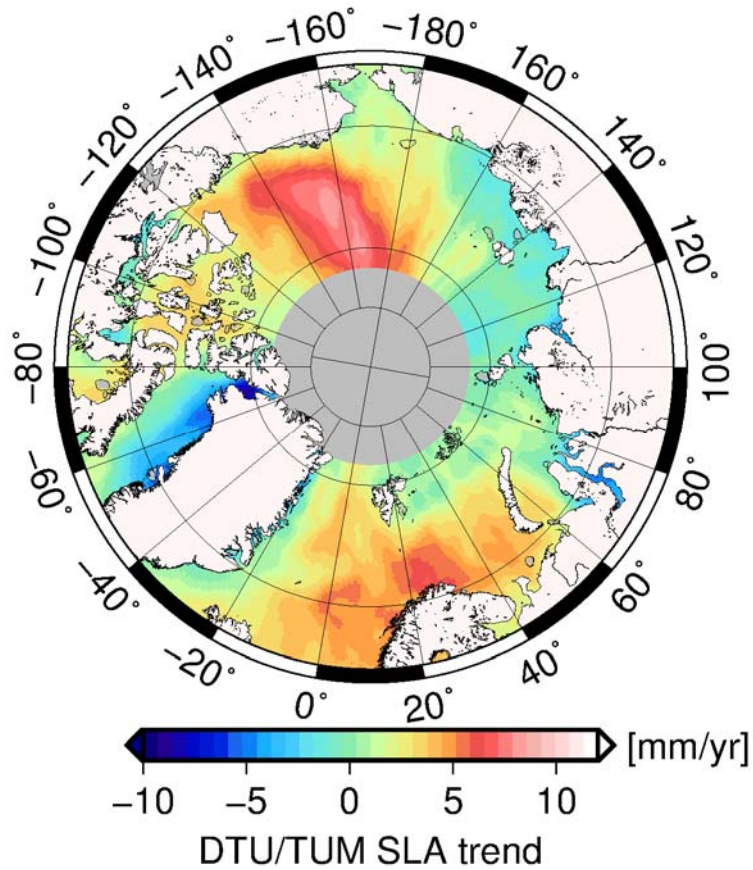


Figure 8.2: Regional trends of ESA CCI DTU/TUM Arctic sea level record between 1996 to 2018

NERSC TOPAZ4: The TOPAZ4 products contain gridded sea surface height (meters; relative to geoid), and steric height (meters).

Files: (1) TopazSSH20032017.nc (sea surface height, SSH)
(2) TopazStericht20032017.nc (steric height)

Geophysical Variable	Name in product	Unit
Longitude	LONGITUDE	degrees_east
Latitude	LATITUDE	degrees_north
Time	TAX	hours since 1950-01-01 00:00:00
(1) Sea Surface Height	SSH	m
(2) Steric Sea Level	STERICHT	m

		<p>CCI Sea Level Budget Closure</p> <p>ESA/ESRIN contract 4000119910/17/I-NB</p> <p>Reference: ESA_SLBC_cci_D2.4.2</p> <p>Version: v1.2</p> <p>Date: 18.06.2019</p> <p>Page: 109 of 116</p>
---	---	---

8.3.2 Coverage and resolution in time and space

DTU Arctic Altimetric Sea Level Record: The SLA data cover the region from 65°N-81.5°N and 180°W-180°E with a resolution of 0.25° in latitudinal direction and 0.5° in longitudinal direction, respectively. Data are given in monthly intervals between January 1996 and October 2018.

There are fewer data points from ERS-2 and Envisat compared to CryoSat-2, and for all of the missions, the data coverage is highest during summer/fall.

NERSC TOPAZ4: The TOPAZ4 covers the Nordic Seas and entire Arctic Oceans bounded by 65°N - 90°N and 180°W to 180°E with a spatial resolution of 0.25°. The temporal coverage is from 2003-2017 at a monthly resolution.

8.3.3 Product data format

DTU Arctic Altimetric Sea Level Record: The Arctic SLA record is provided in a netCDF file. Dimensions are 720 in longitude, 67 in latitude and 273 in time. The variables are: sea level anomaly, 2.5% confidence level, 97.5% confidence level, 95% confidence interval, and standard deviation.

NERSC TOPAZ4: The format of the TOPAZ4 fields is in NetCDF CF 1.6. Dimensions are 1440 in longitude and 100 in latitude and 180 in time, and variables are SSH and STERICHT.

8.3.4 Product grid and projection

DTU Arctic Altimetric Sea Level Record: The data are provided in a grid with a resolution of 0.25 degrees in the latitudinal direction and 0.5 degrees in the longitudinal direction. Data points are located at -180:0.5:180 degrees longitude and 65:0.25:82 degrees latitude.

NERSC TOPAZ4: The TOPAZ4 is provided on a regular 0.25°x0.25° latitude-longitude grid.

8.4 Uncertainty assessment

8.4.1 Sources of error

DTU Arctic Altimetric Sea Level Record: When it comes to satellite altimetry in the Arctic Ocean there are multiple error sources:

		<p>CCI Sea Level Budget Closure</p> <p>ESA/ESRIN contract 4000119910/17/I-NB</p> <p>Reference: ESA_SLBC_cci_D2.4.2</p> <p>Version: v1.2</p> <p>Date: 18.06.2019</p> <p>Page: 110 of 116</p>
---	---	---

- Erroneous range estimates caused by highly reflective melt ponds on top of the sea ice, wet ice and refrozen ice/snow (mostly during summer).
- Inaccurate range corrections from atmospheric models – e.g. the dynamic atmospheric correction.
- Inaccurate tide models. The tidal models are based on altimetry, and in an area with less altimetry data, such as sea ice covered regions in the Arctic Ocean, it is to be expected that the tidal model (in this case FES2014) is less accurate.

However, not all of the above listed error sources are directly quantifiable, and those that are, are difficult to keep track of during interpolation. Here, a block bootstrap method is used to quantify the uncertainties by determine the confidence interval for each grid cell for every month (Lahiri, 2003). Each grid cell is assumed to be uncorrelated.

NERSC TOPAZ4: The sources of error come predominantly arise from deficiency in the TOPAZ4 model system and lack of in-situ data for assimilation.

8.4.2 Methodology for uncertainty assessment

In the bootstrap method data are repeatedly processed 500 times from the first filtering to the final resampled grid point by randomly drawing a new grid cell with replacement from the cells in the original dataset. There can be multiple copies of the cells.

8.4.3 Results of uncertainty assessment

A map of the SLA range difference in the confidence intervals from 2.5% to 97.5% corresponding to a confidence level of 95% is shown in Figure 8.3. The gridded monthly data are not normal distributed, hence the standard deviation should only be used with care. For more information, see Rose et al. (in prep).

8.4.4 Uncertainty documentation in the data products

The estimated uncertainties associated with the SLA are given as two separate variables in the netCDF files. The uncertainty estimates are the lower and upper confidence level of data, the 95% confidence interval range and the standard deviation. The standard deviation should be used with care, while data are not normal distributed everywhere.

		CCI Sea Level Budget Closure ESA/ESRIN contract 4000119910/17/I-NB Reference: ESA_SLBC_cci_D2.4.2 Version: v1.2 Date: 18.06.2019 Page: 111 of 116

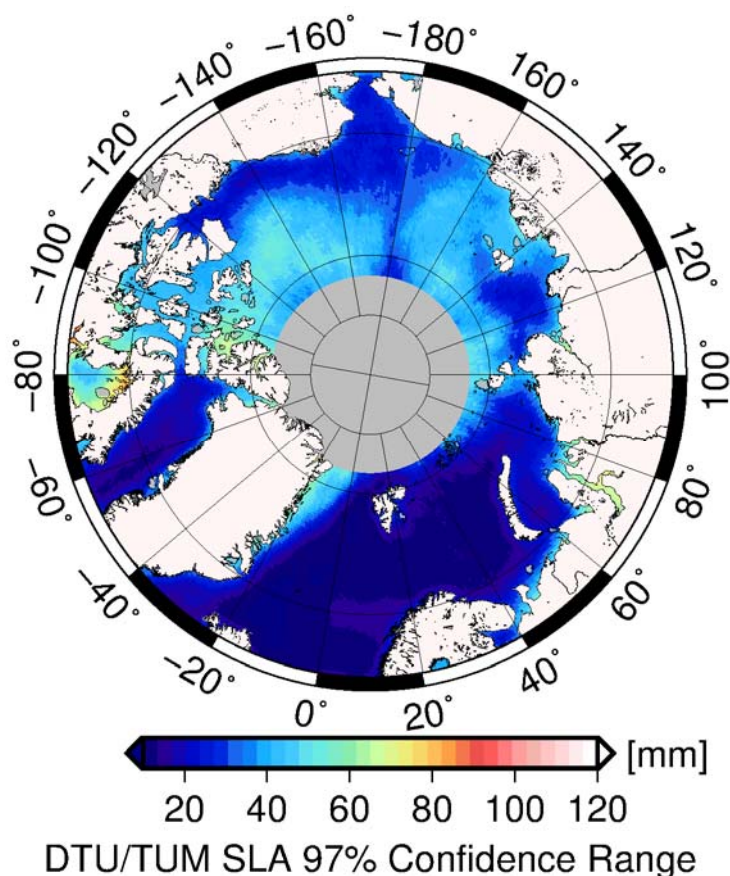



Figure 8.3: The SLA 97% confidence range interval

8.5 References

- Andersen, O. B., and R. Scharroo (2011): Range and geophysical corrections in coastal regions, In: S. Vignudelli, A.G. Kostianoy, P. Cipollini, J. Benveniste (eds.): *Coastal altimetry*, Springer, ISBN: 978-3-642-12795-3.
- Andersen, O., Knudsen, P., and Stenseng, L. (2018): A New DTU18 MSS Mean Sea Surface – Improvement from SAR Altimetry. 172. Abstract from 25 years of progress in radar altimetry symposium, Portugal.
- Andersen, O. B., Stenseng, L., Piccioni, G., and Knudsen, P. (2016): The DTU15 MSS (Mean Sea Surface) and DTU15LAT (Lowest Astronomical Tide) reference surface. Abstract from ESA Living Planet Symposium 2016, Prague, Czech Republic.
- Armitage, T. W. K., and M. W. J. Davidson (2014): Using the Interferometric Capabilities of the ESA CryoSat-2 Mission to Improve the Accuracy of Sea Ice Freeboard Retrievals, *IEEE Transactions on Geoscience and Remote Sensing*, vol. 52, no. 1, pp. 529-536, Jan. 2014. doi: 10.1109/TGRS.2013.2242082. <http://ieeexplore.ieee.org/stamp/stamp.jsp?tp=&arnumber=6479282&isnumber=6675822>

		<p>CCI Sea Level Budget Closure</p> <p>ESA/ESRIN contract 4000119910/17/I-NB</p> <p>Reference: ESA_SLBC_cci_D2.4.2</p> <p>Version: v1.2</p> <p>Date: 18.06.2019</p> <p>Page: 112 of 116</p>
---	---	---

- Brown, G.S. (1977): The average impulse response of a rough surface and its applications. *IEEE Trans. Antennas Propag.* 25, 67–74. <http://dx.doi.org/10.1109/TAP.1977.1141536>.
- Hayne, G.S. (1980): Radar altimeter mean return waveforms from near-normal-incidence ocean surface scattering. *IEEE Trans. Antennas Propag.* 28, 687–692. doi: 10.1109/TAP.1980.1142398.
- Carrere, L., Faugère, Y., and Ablain, M. (2016a): Major improvement of altimetry sea level estimations using pressure-derived corrections based on ERA-Interim atmospheric reanalysis. *Ocean Science*, 12(3), 825–842. doi: 10.5194/os-12-825-2016.
- Carrere L., F. Lyard, M. Cancet, A. Guillot, and N. Picot (2016b): FES 2014, a new tidal model – Validation results and perspectives for improvements: Presentation to ESA Living Planet Conference, Prague 2016.
- Lahiri, S. (2003): *Resampling Methods for dependent Data*. Springer, p. 374, ISBN 978-1-4757-3803-2.
- Passaro, M., Cipollini, P., Vignudelli, S., Quartly, G., and Snaith, H. (2014): ALES: A multimission subwaveform retracker for coastal and open ocean altimetry. *Remote Sens. Environ.* 145, 173–189. doi: 10.1016/j.rse.2014.02.008.
- Passaro, M., S. K. Rose, O. B. Andersen, E. Boergens, F. M. Calafat, D. Dettmering, and J. Benveniste (2018): ALES+: Adapting a homogenous ocean retracker for satellite altimetry to sea ice leads, coastal and inland waters. *Remote Sens. Environ.*, 211, 456–471. doi: 10.1016/j.rse.2018.02.074.
- Peacock, N.R., and Laxon, S.W. (2004): Sea surface height determination in the Arctic ocean from ERS altimetry. *J. Geophys. Res. Oceans* 109. doi: 10.1029/2001JC001026.
- Rose, S.K., Andersen, O.A., Passaro M., Benveniste, J. (*in preparation*): Arctic Ocean Sea Level Record from the Complete Radar Altimetry Era: 1991-2018, *Remote Sens.*
- Sakov, P., F. Counillon, L. Bertino, K. A. Lisæter, P. R. Oke, and A. Korabely (2012): TOPAZ4: an ocean-sea ice data assimilation system for the North Atlantic and Arctic. *Ocean Science*, 8:633-656, doi:10.5194/os-8-633-2012.
- Scharroo, R., Leuliette, E. W., Lillibridge, J. L., Byrne, D., Naeije, M. C., and Mitchum, G. T. (2013): RADS: Consistent multi-mission products, Proceedings of the Symposium on 20 Years of Progress in Radar Altimetry, Venice: ESA Spec. Publ., ESA SP-710, 4.
- Stenseng, L. (2011): *Polar Remote Sensing by CryoSat-type Radar Altimetry*. Ph.D. thesis. National Space Institute, Technical University of Denmark.
- Xie, J., L. Bertino, F. Counillon, K. A. Lisæter, and P. Sakov (2017): Quality assessment of the TOPAZ4 reanalysis in the Arctic over the period 1991-2013, *Ocean Sci.*, 13(1), pp. 123-144, doi:10.5194/os-2016-38, 2016 doi:10.5194/os-13-123-2017.

		<p>CCI Sea Level Budget Closure</p> <p>ESA/ESRIN contract 4000119910/17/I-NB</p> <p>Reference: ESA_SLBC_cci_D2.4.2</p> <p>Version: v1.2</p> <p>Date: 18.06.2019</p> <p>Page: 113 of 116</p>
---	---	---

Appendix

Complementary material for Chapter 7 “Total Land Water Storage Change”

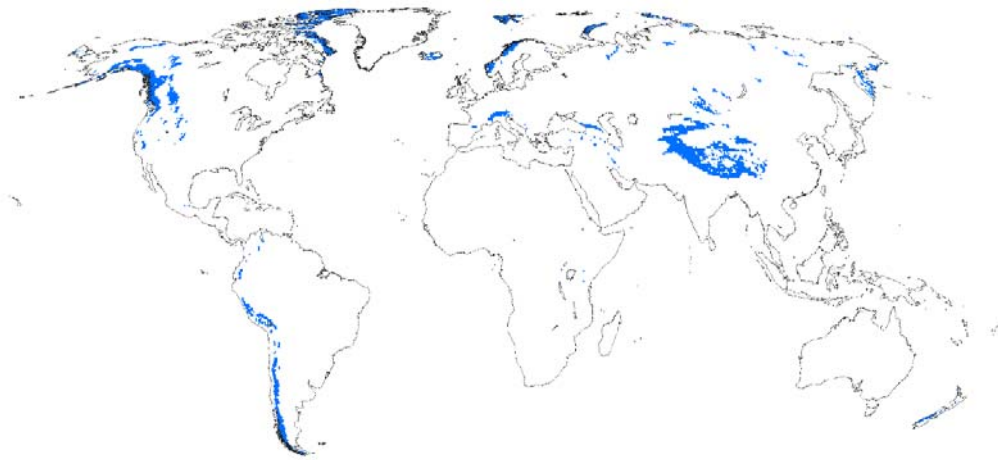


Figure A 1: : Location of glacierized grid cells (from GGM original gridded data) which are within the boundaries of the WATCH-CRU ocean-land mask.



Figure A 2: Location of glacierized grid cells (from GGM original gridded data) which are outside of the boundaries of the WATCH-CRU ocean-land mask (excluded from the analysis).

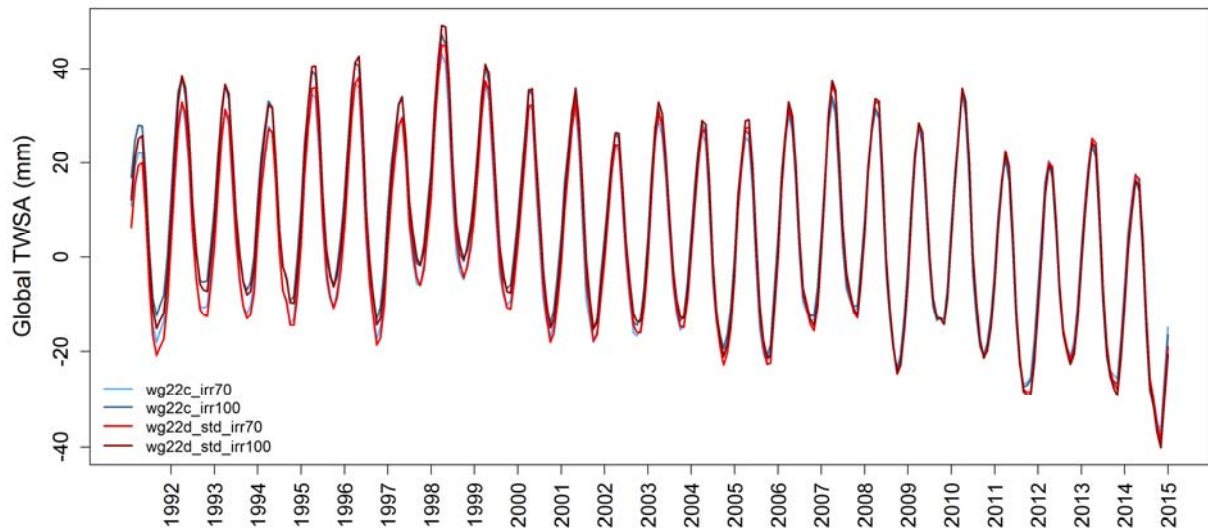


Figure A 3: Comparison of globally averaged TWSA in mm with respect to the global continental area (except Greenland and Antarctica) as computed by WaterGAP2.2c standard (blue curves) and by WaterGAP2.2d standard (red curves) forced with WFDEI-CRU for two irrigation variants, either 70% deficit (irr70) irrigation in groundwater depletion areas or optimal (irr100) irrigation. Anomalies are relative to the mean of 2006-2013.

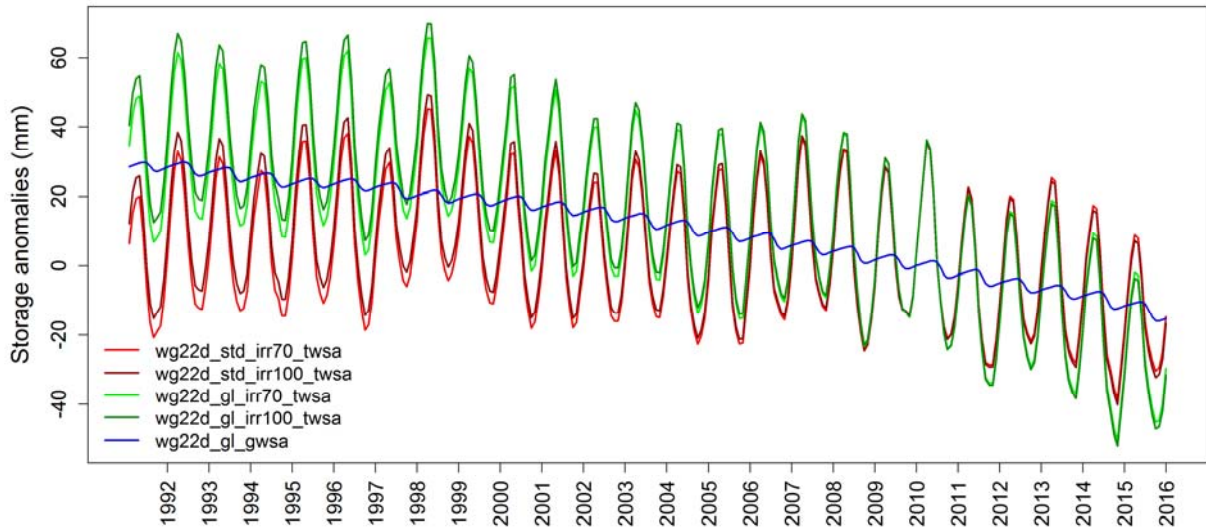


Figure A 4: Effect of adding a glacier water storage compartment on global TWSA in mm with respect to the global continental area (except Greenland and Antarctica) from WaterGAP2.2d forced with WFDEI-CRU for two irrigation variants (70% deficit and optimal irrigation variants). Red curves: TWSA from WaterGAP2.2d standard, green curves: TWSA from WaterGAP2.2d variant including glaciers explicitly, blue curve: glacier water storage anomalies from WaterGAP2.2d variant including glaciers explicitly. All anomalies are relative to the mean of 2006-2015.

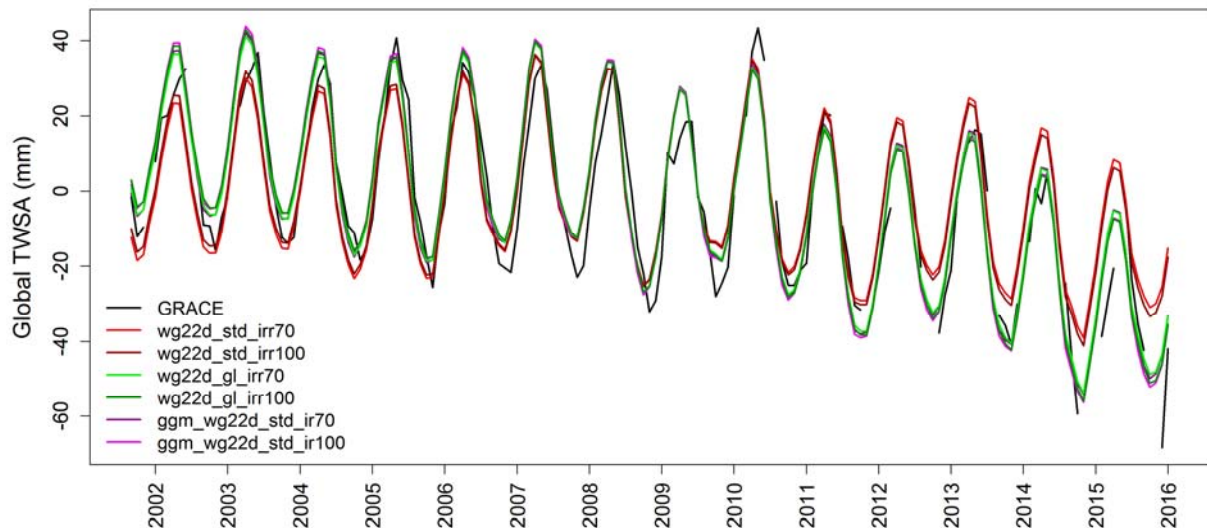


Figure A 5: Comparison between global TWSA in mm with respect to the global continental area (except Greenland and Antarctica) from GRACE (solution provided by WP220 version 1) and from modeling (WFDEI-CRU) for two irrigation variants (70% deficit and optimal irrigation variants). Black curve: GRACE, red curves: WaterGAP2.2d standard, green curves: WaterGAP2.2d variant including glaciers explicitly. The magenta curves were obtained by summing TWS from WaterGAP2.2d standard and glacier water storage from GGM, and deriving anomalies. All anomalies are relative to the mean of January 2003 – January 2016.

End of document